



Non-destructive Classification of Moisture Deterioration in Layered Building Floors Using Ground Penetrating Radar

vorgelegt von
M.Sc.
Tim Klewe

an der Fakultät VI – Planen Bauen Umwelt
der Technischen Universität Berlin
zur Erlangung des akademischen Grades

Doktor der Ingenieurwissenschaften
- Dr.-Ing. -

genehmigte Dissertation

Promotionsausschuss:

Vorsitzender: Prof. Dr. Dietmar Stephan
Gutachterin: Prof. Dr. Sabine Kruschwitz
Gutachter: Dr. Christoph Strangfeld
Gutachter: Prof. Dr. Christian Große
Gutachter: Prof. Dr. Markus Krüger

Tag der wissenschaftlichen Aussprache: 22. September 2023

Berlin 2023

Abstract

In the event of moisture deterioration, rapid detection and localization is particularly important to prevent further deterioration and costs. For building floors, the layered structure poses a challenging obstacle for most moisture measurement methods. But especially here, layer-specific information on the depth of the water is crucial for efficient and effective repairs. Ground Penetrating Radar (GPR) shows the potential to generate such depth information. Therefore, the present work investigates the suitability of GPR in combination with machine learning methods for the automated classification of the typical deterioration cases (i) dry, (ii) wet insulation, and (iii) wet screed.

First, a literature review was conducted to identify the most common methods for detecting moisture in building materials using GPR. Here, it especially became clear that all publications only investigated individual time-, amplitude- or frequency features separately, without combining them. This was seen as a potential aspect for innovation, as the multivariate application of several signal features can help to overcome individual weaknesses and limitations.

Preliminary investigations carried out on drying screed samples confirmed the profitable use of multivariate evaluations. In addition to the general suitability and dependencies of various features, first limitations due to possible interference between the direct wave and the reflection wave could be identified. This is particularly evident with thin or dry materials, for which the two-way travel times of the reflected radar signals become shorter.

An extensive laboratory experiment was carried out, for which a modular test specimen was designed to enable the variation of the material type and thickness of screed and insulation, as well as the simulation of moisture deteriorations. The data collected revealed clear differences between dry and deteriorated structures within measured B-scans. These deviations were to be detected with the newly introduced B-scan features, which evaluate the statistical deviation of A-scan features within a survey line. In this way, deteriorations to unknown floor structures are recognized, regardless of the material parameters present. In a subsequent training and cross-validation process of different classifiers, accuracies of over 88 % of the 504 recorded measurements (252 different experimental setups) were achieved. For that, the combination of amplitude and frequency features, which covered all relevant reflections of the radar signals, was particularly beneficial. Furthermore, the data set showed only small differences between dry floors and deteriorated screeds for the B-scan features, which could be attributed to a homogeneous distribution of the added water in the screeds. The successful separation of these similar feature distributions raised the suspicion of overfitting, which was examined in more detail by means of a validation with on-site data.

For this purpose, investigations were carried out at five different locations in Germany, using the identical measurement method like in the laboratory. By extracting drilling cores, it was possible to determine the deterioration case for each measurement point and thus generate a corresponding reference. However, numerous data had to be sorted out before classification, since disturbances due to underfloor heating, screed reinforcements, steel beams or missing insulation prevented comparability with the laboratory experiments. Validation of the remaining data (72 B-scans) achieved only low accuracy with 53 % correctly classified deterioration cases. Here, the previously suspected overfitting of the small decision boundary between dry setups and deteriorated screeds within the laboratory proved to be a problem. The generally larger deviations within (also dry) on-site

B-scans were thus frequently misclassified as screed deterioration. In addition, there were sometimes strongly varying layer thicknesses or changing cases of deterioration within a survey line, which caused additional errors due to the local limitation of the drilling core reference. Nevertheless, individual on-site examples also showed the promising potential of the applied signal features and the GPR method in general, which partly allowed a profound interpretation of the measurements. However, this interpretation still requires the experience of trained personnel and could not be automated using machine learning with the available database. Nevertheless, such experience and knowledge can be enriched by the findings of this work, which provide the basis for further research.

Future work should aim at building an open GPR data base of on-site moisture measurements on floors to provide a meaningful basis for applying machine learning. Here, referencing is a crucial point, whose limitations with respect to the moisture present and its distribution can easily reduce the potential of such efforts. The combination of several reference methods might help to overcome such limitations. Similarly, a focus on monitoring approaches can also help to reduce numerous unknown variables in moisture measurements and increase confidence in the detection of different deterioration cases.

Kurzfassung

Bei Feuchteschäden ist eine schnelle Erkennung und Lokalisierung von besonderer Bedeutung, um das Ausmaß und zusätzliche Kosten einzugrenzen. In dem speziellen Fall von Fußböden stellt der geschichtete Aufbau für die meisten Feuchtemessverfahren ein unüberwindbares Hindernis dar. Allerdings sind besonders hier genaue schichtspezifische Informationen über die Wassertiefe entscheidend, um eine effiziente und effektive Instandsetzung vornehmen zu können. Ground Penetrating Radar (GPR) hat das Potenzial, solche Tiefeninformationen zu generieren. Die vorliegende Arbeit untersucht daher die Eignung von GPR in Kombination mit Methoden des maschinellen Lernens für die automatisierte Klassifizierung der typischen Schadensfälle (i) trocken, (ii) geschädigte Dämmung, und (iii) geschädigter Estrich.

In einer Literaturrecherche wurden zunächst die gängigsten Methoden zur Detektion von Feuchtigkeit in Baumaterialien mittels GPR erarbeitet. Dabei wurde insbesondere deutlich, dass alle Veröffentlichungen entsprechende Zeit-, Amplituden- oder Frequenzmerkmale separat untersuchten, ohne diese zu kombinieren. Hierin wird eine Innovationsmöglichkeit gesehen, da die multivariate Anwendung mehrerer Signalmerkmale dabei helfen kann, die Schwächen und Einschränkungen einzelner Merkmale zu überwinden.

Voruntersuchungen an trocknenden Estrichproben bestätigten den gewinnbringenden Nutzen einer solchen multivariaten Datenauswertung. Neben der generellen Eignung und den Abhängigkeiten verschiedener Merkmale konnten erste Einschränkungen durch mögliche Interferenzen zwischen der direkten Welle und der Reflexionswelle identifiziert werden. Dies zeigt sich insbesondere bei dünnen oder trockenen Materialien, bei denen sich die Laufzeiten der reflektierten Radarsignale verkürzen.

Es folgten umfangreiche Laboruntersuchungen an einem eigens entworfenen modularer Probekörper, welcher die Variation der Materialart und -dicke von Estrich und Dämmung sowie die Simulation von Feuchtigkeitsschäden ermöglicht. Die gesammelten Daten zeigten innerhalb der gemessenen B-Scans deutliche Unterschiede zwischen trockenen und geschädigten Aufbauten. Diese Unterschiede sollten mit den neu eingeführten B-Scan Merkmalen erkannt werden, welche die statistische Abweichung von A-Scan Merkmalen innerhalb einer Messlinie auswerten. Dies erlaubt die Erkennung von Schäden an unbekanntem Bodenstrukturen und somit unabhängig von den vorhandenen Materialparametern. In einem anschließenden Trainings- und Kreuzvalidierungsprozess verschiedener Klassifikatoren wurden Genauigkeiten von über 88 % bei 504 aufgenommenen B-Scans (252 verschiedene Versuchsaufbauten) erreicht. Besonders vorteilhaft war dabei die Kombination von Amplituden- und Frequenzmerkmalen, welche alle relevanten Reflexionen innerhalb der Radarsignale erfasste. Darüber hinaus zeigten sich innerhalb des Datensatzes nur geringe Unterschiede zwischen trockenen Fußböden und geschädigten Estrichen, was auf eine homogene Verteilung des zugeführten Wassers innerhalb der Estriche zurückgeführt werden konnte. Die dennoch erfolgreiche Trennung dieser ähnlichen Merkmalsverteilungen ließ den Verdacht einer Überanpassung aufkommen, was durch eine Validierung mit Praxisdaten näher untersucht werden sollte.

Zu diesem Zweck erfolgten Untersuchungen an fünf verschiedenen Standorten in Deutschland, wobei die Messmethode identisch zum Labor verblieb. Entnommene Bohrkernen ermöglichten für jeden Messpunkt eine Bestimmung des Schadenfalls und lieferten so eine entsprechende Referenz. Vor der Klassifizierung mussten bereits zahlreiche Daten aussortiert werden, da Störungen durch Fußbodenheizung, Estrichbewehrung, Stahlträger oder fehlende Dämmung eine Vergleichbarkeit mit den Laborversuchen verhinderten.

Die Validierung der verbleibenden Daten (72 B-Scans) ergab mit 53 % korrekt klassifizierten Schadensfällen erheblich geringere Genauigkeiten. Hier erwies sich die zuvor vermutete Überanpassung der Entscheidungsgrenze zwischen trockenen Aufbauten und beschädigten Estrichen innerhalb des Labors als tatsächliches Problem. Die in der Regel größeren Abweichungen für (auch trockene) B-Scans aus der Praxis wurden daher häufig als Estrichschäden fehlinterpretiert. Hinzu kamen teilweise stark variierende Schichtdicken oder wechselnde Schadensfälle innerhalb einer Messlinie, die aufgrund der lokalen Begrenzung der Bohrkernreferenz zusätzliche Fehler verursachten. Dennoch zeigten einzelne Beispiele vor Ort auch das vielversprechende Potenzial der angewandten Signalmerkmale und von GPR im Allgemeinen, was teilweise fundierte Interpretationen ermöglichte. Diese Interpretationen erfordern jedoch nach wie vor die Erfahrung von geschultem Personal und konnten mit der vorhandenen Datenbasis nicht durch maschinelles Lernen automatisiert werden. Dennoch können solche Erfahrungen und Kenntnisse durch die Ergebnisse dieser Studie erweitert werden, was die Grundlage für weitere Forschung bildet.

Zukünftige Arbeiten sollten darauf abzielen eine offene GPR Datenbank mit praxisbezogenen Feuchtemessungen an Fußböden aufzubauen, um eine aussagekräftige Grundlage für die Anwendung von maschinellem Lernen zu schaffen. Hier ist die Referenzierung ein entscheidender Punkt, dessen Einschränkungen in Bezug auf die vorhandene Feuchtigkeit und ihrer Verteilung das Potenzial solcher Bemühungen erheblich verringern können. Die Kombination mehrerer Referenzmethoden könnte helfen, solche Einschränkungen zu überwinden. In ähnlicher Weise kann eine Konzentration auf Ansätze des Monitorings dazu beitragen, die zahlreichen unbekanntenen Variablen bei Feuchtemessungen zu reduzieren und so für eine höhere Sicherheit bei der Erkennung verschiedener Schadensfälle sorgen.

Acknowledgement

I am grateful to have had the support and contributions of so many individuals throughout my research journey. First and foremost, I want to express my sincere appreciation to my supervisors Sabine Kruschwitz and Christoph Strangfeld for their invaluable guidance, expertise, and unwavering encouragement. Their constant efforts were instrumental in the successful completion of my research project.

Furthermore, I would like to acknowledge Thomas Kind and Jens Wöstmann for their fruitful explanations and discussions on the radar method, which greatly enhanced my understanding of the topic. Likewise, I am thankful to Christoph Völker for his enlightening insights on data analysis, that always gave me further understanding and guidance. I would also like to acknowledge Marco Lange and Sean Smith for their diligent assistance with various technical aspects, including sample preparation and construction. Hans-Carsten Kühne and Frank Haamkens are also thanked for their support in producing the screed samples.

Sarah Munsch's contributions in conducting NMR measurements and engaging in insightful discussions on moisture measurements were also deeply appreciated. Christian Köpp's helpful feedback and corrections on my publications are also acknowledged with gratitude. Further, I thank Ozan Tasan and Ahmed Ismail for the contributions to this research in the framework of their final theses.

Last but not least, I would like to express my heartfelt gratitude to my family and friends for their unwavering support throughout this adventure. Their encouragement, love, and understanding have been a source of strength and motivation, and I could not have done this without them. This is especially true for my partner Aleksandra Naydenova, who has always helped me stay on track through her listening, empathy, advice, and constant drive.

.....
Author's signature

Contents

Introduction

1	Motivation	3
1.1	Project Idea and Research Questions.....	5
1.2	Thesis Structure	7
	Bibliography	10
A	Review of Moisture Measurements in Civil Engineering with Ground Penetrating Radar - Applied Methods and Signal Features	11
A.1	Introduction.....	13
A.2	Fundamentals of GPR	13
	A.2.1 Wave propagation and received signals	14
A.3	Configurations and their parameters	16
A.4	Moisture content of building materials.....	17
A.5	Determination of material moisture based on GPR	18
	A.5.1 Travel time and velocity features	19
	A.5.2 Amplitude and attenuation features.....	20
	A.5.3 Features in the frequency domain.....	21
	A.5.4 Inversion-based methods	22
	A.5.5 Problems and limitations of on site investigations	24
A.6	Summary and conclusion	25
	Bibliography	26

Materials and Preliminary Studies

2	Evaluation of Radar Signal Features on Drying Screed Samples	35
2.1	Materials and Methods.....	35
	2.1.1 Casting of Screed Samples	35
	2.1.2 Hardware and Measurement Procedure	37
	2.1.3 Feature Extraction and Evaluation.....	38
2.2	Results and Discussion.....	40
	2.2.1 Moisture Reference	40
	2.2.2 Univariate Analysis on Exemplary Screed Samples	41
	2.2.3 Multivariate Analysis on Entire Dataset	43
2.3	Summary and Conclusion	45
	Bibliography	46

Results

B	Combining Signal Features of Ground-Penetrating Radar to Classify Moisture Damage in Layered Building Floors.....	49
B.1	Introduction.....	51
B.1.1	Moisture Measurement with GPR.....	51
B.2	Materials and Methods.....	53
B.2.1	Modular Test Specimen.....	54
B.2.2	Water Damage in Insulation Layer.....	54
B.2.3	Water Damage in Screed Layer.....	55
B.2.4	Hardware and Measurement Procedure.....	56
B.2.5	Feature Extraction.....	57
B.2.6	Classification of Damage Scenarios.....	59
B.3	Results.....	60
B.3.1	Measurements at Modular Specimen.....	60
B.3.2	Damage Scenario Classification.....	63
B.4	Discussion.....	66
	Bibliography.....	68
C	Classification of On-Site Floor Moisture Damage with GPR - Limitations and Chances.....	71
C.1	Introduction.....	73
C.1.1	Moisture Measurement with GPR.....	74
C.1.2	Preceding Laboratory Study.....	74
C.2	Methods.....	74
C.2.1	On-Site Measurements.....	74
C.2.2	Feature Extraction.....	76
C.2.3	Classification.....	77
C.3	Results.....	78
C.3.1	On-Site Measurements.....	78
C.3.2	Classification of On-Site Measurements.....	82
C.4	Discussion.....	83
C.5	Summary and Conclusion.....	87
	Bibliography.....	89

Synthesis

3	Discussion.....	95
3.1	Summary of Results.....	95
3.2	Literature Review.....	96
3.3	Materials and Preliminary Studies.....	97
3.3.1	Specimens.....	97
3.3.2	Feature Evaluation.....	98
3.4	Laboratory Investigations.....	99
3.4.1	Experimental Design.....	99
3.4.2	Methodology Development.....	101

3.5	On-Site Investigations	103
3.5.1	Measurements	103
3.5.2	Methodology Validation	104
3.6	Concluding Discussion	106
4	Outlook	109
	Bibliography	110
	List of Tables	111
	List of Figures	113
	Abbreviations	116

Appendix

I	Comparison of the Calcium Carbide Method and Darr Drying to Quantify the Amount of Chemically Bound Water in Early Age Concrete	121
II	Poster: Combination of Radar and Neutrone Probe to Determine the Mass Moisture of Screeds	143
	Complete List of Publications	145

Introduction

1	Motivation	3
1.1	Project Idea and Research Questions.....	5
1.2	Thesis Structure	7
	Bibliography	10
A	Review of Moisture Measurements in Civil Engineering with Ground Penetrating Radar - Applied Methods and Signal Featu- res	11
A.1	Introduction.....	13
A.2	Fundamentals of GPR	13
A.3	Configurations and their parameters	16
A.4	Moisture content of building materials.....	17
A.5	Determination of material moisture based on GPR.....	18
A.6	Summary and conclusion	25
	Bibliography	26

1. Motivation

”Water is sometimes sharp and sometimes strong, sometimes acid and sometimes bitter, sometimes sweet and sometimes thick or thin, sometimes it is seen bringing hurt or pestilence, sometime health-giving, sometimes poisonous. It suffers change into as many natures as are the different places through which it passes. [...] Sometimes it starts a conflagration, sometimes it extinguishes one; is warm and is cold, carries away or sets down, hollows out or builds up, tears or establishes, fills or empties, raises itself or burrows down, speeds or is still; is the cause at times of life or death, or increase or privation, nourishes at times and at others does the contrary; at times has a tang, at times is without savor, sometimes submerging the valleys with great floods. In time and with water, everything changes.”

*Leonardo da Vinci, * 1452 - † 1519*

For mankind, water has always been both a source of life and danger, offering a particularly ambivalent fascination. Consequently, it does not seem surprising that our building materials are also exposed to this special relationship. While a large amount of water is necessary or even indispensable for their production [1], unwanted contact with the liquid often poses a risk of deterioration. Degradations like mould [2], corrosion [3], the migration of chloride ions [1], alkali-silica reaction [4], frost-thaw cycle, micro cracking [5], spalling, salt efflorescence [6], etc. are promoted by an increased material moisture. The consequences are not only health-related, such as an increased risk of lung diseases like asthma due to mold [7, 8], but also cause immense repair costs. Statistics from the Insurance Information Institute show that one in 60 insured buildings in the U.S. has a water damage each year [9]. This corresponds to estimated annual costs of 16.3 billion USD [10, 11]. Between 2000 and 2020, the annual costs of pipe water damage in Germany increased by 165 % to the latest amount of 3.3 billion Euro [12]. Thus, pipe water causes greater financial damage than the sum of natural hazards, severe weather and fire damage combined. Unlike the latter causes of damage, which are usually associated with a clear event, the extent of pipe water damage often remains partially or completely undetected, which further increases the damage and costs. It is therefore clear that in the event of damage, determining and localizing the moisture and its cause is an important first step in estimating and efficiently carrying out the necessary renovation.

There are numerous methods for measuring moisture in building materials, which can basically be divided into destructive and non-destructive procedures [13]. In the determination of moisture, the destructive methods aim at an actual separation of water and the building material, while the non-destructive methods observe changes in physical material properties. The most commonly used destructive method is Darr drying [14]. For this purpose, samples are taken destructively and stored in a drying oven for several days, whereby the weight loss that occurs allows the moisture content to be determined. The procedure is simple and accurate, however time consuming and costly. A faster and also direct approach is the calcium-carbide method (CCM) [15]. Here, small sample sizes of 3 g to 100 g are crushed together with calcium carbide in a shaker. The calcium carbide reacts with the containing water, resulting in a measurable pressure increase inside the shaker that can be directly related to the moisture content. For both destructive methods, the relatively small sample size only allows spatially limited, however quantitatively accurate statements about present water, which is why it is often used to reference non-destructive measurements.

Non-destructive measurement methods offer a much larger number of possible techniques. The possibilities range from electric (resistive [16, 17], capacitive [18, 19, 20]) over radiometric [21, 22], hygrometric [23], and chemical [24], to thermal methods [25], whereby their suitability highly depends on the individual problem.

A quite special case is the investigation of building floors, as they have a layered structure and are therefore particularly difficult to measure in their entirety. In addition, there is a wide range of possible material types and their thicknesses, which makes each floor construction a very individual case. Most of the common non-destructive moisture measurement methods are not suitable for a comprehensive investigation of building floors. They often provide only moisture information on superficial areas or are hindered by the layered structure. In addition, floor constructions often contain a floor covering above screed and insulation, which can affect the validity of the applied method. Especially the moisture state of the insulation, which lies deepest, is unrecognized by most methods and presents a particular challenge when performing moisture investigations on building floors.

Neutron probes are a suitable exception, since they can reach penetration depths of almost 30 cm, regardless of the layered structure. With these probes it is possible to get an overview of the total amount of water in a defined floor area, however liquid water cannot be distinguished from chemically bound water. This is due to the physical principle in which so-called 'fast' neutrons with high kinetic energy are irradiated into the medium under investigation. These neutrons interact with the atoms of the matter, causing scattering, diffusion and, above all, deceleration [26]. While heavy atoms essentially cause a change in direction of the neutrons, the collision with hydrogen atoms, i.e. those with the lowest atomic mass, results in the greatest possible energy loss [27]. According to [28], already 18 collisions with hydrogen atoms are sufficient to convert a fast neutron into a slow, thermal neutron. The number of these thermal neutrons is recorded by counter tubes installed in the neutron probe and thus allows conclusions to be drawn about the quantity of hydrogen atoms present in the measurement volume. Therefore, an appropriate calibration of the measured values is required for the quantitative determination of the mass moisture, which can be carried out by the destructive removal of drilling cores and a subsequent gravimetric investigation. Further, the taken cores offer so far the only possibility for a vertical localization of the moisture deterioration in layered floor structures, since the integral measurement method of the neutron probe does not allow depth

information. In addition, the sensitivity to water also decreases with increasing distance from the radiation source, which further hinders the detection of insulation deterioration. With its strong sensitivity to water, Ground Penetrating Radar (GPR) is the most promising non-destructive method for obtaining the valuable depth information needed to fully assess moisture deterioration in building floors. Not only, but also for moisture measurements, it has long been an established method in geophysics [29, 30], whereas its application in civil engineering is increasing [31, 32]. The literature therefore already contains numerous processing methods that allow conclusions to be drawn about the moisture content of the medium under investigation, such as asphalt [33, 34], concrete [35, 36, 37], brick [38], or screed [39]. Distinctive features can be found in the time as well as in the frequency domain of the measured data, whereby users often only apply a single feature for moisture determination. This results in greater uncertainties, since other influencing factors, such as the reflector depth or the underlying permittivity, are usually unknown, but have a major impact on the evaluation. Possible misinterpretations could be reduced by combining several signal features with the use of multivariate data analysis and machine learning. The thus potential advances may enable reliable information about the extent of deterioration and the exact depth of moisture in building floors. Combined with the ability to quickly measure large areas, it would make GPR the primary approach for floor deterioration assessment to significantly save renovation costs. With the above-mentioned costs of 3.3 billion euros per year, the potential in Germany alone is enormous. A reduction of just 3 % would mean savings of 100 million Euro per year, which can have a direct impact on insurance premiums for buildings.

1.1 Project Idea and Research Questions

Due to of the aforementioned advantages when applied to layered structures, neutron probes are a suitable means to assess moisture deteriorations in building floors. Therefore, the engineering office 'Ingenieurbüro Tobias Ritzer GmbH', the industrial partner of the project, has been using this methodology for more than 2 decades. Their experience has shown that in the case of pipe water damage, floors are mainly affected, as they either include the broken pipe system in the insulation or are flooded from above. This results in two primary types of deterioration: wet insulation or wet screed. Moisture barriers in the form of polyethylene foils usually prevent the exchange of water between the two layers. However, in the rare case of poor functionality, both layers can be deteriorated simultaneously. Knowledge of the presence and distribution of these different cases is of great importance in order to carry out an efficient and effective repair.

The idea of the project is to supplement the neutron probe with GPR to generate the missing depth information for moisture deteriorations in building floors. In this context, methods are developed that allow a valid classification of the two commonly occurring deterioration cases, wet insulation and wet screed. This additional valuable information is expected to reduce the need for destructive drilling cores or replace them completely. Figure 1.1 shows the conceptual plan, where a detailed data acquisition in the laboratory is to take place at the beginning. The collected data is then used to study and assess distinctive signal features that allow the differentiation and classification of common deterioration cases. In particular, methods of multivariate data analysis and machine learning shall be tested to achieve this goal.

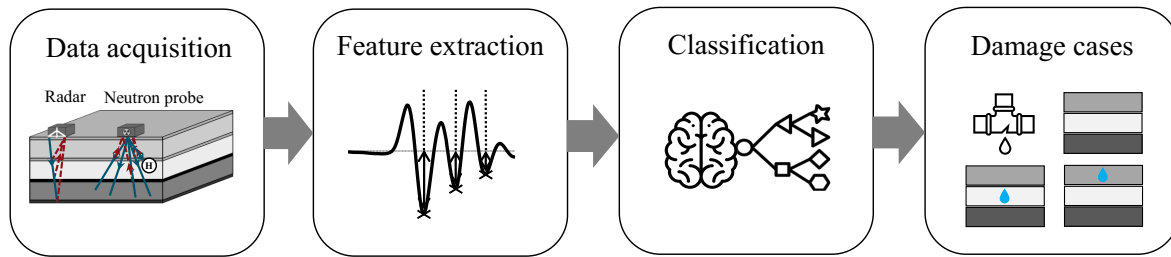


Figure 1.1: Project plan to classify the two common damage cases on building floors (wet insulation and wet screed) by extracting and combining distinctive signal features of GPR.

The application of machine learning for non-destructive testing in civil engineering (NDT-CE) offers both great potential and possible pitfalls. On the one hand, it can accelerate the investigation and evaluation of large areas with a wide variety of deterioration conditions, that usually require both, an extensive analysis by trained personnel, and the calibration on destructively extracted drilling cores. Further, machine learning offers the possibility to provide further insights into the data structure and into yet unknown relationships within NDT-CE. On the other hand, the successful use of these new techniques requires a profound and diverse training database. Compared to popular and successful examples in computer vision applications such as autonomous driving or facial recognition, the availability of labeled nondestructive testing (NDT) data is often limited in civil engineering. Compared to other materials like metals or polymers, building materials are more heterogeneous and may differ a lot from each other. This implies the risk of an insufficient representation of the space of possibility [40]. Unfortunately, referencing training data for machine learning is not always straightforward for NDT-CE. Therefore, the project approaches these problems and questions by producing referenced training data within laboratory conditions. The developed methods are then applied to classify new, also referenced on-site measurements on real deterioration cases.

From the foregoing, two research questions arise for this thesis:

Primary research question

- To what extent is the GPR method suitable for the valid classification of commonly occurring moisture deterioration cases in building floors?

In order to answer this question, possibilities and limits of the method are to be worked out by means of a profound experimental program in the laboratory and on-site, followed by a meaningful data evaluation. In the process, all measurements are also performed with the neutron probe for comparison.

Secondary research question

- What are the opportunities and problems in applying machine learning on a practical example within NDT-CE?

For the evaluation, training data generated in the laboratory are used to classify new, referenced on-site deterioration cases. The validation should thus allow a statistical evaluation of the achieved accuracy.

1.2 Thesis Structure

The research questions posed are investigated and discussed in the form of a cumulative dissertation. Therefore, both, corresponding publications and additional chapters are included in this thesis. A clear distinction is made by the section's numbering. While the published works are marked by alphabetic numerals, the additional sections carry Arabic numerals. The incrementing is done independently for both types.

After the motivation and the formulation of the resulting research questions in the previous sections, the remaining part of the introduction will be dedicated to the theoretical basics and the current state of the art of GPR. This will be given in the form of the first publication A - a review paper. This paper provides a comprehensive overview of the application of GPR for moisture measurement on building materials, with particular reference to the signal features used for this purpose. It provides a basis for the subsequent preliminary investigations, which will be introduced in chapter 2. Here, both the production of the relevant test specimens and the subsequent first studies are presented, which provide initial insights into the properties of various GPR signal features from the literature. The results obtained had a direct impact on the following main part of the thesis, which is presented by the publications B and C. The former publication deals with the extensive laboratory investigations and the resulting method development for the classification of various moisture deterioration cases on floor constructions with unknown material parameters like type and thickness. This method will then be applied on new on-site measurement, which is covered by the latter publication. The synthesis of all the collected findings then follows in section 3, where a comprehensive discussion of all collected findings and their critical review is conducted. In closing, an outlook for possible future works is provided.

The terms 'damage' and 'deterioration'

In the following thesis the term 'damage' may be used as a synonym for 'deterioration'. Neither term is uniformly defined in the literature and does not indicate the conditions needed (e.g. moisture content) to evaluate a floor structure as damaged or deteriorated. However, a definition within this thesis is given for insulation and screed in the sections B.2.2 and B.2.3, respectively, and critically discussed in section 3.4.1.

Bibliography

- [1] R. H. Crawford and G. Treloar. An assessment of the energy and water embodied in commercial building construction. In *4th Australian Life-Cycle Assessment Conference*, 2005.
- [2] K. F. Nielsen, G. Holm, L. P. Uttrup, and P. A. Nielsen. Mould growth on building materials under low water activities. Influence of humidity and temperature on fungal growth and secondary metabolism. *International Biodeterioration & Biodegradation*, 54(4):325–336, dec 2004. <https://doi.org/10.1016/j.ibiod.2004.05.002>.
- [3] A. Bentur, N. Berke, and S. Diamond. *Steel corrosion in concrete: fundamentals and civil engineering practice*. CRC Press, 1997.
- [4] D. W. Hobbs. *Alkali-silica reaction in concrete*. Thomas Telford Publishing, 1988.
- [5] S. Jacobsen, J. Marchand, and L. Boisvert. Effect of cracking and healing on chloride transport in OPC concrete. *Cement and Concrete Research*, 26(6):869–881, jun 1996. [https://doi.org/10.1016/0008-8846\(96\)00072-5](https://doi.org/10.1016/0008-8846(96)00072-5).
- [6] C. Dow and F. P. Glasser. Calcium carbonate efflorescence on Portland cement and building materials. *Cement and Concrete Research*, 33(1):147–154, jan 2003.
- [7] J. Lohi, T. Tuomela, and T. Tuuminen. Exposure to Mould and Moisture Damage Is a Potential Risk Factor for the Development of Respiratory Diseases Opinion. *International Journal of Immunology*, 8(3):38, 2020.
- [8] G. Smedje and D. Norbäck. Incidence of asthma diagnosis and self-reported allergy in relation to the school environment—a four-year follow-up study in schoolchildren. *The International Journal of Tuberculosis and Lung Disease*, Vol. 5(11), 2001.
- [9] Insurance Information Institute. Facts + Statistics: Homeowners and renters insurance. <https://www.iii.org/fact-statistic/facts-statistics-homeowners-and-renters-insurance>, 2023.
- [10] E. Duffin. Number of households in the U.S. from 1960 to 2022 [infographic]. <https://www.statista.com/statistics/183635/number-of-households-in-the-us/>, December 2022.
- [11] Statista Research Department. Homeownership rate in the United States from 1990 to 2022 [infographic]. <https://www.statista.com/statistics/184902/homeownership-rate-in-the-us-since-2003/>, February 2023.
- [12] GDV. Annual of Gesamtverband der Deutschen Versicherungswirtschaft e.V. <https://www.gdv.de/de/zahlen-und-fakten/versicherungsgebiete/wohngebaeude-24080>, 2020. Accessed on 20/07/2021.
- [13] S. Kruschwitz. Feuchtemessung im Bauwesen - ein Überblick. *Fachtagung Bauwerksdiagnose, Vortrag 5*, 2014.
- [14] Deutsches Institut für Normen. *DIN EN ISO 12570 : 2000 - Bestimmung des Feuchtegehalts durch Trocknen bei erhöhter Temperatur*, 2000.

- [15] F. Radtke. *Schnellbestimmung der Feuchtigkeit beliebiger Materialien mit der Carbid-Methode*. [https://www.radtke-messtechnik.com/wp-content/uploads/2021/06/Anleitung-CM-Ger2.05 edition](https://www.radtke-messtechnik.com/wp-content/uploads/2021/06/Anleitung-CM-Ger2.05%20edition%202021.pdf), 2021.
- [16] J. Priou, Y. Lecieux, M. Chevreuil, V. Gaillard, C. Lupi, D. Leduc, E. Rozière, R. Guyard, and F. Schoefs. In situ DC electrical resistivity mapping performed in a reinforced concrete wharf using embedded sensors. *Construction and Building Materials*, 211:244–260, jun 2019.
- [17] M. Cheytani and S. L. I. Chan. The applicability of the Wenner method for resistivity measurement of concrete in atmospheric conditions. *Case Studies in Construction Materials*, 15:e00663, dec 2021.
- [18] H. Eller and A. Denoth. A capacitive soil moisture sensor. *Journal of Hydrology*, 185(1-4):137–146, nov 1996.
- [19] E. Nyfors. Industrial Microwave Sensors - A Review. *Subsurface Sensing Technologies and Applications*, 1(1):23–43, 2000.
- [20] R. Černý. Time-domain reflectometry method and its application for measuring moisture content in porous materials: A review. *Measurement*, 42(3):329–336, apr 2009.
- [21] J. Kodikara, P. Rajeev, D. Chan, and C. Gallage. Soil moisture monitoring at the field scale using neutron probe. *Canadian Geotechnical Journal*, 51(3):332–345, mar 2014.
- [22] S. M. Nagel, C. Strangfeld, and S. Kruschwitz. Application of ^1H proton NMR relaxometry to building materials - A review. *Journal of Magnetic Resonance Open*, 6-7:100012, jun 2021.
- [23] C. Strangfeld and T. Klewe. Hygrometric Moisture Measurements Based on Embedded Sensors to Determine the Mass of Moisture in Porous Building Materials and Layered Structures. pages 213–225, 2021.
- [24] ASTM International. Standard Test Method for Measuring Moisture Vapor Emission Rate of Concrete Subfloor Using Anhydrous Calcium Chloride. *F1869-16b*, 2016.
- [25] E. Grinzato, G. Cadelano, and P. Bison. Moisture map by IR thermography. *Journal of Modern Optics*, 57(18):1770–1778, oct 2010.
- [26] M. A. Berliner. *Feuchtemessung*. Verlag Technik, 1980.
- [27] K. Kupfer. *Materialfeuchtemessung: Grundlagen, Meßverfahren, Applikationen, Normen*. Expert-Verlag, 1997.
- [28] W. Lück. *Feuchtigkeit - Grundlagen, Messen, Regeln*. R. Oldenbourg, 1964.
- [29] J. A. Huisman, S. S. Hubbard, J. D. Redman, and A. P. Annan. Measuring Soil Water Content with Ground Penetrating Radar: A Review. *Vadose Zone Journal*, 2(4):476–491, nov 2003.

- [30] L. Slater and X. Comas. The Contribution of Ground Penetrating Radar to Water Resource Research. In *Ground Penetrating Radar: Theory and Applications*. Elsevier, 2009.
- [31] F. Lombardi, F. Podd, and M. Solla. From Its Core to the Niche: Insights from GPR Applications. *Remote Sensing*, 14(13):3033, jun 2022.
- [32] W. Wai-Lok Lai, X. Dérobert, and P. Annan. A review of Ground Penetrating Radar application in civil engineering: A 30-year journey from Locating and Testing to Imaging and Diagnosis. *NDT&E International*, 96:58–78, jun 2018.
- [33] T. Saarenketo and T. Scullion. Road evaluation with ground penetrating radar. *Journal of Applied Geophysics*, 43(2-4):119–138, mar 2000.
- [34] F. M. Fernandes, Andreia Fernandes, and Jorge Pais. Assessment of the density and moisture content of asphalt mixtures of road pavements. *Construction and Building Materials*, 154:1216–1225, nov 2017. <https://doi.org/10.1016/j.conbuildmat.2017.06.119>.
- [35] G. Klysz and J.-P. Balayssac. Determination of volumetric water content of concrete using ground-penetrating radar. *Cement and Concrete Research*, 37(8):1164–1171, aug 2007.
- [36] S. Laurens, J. P. Balayssac, J. Rhazi, G. Klysz, and G. Arliguie. Non-destructive evaluation of concrete moisture by GPR: experimental study and direct modeling. *Materials and Structures* 38, 38(9):827–832, nov 2005.
- [37] W. L. Lai, S. C. Kou, W. F. Tsang, and C. S. Poon. Characterization of concrete properties from dielectric properties using ground penetrating radar. *Cement and Concrete Research*, 39(8):687–695, aug 2009.
- [38] W. L. Lai, T. Kind, S. Kruschwitz, J. Wöstmann, and H. Wiggenhauser. Spectral absorption of spatial and temporal ground penetrating radar signals by water in construction materials. *NDT & E International*, 67:55–63, oct 2014.
- [39] F. Kurz and H. Sgarz. Measurement of Moisture Content in Building Materials using Radar Technology. *International Symposium Non-Destructive Testing in Civil Engineering (NDT-CE)*, 2015.
- [40] J. B. Harley and D. Sparkman. Machine learning and NDE: Past, present, and future. 2019.

A. Review of Moisture Measurements in Civil Engineering with Ground Penetrating Radar - Applied Methods and Signal Features

Abstract

When applying Ground Penetrating Radar (GPR) to assess the moisture content of building materials, different medium properties, dimensions, interfaces and other unknown influences may require specific strategies to achieve useful results. Hence, we present an overview of the various approaches to carry out moisture measurements with GPR in civil engineering (CE). We especially focus on the applied signal features such as time, amplitude and frequency features and discuss their limitations. Since the majority of publications rely on one single feature when applying moisture measurements, we also hope to encourage the consideration of approaches that combine different signal features for further developments.

Bibliographic Information

T. Klewe, C. Strangfeld, S. Kruschwitz, (2021, February). Review of moisture measurements in civil engineering with ground penetrating radar – Applied methods and signal features, *Construction and Building Materials*, Volume 278, 122250, ISSN 0950-0618, <https://doi.org/10.1016/j.conbuildmat.2021.122250>.

Author's contribution

Conceptualization, T.K., C.S., and S.K.; methodology, T.K.; software, T.K.; validation, T.K.; formal analysis, T.K.; investigation, T.K.; resources, C.S. and S.K.; data curation, T.K.; writing—original draft preparation, T.K. and C.S.; writing—review and editing, T.K., C.S. and S.K.; visualization, T.K.; supervision, C.S. and S.K.; project administration, C.S. and S.K.; funding acquisition, C.S. and S.K.

Copyright Notice

This is a published article accessible by <https://doi.org/10.1016/j.conbuildmat.2021.122250>.
It is licensed under an open access Creative Commons CC BY 4.0 license.

A.1 Introduction

In civil engineering (CE), all constructions are facing several types of degradation, which cause expensive costs of repair. Frequently occurring degradations are the migration of chloride ions [1], leading to corrosion [2], alkali-silica reaction [3], mould [4], frost-thaw cycle, micro cracking [5], spalling, salt efflorescence [6], etc. All these degradation processes are promoted by an increased amount of material moisture and affect building materials such as concrete, steel, wood, stones, bricks, and screed [7]. Constructions in the field of transport infrastructure, building constructions, or hydraulic structures are mainly made of reinforced concrete [8]. Therefore, the moisture content in the porous cement matrix of concrete is an important and crucial parameter. However, a reliable and non-destructive investigation of the moisture content is still very complex and challenging, while the costs of repair rise continuously. Especially in the field of building constructions, ageing pipe systems are becoming a high burden for insurance. In 2018, 2.9 billion Euro of damage was caused by piped water, accounting for the largest share (49%) of building insurance claims in Germany [9]. In the event of damage, the accurate determination and localization of water ingress is essential to plan for and perform efficient renovations.

There are various methods to approach this task, ranging from destructive (Darr test, calcium carbide method) to non-destructive procedures (electrical, capacitive, radiometric, thermal and hygromatic) [10, 11]. While destructive methods are time and cost intensive, most non-destructive measurements are comparatively easy to perform, however, without the use of complex processing and interpretation procedures, they deliver only qualitative results.

Ground Penetrating Radar (GPR) is a fast and widely used measurement method based on electromagnetic waves. Although Radio Detection And Ranging (Radar) is commonly applied for aircraft and ship detection [12], it is used in many other applications like weather forecasts [13] or collision avoidance in the automotive industry [14]. Apart from that, it recently received attention from a wider audience with its application to prove the existence of water on Mars [15]. Over the last decades, many publications already demonstrated the high sensitivity of GPR for water, especially in geophysics [16, 17]. However, also in CE it is increasingly used for nondestructive moisture measurements (e.g. [18, 19, 20, 21, 22]).

A variety of publications have shown multiple ways to assess moisture with GPR. Different building materials and inspection purposes require individual methods concerning the antenna configuration or the used frequency. The applied setup as well as the underlying structure highly influence the subsequent interpretation of the recorded data, which is why also numerous signal features have been established. Due to the many possibilities to perform moisture measurements with GPR, this review gives an overview of the various methods and their limitation in the context of CE. It shall serve as a basis for inexperienced readers, as well as for advanced users, to encourage further development. Approaches that combine different features or even methods, like data fusion and machine learning, could also benefit from this overview.

A.2 Fundamentals of GPR

GPR signals are electromagnetic waves whose dynamic behavior is mathematically expressed by Maxwell's equations [23, 24]. The wave propagation in investigated objects is highly dependent on the particular electrical properties of the underlying material.

Those properties are described by dielectric permittivity ε , electrical conductivity σ , and magnetic permeability μ .

While an influence of μ is neglectable in the majority of GPR applications, ε and σ are of high importance [25]. A low electrical conductivity σ provides the best conditions for an effective use of GPR since the energy is primarily maintained in low-loss materials. Less attenuation allows signals to penetrate deeper into a given material, which results in a better signal-to-noise ratio for low-lying regions of interest. The velocity of wave propagation in low-loss and nonmagnetic materials can be calculated with Eq. (A.1) [26, 25].

$$v = \frac{c_0}{\sqrt{\varepsilon_r}} \quad (\text{A.1})$$

As the speed of light c_0 is constant, the wave velocity is a function of the relative permittivity ε_r (with $\varepsilon_r = \frac{\varepsilon}{\varepsilon_0}$ and the electric permittivity in vacuum $\varepsilon_0 = 8.854 \cdot 10^{-6} \frac{\text{As}}{\text{Vm}}$). The relative permittivity describes the dielectric characteristics of materials and is defined as a complex value, where the real and imaginary part are associated with energy storage and dissipation, respectively [16]. While the real part of most building materials is considered as constant and dominant between 10 MHz to 1000 MHz, the frequency-dependent loss becomes relevant as you get closer to the water relaxation frequency between 10 GHz to 20 GHz [19, 25]. According to the popular models of Debye [27] and Cole-Cole [28] this results in a decreasing real part and an increasing imaginary part of ε_r for higher frequencies. Following Eq. A.1 smaller real parts of ε_r cause higher velocities. However, this effect is not measurable in common GPR applications on building materials, since the high frequency components of transmitted broadband impulses also experience more attenuation due to an increased imaginary part. The frequency dependent attenuation leads to a shift towards lower frequencies that can be observed with rising water contents (see section A.5.3). Furthermore, the enhanced scattering of higher frequencies on heterogeneities leads to additional damping, which limits the possible penetration depth [29, 30].

The real value of ε_r is 1 for air and approximately 81 for pure water in liquid phase. For most of dry soils and building materials ε_r is in the range of 2 to 9 [26] and increases with a higher water content (e.g. ε_r is 10 to 20 for wet concrete). Due to these significant differences, the water content is considered as the main influence on dielectric properties of building materials, which highly justifies the use of GPR for moisture measurements [31].

A related method that also utilizes the influence of water on the electric permittivity and the resulting attenuation of electromagnetic waves is the application of microwave measurements. A review of the various concepts is presented by Okamura [32].

A.2.1 Wave propagation and received signals

The occurrence of reflection, refraction, and transmission on boundaries between two different permittivities is an important behavior to describe the propagation of electromagnetic waves. The simplified ray-based wave paths describing these principles are shown in Figure A.1.

The amount of reflected energy (R, black) of a transmitted pulse is dependent on the difference between the permittivities ε_1 and ε_2 of two considered materials. Expressed as a factor in the range of -1 and 1 , the reflection coefficient r is calculated as follows:

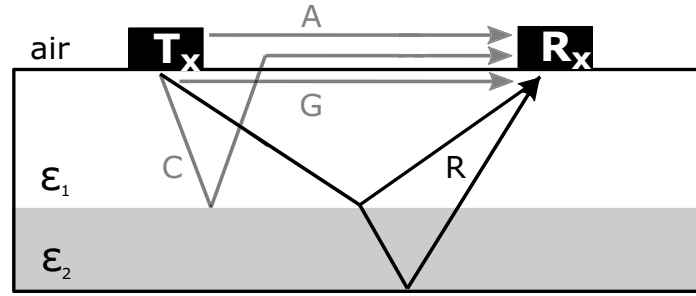


Figure A.1: Principle of GPR reflection and underlying signal paths between a transmitter T_x and a receiver R_x : A - direct air wave, G - direct ground wave, R - reflected wave, C - critical refracted wave (according to [16] and [25]).

$$r = \frac{\sqrt{\epsilon_1} - \sqrt{\epsilon_2}}{\sqrt{\epsilon_1} + \sqrt{\epsilon_2}} \quad (\text{A.2})$$

Another important wave path is taken by the direct air (A, grey) and direct ground (G, grey) wave, which propagate in their respective medium on the shortest way between transmitter and receiver. With a small antenna spacing, both waves superpose and form the direct wave (DW) that is seen first in the received signal. A qualitative example of such a recorded energy-signal in time domain (A-Scan) is shown in Figure A.2. The DW is followed by a reflection wave (RW), with a certain peak-to-peak amplitude $A_{RW,p-p}$ and a time difference Δt_{RW} between DW and RW. These basic signal features, as well as the peak-to-peak amplitude of the DW, can already serve as good indicators for moisture measurements on building materials, which will be further discussed in section A.5.

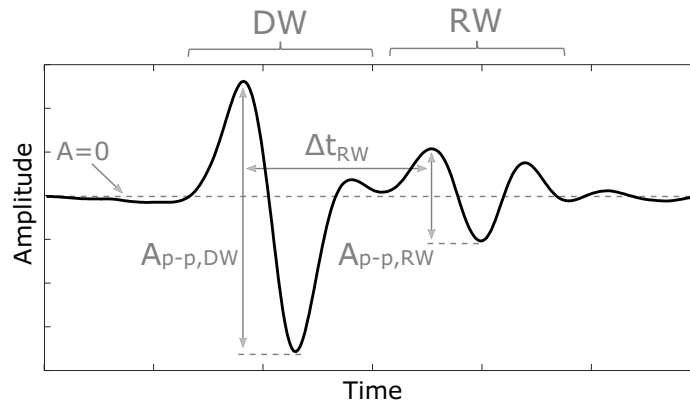


Figure A.2: Example of a recorded energy-signal in time domain (A-Scan) including the direct wave (DW) and reflection wave (RW). Basic signal features are the peak-to-peak amplitudes $A_{DW,p-p}$ and $A_{RW,p-p}$ located at the first peaks of DW and RW. The time difference Δt_{RW} between both peaks is often considered as the travel time.

Similar to optics, refraction is described by Snell's law that deals with the relationship of occurring angles on interfaces. For reasons of clarity, the occurring refraction from ϵ_2 to ϵ_1 is not depicted in Figure A.1. Critical refractions and reflections (C, grey) also exist. They often superpose with the reflected wave R, which makes a separate investigation

difficult. In general, the received A-Scan is always a superposition of all different wave paths, whereas their individual amplitude and separation in time and space depend on the spacing between transmitter and receiver as well as on the target depth and on the elevation of the antenna [30]. Different GPR configurations, therefore, have a considerable influence on the received signals and their interpretation. The commonly used set-ups for moisture measurements in building materials and their underlying parameters are discussed in the following section.

A.3 Configurations and their parameters

GPR configurations are divided into two types: reflection and transillumination measurements. Transillumination is rarely performed in civil engineering since a suitable back wall is often inaccessible (e.g tunnels, foundations, containments). Also, the transmission between a pair of boreholes, as it is applied by geophysicists for soil moisture measurements [33, 24], is commonly not used to investigate building materials. This paper, therefore, focuses on reflection configurations. Here, the common-offset reflection survey, as shown in Figure A.3, is the simplest and mostly applied configuration.

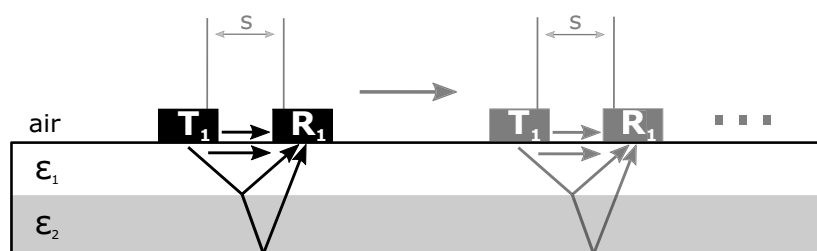


Figure A.3: Principle of a line measurement with GPR in common-offset configuration and its most important signal paths: Direct air wave, direct ground wave and the reflected waves.

As the name of the method suggests, the spacing s between a single transmitter and a receiver is kept constant for every measurement position on a survey line. The most significant parameter is the applied center frequency, which describes the dominant frequency of the transmitted broadband pulse. As mentioned in section A.2, it influences the general attenuation and, therefore, the penetration depth. When it comes to multi-layered mediums or rebar localization, the spatial resolution becomes more relevant since it rises with shorter wavelengths. This creates a trade-off between resolution and penetration depth when choosing the most suitable center frequency. GPR frequencies used for material moisture measurements are mainly between 100 kHz and 10 GHz. In case of concrete, frequencies between 1 GHz to 3 GHz yield a good trade-off between spatial resolution and penetration depth. Other essential parameters are the antenna spacing s , the antenna orientation, the bit resolution, recording time window, sampling frequency, the distance between each measurement and the parallel line spacing (when performing more than one survey line) [24]. The suitable choice of these values highly depends on the particular test object and purpose.

When using GPR in reflection configuration, one rarely has precise information about the underlying layer depth. In that case, a profound water content estimation through the use of velocity data is impossible since the traveled distance is unknown. Here, multi-offset

configurations like common-midpoint (CMP) and wide angle reflection and refraction (WARR), as shown in Figure A.4, can be used. While the CMP method uses a fixed midpoint with a stepwise increasing spacing between transmitter and receiver, WARR configurations often have one source at a constant location with multiple receivers in defined distances. WARR can also be performed by using a single receiver (or transmitter) that is moved further from the corresponding transmitter (or receiver) with every measurement.

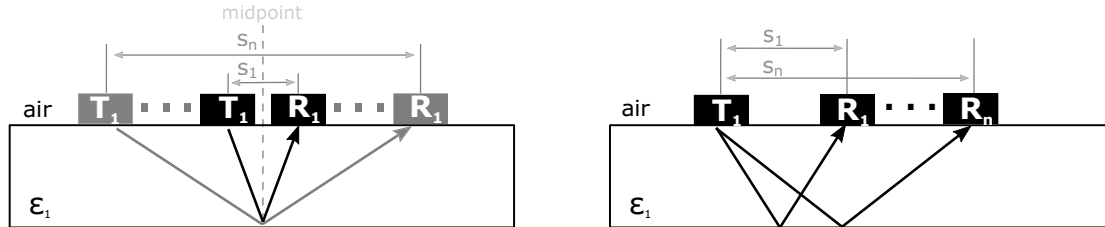


Figure A.4: GPR with multiple offsets: common-midpoint (CMP, left) and wide angle reflection and refraction (WARR, right) configuration.

The series of reflection waves (B-Scan) collected by multi-offset techniques form a hyperbola from which velocity and layer depth can be estimated [34][35][36]. After that, the obtained vertical velocity model allows a layer specific permittivity estimation.

A.4 Moisture content of building materials

As discussed in section A.2, the permittivity of an investigated material heavily depends on the moisture content and, therefore, changes when water is adsorbed. Water adsorption or desorption generally requires an open porosity as well as a hydrophobic behavior. Several building materials possess these material properties such as: concrete, screed, mineral rock wool, calcium silicate plate, etc. In these, the adsorbed water is located in completely filled pores and partially saturated pores [37].

Concrete is a highly heterogeneous material. Every concrete mixture has its own composition of water, cement, minerals, aggregates, additives, etc. This defines the resulting material properties, e.g. comprehensive strength, the dry density, and resistance to water and chlorides. Furthermore, the resulting pore system is also influenced significantly by the concrete composition as well as by the ambient temperature and humidity. On the long-term, the pore system might vary due to carbonation, micro-cracking, and sulphate attack. Thus, every pore system and hence every concrete is unique, and a general calibration function does not exist. Furthermore, the properties of the pore water are not time constant. Chloride and sulphate ingress change the surface tension of water, which changes the moisture content as well as the relative permittivity. In conclusion, quantitative moisture measurements of concrete would require intensive calibration for all the influencing factors mentioned above. Also in case of assumed perfect dry concrete samples (all evaporable pore water is released), no uniform permittivity exists. Every cement mixture contains different amounts of chemically bound water, calcium, aluminum, iron, etc. which influence the final permittivity.

The open porosity varies between 5 % and 25 % in most cases. The pore sizes are distributed over several magnitudes and are described by a representative diameter. Micro-pore

diameters are between 0.4 nm and 2 nm, so called meso-pores are in the range of 2 nm to 100 nm, and macro-pores range from 100 nm up to 100 μm [38]. In these pores, the material moisture is located in liquid phase at the pore surface/ fringe and in vapor phase in the pore center. Occurring transportation processes are a two-phase flow including both phases, vapour and liquid. The total porosity and the distribution of the different pore sizes determine the capability of adsorption and desorption of water. The function which relates the water vapour partial pressure, i.e. relative humidity and the resulting material moisture is the so-called sorption isotherm.

In most cases, the moisture content of concrete is between 0.15 M% and 10 M%. It is defined as the ratio between the mass of moisture divided by the mass of the dry material. Besides this definition, sometimes the moisture content is based on the mass of the wet material or the volumetric moisture content is given [39]. For comparison, these values must be converted to each other. In the following, we use the definition based on the mass of the dry material. Obviously, this requires the knowledge of the dry mass. One common approach is oven drying to evaporate the mobile water in the pores [40]. Depending on the sample size, this might take up to several days. If mass constant is reached, the sample is considered as dry and all evaporable/ mobile water is released. Nevertheless, the cement matrix still contains a lot of chemically bound water. This water is immobile and never contributes to the moisture transport [11]. However, if the oven temperature is too high, this chemically bound water is partially released as well, which leads to systematic deviations from the “true” moisture content. In practice, various drying temperatures are established for different materials (cement based, calcium-sulphate based, clay minerals, etc.) and different testing purposes. Therefore, we will emphasize to consider clearly the drying method and a suitable temperature (in case of oven drying) when using moisture content values for calibration.

A.5 Determination of material moisture based on GPR

After the reflected energy-signals are recorded (Fig. A.2), there are two possible ways to estimate the underlying water content θ . The first is illustrated by the steps A and B in Figure A.5, where the θ -estimation is based on a preceding ϵ -estimation. This is an appropriate approach, since the electric permittivity ϵ strongly depends on the material moisture [41]. However, such two-step calculations may increase the risk of error accumulation and therefore, already require a precise determination of ϵ . With a known ϵ , petrophysical models derived from empirical studies can be applied to calculate $\theta(\epsilon)$. Topp’s equation [42] is the most commonly used model in geophysics to estimate soil moisture [16, 17]. Therefore, it is also applied in civil engineering to derive θ of subgrades below pavement and railway structures [43, 44, 20]. It provides a basic polynomial approximation for $\theta(\epsilon)$, which only regards the real part of ϵ . For asphalt mixes, Fernandes et al. [45] applied a modification of the complex refractive index model (CRIM) derived by Wang and Lytton [46] to estimate the moisture content. CRIM offers a more complex approach, which requires further knowledge about the volumetric fraction of different material components. An overview of various petrophysical models and further literature can be found in [47].

When there is no established model for the investigated material, like for concrete, site-specific relationships based on the collected data serve as a suitable way to evaluate θ

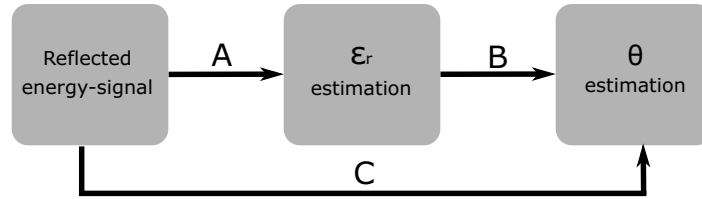


Figure A.5: Principle of signal processing to estimate the moisture content θ by using the reflected energy-signal of GPR.

[48]. However, those fitted models always require an accurate reference of the underlying water contents. Here, the gravimetric method, as discussed in the previous section, provides results by drying and weighing collected samples (e.g. drilling cores) according to ASTM D2216-19 [23].

Such references also enable the second possible way to estimate θ , which is shown by step C in Figure A.5. This approach skips the ϵ -estimation by formulating a direct relationship between the received GPR signals and the obtained moisture data.

Both approaches, AB and C, require characteristic signal features that correlate with θ . Those features commonly applied in civil engineering can be divided into time, amplitude, and frequency features. Their related methods and limitations will be discussed in the following sections.

A.5.1 Travel time and velocity features

Measuring the time Δt that it takes for a transmitted and reflected impulse to travel back to its origin is by far the oldest signal feature in radar technology [49]. It is generally used to detect objects and to calculate their distance d with Eq. A.3 by means of the known wave velocity v .

$$v = \frac{2d}{\Delta t} \quad (\text{A.3})$$

When performing moisture inspections with GPR, the permittivity of an investigated medium and hence the propagation velocity (Eq. A.1) is obviously unknown. Therefore, a known reflector depth is one possibility to calculate v and ϵ by measuring Δt . It is usually performed in laboratory studies where the dimensions of test specimens are given, like in the works of Fernandes et al. [45], Lai et al. [22] and Laurens et al. [21]. Such set-ups allow an accurate determination of ϵ depending on the water content θ with a normal common-offset survey. This approach is also applicable to multilayered structures, as shown by Grote et al. [20]. Here, Δt is the time passing between two reflections from the top and bottom of a specific layer. In singlelayered mediums, Δt is often defined as the time difference between the first peak of the direct and the reflection wave (see Figure A.2), since the true time-zero is not available [50]. In the study of Viriyametant et al. [51], the authors even propose a delay correction when using the direct wave as a time reference. This is motivated by a measurable influence of the underlying moisture content on the direct wave velocity, which can vary in near surface areas. The correction is calculated with a given transmitter to receiver offset and the wave velocity obtained from various rebar reflections in known depths.

In practice, usually the propagation velocity, as well as the reflector depth, are unknown.

In this case, ASTM D6432-11 [36] suggests two techniques to obtain v from measured travel times. The first is called hyperbolic geometry and can be performed in common-offset configuration. It requires point reflectors such as pipes or rebars that cause a hyperbolic pattern in the radargram (B-Scan), from which the propagation velocity can be derived. Cheung and Lai [52] recently used this technique to detect water-pipe leakages by observing significant velocity drops compared to undamaged dry areas. A quantitative approach was studied by Koyan et al. [53] who presented a migration-based velocity analysis on multiple rebar reflections, however, this was done with known reflector depths to conduct a time-zero correction. Here, occurring uncertainties were mainly caused by interferences due to a small spacing between the rebars and a limited vertical resolution for shallow rebar depths.

The second way to obtain v without a known d is called velocity sounding which describes the use of the CMP and WARR survey method, as mentioned in section A.3. CMP measurements were applied by Cai et al. [44] and Grote et al. [20] to obtain a vertical velocity characterization for railway and pavement structures, respectively. The use of such multi-offset configurations also allows greater spacing between transmitter and receiver. Therefore, the travel time of the direct wave gets more relevant while it is barely considered in common-offset configuration. Klysz and Balayssac [19] suggest the analysis of direct wave travel times with WARR configuration to estimate the moisture content of concrete covers. However, it is important to mention that only near surface moisture can be measured with this technique, since the penetration depth of the ground wave is limited [54].

A.5.2 Amplitude and attenuation features

Quantitative estimation of underlying permittivities by analyzing the received signal amplitudes is very challenging compared to the use of travel times [20]. The theoretical approach is given with Eq. A.2, which suggests the evaluation of occurring reflections on a boundary of two different permittivities. Besides the need of one given ϵ , this method often leads to inaccuracies due to several other influences on the amplitude. In complex mediums, like concrete, the propagating waves experience a lot of scattering through heterogeneously distributed electrical properties [25]. An increased moisture content leads to the presence of more water filled pores and thus to more heterogeneities and a higher conductivity. Furthermore, attenuation grows with longer travel paths and rising frequencies, which distorts an amplitude-based ϵ -estimation even more.

The use of an air-launched and, therefore, air-coupled antenna configuration makes it possible to analyze the reflection that occurs on the air-material interface. Air, as the overlying medium, has a known permittivity $\epsilon_{air} = 1$ and causes comparatively low losses. Thus, the permittivity of the underlying material ϵ_m can be calculated with the following equation:

$$\epsilon_m = \left[\frac{1 + \frac{A_0}{A_m}}{1 - \frac{A_0}{A_m}} \right]^2 \quad (\text{A.4})$$

Here, the reflection coefficient is defined as $r = A_0/A_m$ with the reflected air-surface amplitude A_0 , that is scaled by the highest possible amplitude A_m . This maximum can be easily obtained with the use of a metallic reflector in the same distance as the investigated surface. Benedetto et al. [43] used this technique to map the spatial variation of soil moisture as a preinvestigation for pavement applications. However, this approach

only covers moisture near the surface and ignores possible permittivity changes in deeper areas. To capture those, Maser and Scullion [55] also analyzed the reflections from the asphalt-bottom to estimate the moisture content of the underlying base layer. Obviously, this method encounters all the aforementioned uncertainties with the additional risk of error accumulation by the use of previously estimated asphalt permittivities.

Due to the numerous unknown influences for on site investigations, most of the works that study the correlation between amplitudes and water content were performed under laboratory conditions. A controlled environment also allows the use of additional metallic reflectors below the investigated specimens to emphasize the occurring reflections or to generate reference amplitudes for scaling/ normalization. As a signal feature, Hugenschmidt and Loser [56] used the quotient between the reflected amplitudes at the concrete surface and those at an aluminum sheet below the bottom. The authors observed a qualitative correlation with the water content of concrete as well as with ingressed chlorides that increase the underlying conductivity and therefore cause additional attenuation. This is particularly an issue in countries where salt is used for de-icing roads and pavements. The concurrent influence of moisture and chlorides in concrete was also studied by Senin and Hamid [57]. It was observed that ingressed chlorides attenuate the amplitude even more with rising water contents, which is explained by a rising mobility of the chloride ions in water filled pores. To obtain a signal feature, the authors defined an amplitude attenuation per meter with known sample thicknesses. Here, the received amplitude of a completely dry and chloride free reference-sample served as the normalizing factor. Lai et al. [22] used a similar attenuation feature expressed in dB/m to observe the hydration process of concrete. The authors normalized the reflection-amplitudes with those of the direct wave. This may lead to errors since the amplitude of the direct wave is also sensitive to the underlying moisture content, as shown in the works of Klysz and Balayssac [19] and Sbartai et al. [58]. The latter took the amplitude of the direct wave in air as the normalizing factor to ensure a material-independent reference. Another possibility to scale received amplitudes is shown by Laurens et al. [21] who use the reflection of a fully saturated specimen to emphasize the contrast of different moisture contents.

In Klee and Kind [59], the authors presented a statistical approach in which they analyzed the root mean square (RMS) of time-slices (C-Scans) during the hydration process of concrete. The general procedure is described in Kind et al. [60]. C-Scans can be obtained by measuring more than one survey line with a parallel spacing to each other, which generates a data cube (e.g. in the work of Weise et al. [61]). A horizontal slice out of that data cube includes all samples (amplitudes) for a certain time value of all recorded reflection signals. During hydration, the RMS significantly rose in the time range of the back wall reflections, but did not show any remarkable changes for other time ranges.

In most cases outside the laboratory, practical studies only allow qualitative statements on moisture contents. An example is the work of Alani et al. [62], where the general signal attenuation served as a suitable indicator for specific bridge areas affected by moisture ingress.

A.5.3 Features in the frequency domain

In comparison to the classical features like amplitude and travel time, represented by specific points in time domain, frequency related features include the information of certain time ranges or the complete time signal. Extracting these features makes it possible to observe a shift to lower frequencies in the received waveforms with rising water contents

[21].

One way to explain this phenomenon is the occurrence of Rayleigh scattering [16]. It describes the scattering on heterogeneities that are much smaller in size than the applied wavelength of the electromagnetic wave [25]. As mentioned before, higher water contents go along with a higher number of water filled pores. The additional heterogeneities attenuate higher frequencies even more which results in the observable shift. To capture this dependency, Benedetto and Tedeschi [63] compare the peak frequencies of different spectra obtained by fast fourier transformation (FFT) to indicate qualitative changes in the water content. In addition to that, the authors extract the spectrum's second, third, and fourth standardized moments, which represent the variance, skewness and kurtosis, respectively. However, the use of higher order statistics requires a larger sample size to maintain the same level of accuracy, which is discussed in [64].

Another explanation for the frequency shift is dielectric dispersion, which describes the frequency dependent behavior of ϵ . As stated in section A.2, free water has a relaxation frequency between 10 to 20 GHz, which marks the highest possible imaginary part of ϵ and thus the highest frequency dependent attenuation. For composite materials with bound water, like soil or concrete, the relaxation frequency is significantly smaller compared to free water [65]. The influence of free and bound water on the frequencies of an reflected signal was studied by Lai et al. [66] on hydrating concrete samples. By using the short-time Fourier transformation (STFT), it was shown that the higher frequency components of the reflection wave get less attenuated with a rising share of bound water, which can be explained with the increased inertia of bound molecules [47]. The use of STFT, as a joint time-frequency analysis, makes it possible to analyze the spectra of different time steps in the received signal. Thus, occurring changes for different wave types like the direct and reflected wave are detectable, as their occurrence is separated in time. In comparison, the fast fourier transformation (FFT) analyzes the entire signal only, which may lead to a lower sensitivity for spectral shifts in specific time ranges.

In Lai et al. [67] the authors used the STFT to qualitatively observe the drying of a brick wall by evaluating the spectral shift of the direct wave. The same data was later analyzed with the wavelet transformation (WT), which is presented in Lai et al. [68]. Compared to the fixed time-frequency resolution of the STFT, the WT offers varying resolution characteristics. This results in a more accurate analysis of both lower and higher frequency components with a decreasing time resolution for lower and an increasing time resolution for higher frequencies. For the direct and reflection wave, the drying process becomes more detectable with the use of WT compared to the application of STFT.

All mentioned publications concerning variations in the frequency spectra present a qualitative approach since the theoretical influences are not completely understood. Nevertheless, frequency features can serve as an appropriate addition to previously mentioned techniques.

The discussed publications that used an amplitude, time, or frequency feature to detect moisture in the context of civil engineering are listed in Table A.1.

A.5.4 Inversion-based methods

The available computing power motivates sophisticated approaches, like full-waveform inversion, that include the accurate modeling of electromagnetic wave propagation [70]. The idea is to incrementally change the unknown model parameters (permittivity ϵ and conductivity σ) until the misfit between synthetic and collected data is minimized. Hence,

Table A.1: Overview of publications that perform moisture measurements in civil engineering based on signal features of the radar signal. DW - direct wave; RW - reflection wave; CO(al) - common-offset (air-launched); A, B, C - according to Fig. A.5; f_c - applied center frequency

Reference	Signal Feature	Signal Part	Survey Method	Estimation Method	f_c [GHz]
Alani et al. [62]	Amplitude	DW, RW	CO	Qualitative	2
Benedetto et al. [43]	Amplitude Frequency	RW, A-Scan	CO(al)	A, B (Topp)	0.6, 1.6
Benedetto and Tedeschi [63]	Frequency	A-Scan	CO	Qualitative	0.6, 1.6
Cai et al. [44]	Time	RW	CMP	A, B (Topp)	0.1
Cheung and Lai [52]	Time	RW	CO	Qualitative	0.2, 0.25, 0.4, 0.6, 0.9
Fernandes et al. [45]	Time	RW	CO	A, B (Wang)	1.6
Grote et al. [20]	Amplitude Time	DW, RW	CO, CMP	A, B (Topp and site-specific)	0.9, 1.2
Hugenschmidt and Loser [56]	Amplitude	RW	CO(al)	Qualitative	2.5
Klee and Kind [59]	Amplitude	C-Scan	CO	Qualitative	1.5, 2.6
Klysz and Balayssac [19]	Amplitude Time	DW, RW	CO, WARR	C	1.5
Koyan et al. [53]	Time	RW	CO	A, B (CRIM)	2
Lai et al. [22]	Amplitude Time	DW, RW	CO	A	1
Lai et al. [66] Lai et al. [67] Lai et al. [68]	Frequency	A-Scan	CO	Qualitative	1.5, 2.6
Laurens et al. [21]	Amplitude Time Frequency	DW, RW	CO	A, C	1.5
Maser and Scullion [55]	Amplitude	RW	CO(al)	A, B (CRIM)	1
Senin and Hamid [57]	Amplitude	DW, RW	CO	C	1.6
Sbartai et al. [58]	Amplitude	DW, RW	CO	C	1.5
Válek et al. [69]	Time	RW	CO	Qualitative	1.5
Viriyametantont et al. [51]	Time	RW	CO	A	1.5
Weise et al. [61]	Time	RW	CO	Qualitative	2.6

a precise model of the applied GPR system and the underlying medium is of high importance to ensure appropriate results. In addition to increasing applications for geophysical studies using GPR [71], full-waveform inversion is also used to assess moisture and chlorides in concrete [72, 73].

Another inversion-based approach evaluates the occurring dispersion caused by thin low-velocity layers that act as waveguides [74, 75, 76]. Xiao et al. recently applied this principle to monitor the water ingress and transfer in concrete [77, 78].

The inversion-based methods show promising results, however they are still considered as advanced research, that requires skilled and experienced users [79]. As a tool for modeling synthetic data, open source simulation software like GprMax [80] can be used.

A.5.5 Problems and limitations of on site investigations

Numerous works in this review were performed in laboratory conditions, where the authors are able to measure and control crucial parameters. Knowledge about the thickness of objects, the material composition, a uniform water distribution, available reference measurements from dry states or the surrounding temperature and humidity are necessary for a reliable quantification of moisture contents. While these works reveal important information and experience about the application of GPR, their transfer to a practical on site investigation is not straightforward. Here, most of or even all of the aforementioned parameters are initially unknown. Thus, we want to emphasize that on site investigations should always be performed or supervised by trained personnel who is familiar with the difficulties between laboratory and field tests.

One of the most common reasons for misinterpretation is an imprecise assumption of the actual wave travel path, since it provides the basis for an accurate velocity analysis as discussed in section A.5.1 and influences received amplitudes as well. Extracting drilling cores or perform bigger excavations are direct ways to overcome this problem, like shown in the works of Alani et al. [62], Maser and Scullion [55] and Weise et al. [61]. However, these inspections often can only be done selectively, whereby some thickness variations may remain unnoticed. Here, former collected reference measurements from dry states can provide precise information [20], which generally justifies long term monitoring of certain objects that might constitute a risk to security like roads and bridges. CMP measurements performed in the works of Cai et al. [44] and Grote et al. [20] also deal with the problem of unknown object thicknesses. However, interference between certain wave parts or reflections due to shallow structures might lead to errors. Cai et al. [44] performed simulations with GprMax to identify advantageous trace ranges for their calculations. Furthermore, the choice of a more suitable center frequency may provide better resolution in such cases.

Besides unknown wave travel paths, changing material properties caused by e.g. density or moisture gradients can also cause misinterpretations, since the applied calculations often assume uniform distributions. Here again, the extraction of drilling cores can give good insights into such variations.

Apart from verifying structural properties like the material thickness or composition, indicating the presence of water with other methods like capacitive probes [43] or the use of nuclear magnetic resonance (NMR) [61] may support the correct interpretation of GPR data. Sometimes, even the visual inspection of small surface cracks that serve as ingress ways for moisture [62] or darker areas of a concrete road [61] provide significant hints.

The amount of unknown parameters when performing on site measurements with GPR

underlines the general need of trained and experienced personnel. A comprehensive knowledge about the influence of moisture on the various signal features as well as a detailed assessment of possible errors is necessary to achieve meaningful results.

A.6 Summary and conclusion

In this work, we presented an overview of applied methods to perform moisture measurements with GPR in the context of civil engineering. It focused especially on the variety of used signal features in the reflected energy signal as well as on the respective survey methods and the differing approaches to estimate θ .

While the quantitative determination of underlying water contents already delivers good results in laboratory conditions, users have to deal with a lot of uncertainties when it comes to on site investigations. Unknown underlying component dimensions or material properties can easily lead to misinterpretations as they may have a significant influence on the applied signal features. Therefore, destructive methods like the analysis of drilling cores are often necessary to obtain the missing information or to calibrate collected data. However, the knowledge about the presented methods and signal features, as well as their limitations, can already provide a good basis for qualitative on site assessments of moisture ingress and damage.

Future works should investigate the combination of different signal features or methods, as it is remarkable that most of the studies either focused on a single feature or analyzed a number of them separately. An advanced approach is already given with the emerging inversion-based methods, that even consider the entire waveform and include the conductivity as an additional model parameter. Furthermore, combining different features with the use of data fusion and machine learning may also drive progress towards automation. However, such approaches require a representative data basis, which is usually not available. The trend towards open data could close this gap and encourage further studies on the suitability of learning-based strategies.

Bibliography

- [1] Y. Zhang and G. Ye. A model for predicting the relative chloride diffusion coefficient in unsaturated cementitious materials. *Cement and Concrete Research*, 115:133–144, jan 2019.
- [2] A. Bentur, N. Berke, and S. Diamond. *Steel corrosion in concrete: fundamentals and civil engineering practice*. CRC Press, 1997.
- [3] D. W. Hobbs. *Alkali-silica reaction in concrete*. Thomas Telford Publishing, 1988.
- [4] K. F. Nielsen, G. Holm, L. P. Uttrup, and P. A. Nielsen. Mould growth on building materials under low water activities. Influence of humidity and temperature on fungal growth and secondary metabolism. *International Biodeterioration & Biodegradation*, 54(4):325–336, dec 2004. <https://doi.org/10.1016/j.ibiod.2004.05.002>.
- [5] S. Jacobsen, J. Marchand, and L. Boisvert. Effect of cracking and healing on chloride transport in OPC concrete. *Cement and Concrete Research*, 26(6):869–881, jun 1996. [https://doi.org/10.1016/0008-8846\(96\)00072-5](https://doi.org/10.1016/0008-8846(96)00072-5).
- [6] C. Dow and F. P. Glasser. Calcium carbonate efflorescence on Portland cement and building materials. *Cement and Concrete Research*, 33(1):147–154, jan 2003. [https://doi.org/10.1016/S0008-8846\(02\)00937-7](https://doi.org/10.1016/S0008-8846(02)00937-7).
- [7] L. Pel, K. Kopinga, and H. Brocken. *Moisture transport in porous building materials*. PhD thesis, Technische Universiteit Eindhoven, 1995.
- [8] J. MacGregor, J. K. Wight, S. Teng, and P. Irawan. *Reinforced concrete: Mechanics and design*, volume 3. Prentice Hall Upper Saddle River, NJ, 1997.
- [9] GDV. Annual of Gesamtverband der Deutschen Versicherungswirtschaft e.V. <https://www.gdv.de/de/zahlen-und-fakten/versicherungsgebiete/wohngebaeude-24080>, 2018. Accessed on 11/07/2019.
- [10] S. Kruschwitz. Feuchtemessung im Bauwesen - ein Überblick. *Fachtagung Bauwerksdiagnose, Vortrag 5*, 2014.
- [11] L.-O. Nilsson, editor. *Methods of Measuring Moisture in Building Materials and Structures*. Springer International Publishing, <https://doi.org/10.1007/978-3-319-74231-1> 2018.
- [12] M. I. Skolnik. An introduction to radar. *Radar handbook*, 2:1–21, 1962.
- [13] D. Atlas. *Radar in Meteorology: Battan Memorial and 40th Anniversary Radar Meteorology Conference*. Springer, 2015.
- [14] M. Schneider. Automotive radar-status and trends. In *German microwave conference*, pages 144–147, 2005.
- [15] R. Orosei, S. E. Lauro, E. Pettinelli, A. Cicchetti, M. Coradini, B. Cosciotti, F. Di Paolo, E. Flamini, E. Mattei, M. Pajola, F. Soldovieri, M. Cartacci, F. Cassenti, A. Frigeri, S. Giuppi, R. Martufi, A. Masdea, G. Mitri, C. Nenna, R. Noschese, M. Restano, and R. Seu. Radar evidence of subglacial liquid water on Mars. *Science*, page eaar7268, jul 2018. <https://doi.org/10.1126/science.aar7268>.

- [16] J. A. Huisman, S. S. Hubbard, J. D. Redman, and A. P. Annan. Measuring Soil Water Content with Ground Penetrating Radar: A Review. *Vadose Zone Journal*, 2(4):476–491, nov 2003. <https://doi.org/10.2113/2.4.476>.
- [17] L. Slater and X. Comas. The Contribution of Ground Penetrating Radar to Water Resource Research. In *Ground Penetrating Radar: Theory and Applications*. Elsevier, 2009.
- [18] T. Saarenketo and T. Scullion. Road evaluation with ground penetrating radar. *Journal of Applied Geophysics*, 43(2-4):119–138, mar 2000. [https://doi.org/10.1016/s0926-9851\(99\)00052-x](https://doi.org/10.1016/s0926-9851(99)00052-x).
- [19] G. Klysz and J.-P. Balayssac. Determination of volumetric water content of concrete using ground-penetrating radar. *Cement and Concrete Research*, 37(8):1164–1171, aug 2007. <https://doi.org/10.1016/j.cemconres.2007.04.010>.
- [20] K. Grote, S. Hubbard, J. Harvey, and Y. Rubin. Evaluation of infiltration in layered pavements using surface GPR reflection techniques. *Journal of Applied Geophysics* 57, 57(2):129–153, feb 2005. <https://doi.org/10.1016/j.jappgeo.2004.10.002>.
- [21] S. Laurens, J. P. Balayssac, J. Rhazi, G. Klysz, and G. Arliguie. Non-destructive evaluation of concrete moisture by GPR: experimental study and direct modeling. *Materials and Structures* 38, 38(9):827–832, nov 2005. <https://doi.org/10.1007/BF02481655>.
- [22] W. L. Lai, S. C. Kou, W. F. Tsang, and C. S. Poon. Characterization of concrete properties from dielectric properties using ground penetrating radar. *Cement and Concrete Research*, 39(8):687–695, aug 2009. <https://doi.org/10.1016/j.cemconres.2009.05.004>.
- [23] J. C. Maxwell. A dynamical theory of the electromagnetic field. *Philosophical Transactions of the Royal Society of London*, 155:459–512, jan 1865. <https://doi.org/10.1098/rstl.1865.0008>.
- [24] A. P. Annan. GPR methods for hydrogeological studies. In *Hydrogeophysics*, chapter 7, pages 185–213. Springer, 2005. <https://doi.org/10.1007/1-4020-3102-5>.
- [25] A. P. Annan. Electromagnetic Principles of Ground Penetrating Radar. In Harry M. Jol, editor, *Ground Penetrating Radar: Theory and Applications*, chapter 1, pages 4–38. Elsevier, 2009.
- [26] D. J. Daniels. *Ground Penetrating Radar - 2nd Edition*. The Institution of Engineering and Technology, 2007.
- [27] P. J. W. Debye. *Polar molecules*. New York, The Chemical Catalog Company, Inc., 1929.
- [28] K. S. Cole and R. H. Cole. Dispersion and Absorption in Dielectrics I. Alternating Current Characteristics. *The Journal of Chemical Physics*, 9(4):341–351, apr 1941.
- [29] C. Bohren and D. Huffman. *Absorption and Scattering of Light by Small Particles*. Wiley, 1983.

- [30] A. P. Annan. Ground Penetrating Radar Principles, Procedures & Applications. Technical report, Sensors & Software Inc., 2003.
- [31] M. N. Soutsos, J. H. Bungey, S. G. Millard, M. R. Shaw, and A. Patterson. Dielectric properties of concrete and their influence on radar testing. *NDT&E International*, 34(6):419–425, sep 2001. [https://doi.org/10.1016/S0963-8695\(01\)00009-3](https://doi.org/10.1016/S0963-8695(01)00009-3).
- [32] S. Okamura. Microwave Technology for Moisture Measurement. *Subsurface Sensing Technologies and Applications*, 1(2):205–227, 2000.
- [33] E. W. Gilson, J. D. Redman, J. Pilon, and A. P. Annan. Near Surface Applications of Borehole Radar. *Symposium on the Application of Geophysics to Engineering and Environmental Problems*, jan 1996. <https://doi.org/10.4133/1.2922317>.
- [34] C. Hewitt Dix. SEISMIC VELOCITIES FROM SURFACE MEASUREMENTS. *GEOPHYSICS*, 20(1):68–86, jan 1955.
- [35] J. Hugenschmidt. Multi-offset analysis for man-made structures. *8th International Conference on Ground Penetrating Radar*, apr 2000.
- [36] ASTM D6432-11. Standard Guide for Using the Surface Ground Penetrating Radar Method for Subsurface Investigation. *ASTM Vol. 04.09*, 2011.
- [37] C. Strangfeld and S. Kruschwitz. Monitoring of the absolute water content in porous materials based on embedded humidity sensors. *Construction and Building Materials*, 177:511–521, 2018. <https://doi.org/10.1016/j.conbuildmat.2018.05.044>.
- [38] ISO. ISO 15901-2:2006(E): Pore size distribution and porosity of solid materials by mercury porosimetry and gas adsorption - Part 2: Analysis of mesopores and macropores by gas adsorption. *International Standard*, 2006.
- [39] U. Kaatze. Complex permittivity of water as a function of frequency and temperature. *Journal of Chemical & Engineering Data*, 34(4):371–374, oct 1989. <https://doi.org/10.1021/je00058a001>.
- [40] ASTM D2216-19. Standard Test Methods for Laboratory Determination of Water (Moisture) Content of Soil and Rock by Mass. *ASTM Vol. 04.08*, 2019.
- [41] J. L. Davis and A. P. Annan. Electromagnetic Detection of Soil Moisture: Progress Report I. *Canadian Journal of Remote Sensing*, 3(1):76–86, dec 1977. <https://doi.org/10.1080/07038992.1977.10854959>.
- [42] G. C. Topp, J. L. Davis, and A. P. Annan. Electromagnetic Determination of Soil Water Content: Measurements in Coaxial Transmission Lines. *Water Resources Research*, 16(3):574–582, jun 1980. <https://doi.org/10.1029/WR016i003p00574>.
- [43] A. Benedetto, F. Tosti, B. Ortuani, M. Giudici, and M. Mele. Soil moisture mapping using GPR for pavement applications. *7th International Workshop on Advanced Ground Penetrating Radar*, jul 2013. <https://doi.org/10.1109/iwagpr.2013.6601550>.
- [44] J. Q. Cai, S. X. Liu, L. Fu, and Y. Q. Feng. Detection of railway subgrade moisture content by GPR. *16th International Conference on Ground Penetrating Radar (GPR)*, jun 2016. <https://doi.org/10.1109/ICGPR.2016.7572613>.

- [45] F. M. Fernandes, Andreia Fernandes, and Jorge Pais. Assessment of the density and moisture content of asphalt mixtures of road pavements. *Construction and Building Materials*, 154:1216–1225, nov 2017. <https://doi.org/10.1016/j.conbuildmat.2017.06.119>.
- [46] F. Wang and R. L. Lytton. System Identification Method for Backcalculating Pavement Layer Properties. *Transportation Research Record 1384*, 1993.
- [47] N. J. Cassidy. Electrical and Magnetic Properties of Rocks, Soils and Fluids. In *Ground Penetrating Radar: Theory and Applications*, pages 41–72. Elsevier, 2009. <https://doi.org/10.1016/B978-0-444-53348-7.00002-8>.
- [48] C. Chen and J. Zhang. A Review on GPR Applications in Moisture Content Determination and Pavement Condition Assessment. *GeoHunan International Conference*, jul 2009. [https://doi.org/10.1061/41041\(348\)20](https://doi.org/10.1061/41041(348)20).
- [49] C. Hülsmeier. Patent DE169154: Verfahren zur Bestimmung der Entfernung von metallischen Gegenständen (Schiffen o. dgl.), deren Gegenwart durch das Verfahren nach Patent 165546 festgestellt wird. *Patent*, claimed 11/11/1904, published 04/02/1996, 1904.
- [50] R. Yelf. Where is true time zero? *Proceedings of the Tenth International Conference on Ground Penetrating Radar*, 2004. <https://doi.org/10.1109/ICGPR.2004.179979>.
- [51] K. Viriyametant, S. Laurens, G. Klysz, J.-P. Balayssac, and G. Arliguie. Radar survey of concrete elements: Effect of concrete properties on propagation velocity and time zero. *NDT&E International*, 41(3):198–207, apr 2008. <https://doi.org/10.1016/j.ndteint.2007.10.001>.
- [52] B. W.-Y. Cheung and W. L. Lai. Field validation of water-pipe leakage detection through spatial and time-lapse analysis of GPR wave velocity. *Near Surface Geophysics*, 17(3):231–246, may 2019. <https://doi.org/10.1002/nsg.12041>.
- [53] P. Koyan, J. Tronicke, N. Allroggen, A. Kathage, and M. Willmes. Estimating moisture changes in concrete using GPR velocity analysis: potential and limitations. *17th International Conference on Ground Penetrating Radar (GPR)*, jun 2018. <https://doi.org/10.1109/ICGPR.2018.8441572>.
- [54] K. Grote, T. Crist, and C. Nickel. Experimental estimation of the GPR groundwave sampling depth. *Water Resources Research*, 46(10), oct 2010. <https://doi.org/10.1029/2009WR008403>.
- [55] K. R. Maser and T. Scullion. Automated Pavement Subsurface Profiling Using Radar: Case Studies of Four Experimental Field Sites. *Transportation Research Record 1344*, (1344):148–154, 1991.
- [56] J. Hugenschmidt and R. Loser. Detection of chlorides and moisture in concrete structures with ground penetrating radar. *Materials and Structures*, 41(4):785–792, jul 2008. <https://doi.org/10.1617/s11527-007-9282-5>.

- [57] S. F. Senin and R. Hamid. Ground penetrating radar wave attenuation models for estimation of moisture and chloride content in concrete slab. *Construction and Building Materials*, 106:659–669, mar 2016. <https://doi.org/10.1016/j.conbuildmat.2015.12.156>.
- [58] Z. M. Sbartai, S. Laurens, J.-P. Balayssac, G. Ballivy, and G. Arliguie. Effect of Concrete Moisture on Radar Signal Amplitude. *ACI Materials Journal*, 2006.
- [59] M. Klee and T. Kind. Untersuchung des Einflusses von Hydratisierung und Feuchte auf die Radarstreuung an der Heterogenität von Beton. *77. Jahrestagung der DGG*, 2017.
- [60] T. Kind, C. Trela, M. Schubert, and J. Wostmann. Aggregates scattering of GPR waves in concrete. *Proceedings of the 15th International Conference on Ground Penetrating Radar*, jun 2014. <https://doi.org/10.1109/ICGPR.2014.6970557>.
- [61] F. Weise, T. Kind, L. Stelzner, and M. Wieland. Dunkelfärbung der betonfahrbahndecke im AKR-kontext. *Beton- und Stahlbetonbau*, 113(9):647–655, may 2018. <https://doi.org/10.1002/best.201800020>.
- [62] A. M. Alani, M. Aboutalebi, and G. Kilic. Applications of ground penetrating radar (GPR) in bridge deck monitoring and assessment. *Journal of Applied Geophysics*, 97:45–54, 2013. <https://doi.org/10.1016/j.jappgeo.2013.04.009>.
- [63] F. Benedetto and A. Tedeschi. Moisture content evaluation for road-surfaces monitoring by GPR image and data processing on mobile platforms. *3rd International Conference on Future Internet of Things and Cloud*, pages 602–607, aug 2015. <https://doi.org/10.1109/FiCloud.2015.44>.
- [64] A. Benedetto and F. Benedetto. Remote Sensing of Soil Moisture Content by GPR Signal Processing in the Frequency Domain. *IEEE Sensors Journal*, 11(10):2432–2441, oct 2011. <https://doi.org/10.1109/JSEN.2011.2119478>.
- [65] T. Saarenketo. Electrical properties of water in clay and silty soils. *Journal of Applied Geophysics*, 40(1-3):73–88, oct 1998. [https://doi.org/10.1016/S0926-9851\(98\)00017-2](https://doi.org/10.1016/S0926-9851(98)00017-2).
- [66] W. L. Lai, T. Kind, and H. Wiggenhauser. A Study of Concrete Hydration and Dielectric Relaxation Mechanism Using Ground Penetrating Radar and Short-Time Fourier Transform. *EURASIP Journal on Advances in Signal Processing*, 2010(1), jul 2010. <https://doi.org/10.1155/2010/317216>.
- [67] W. L. Lai, T. Kind, and H. Wiggenhauser. Using ground penetrating radar and time–frequency analysis to characterize construction materials. *NDT & E International*, 44(1):111–120, jan 2011. <https://doi.org/10.1016/j.ndteint.2010.10.002>.
- [68] W. L. Lai, T. Kind, S. Kruschwitz, J. Wöstmann, and H. Wiggenhauser. Spectral absorption of spatial and temporal ground penetrating radar signals by water in construction materials. *NDT & E International*, 67:55–63, oct 2014. <https://doi.org/10.1016/j.ndteint.2014.06.009>.

- [69] J. Válek, S. Kruschwitz, J. Wöstmann, T. Kind, J. Valach, C. Köpp, and J. Lesák. Nondestructive Investigation of Wet Building Material: Multimethodical Approach. *Journal of Performance of Constructed Facilities*, 24(5):462–472, oct 2010. [https://doi.org/10.1061/\(ASCE\)CF.1943-5509.0000056](https://doi.org/10.1061/(ASCE)CF.1943-5509.0000056).
- [70] S. Busch, J. van der Kruk, J. Bikowski, and H. Vereecken. Quantitative conductivity and permittivity estimation using full-waveform inversion of on-ground GPR data. *Geophysics*, 77(6):H79–H91, nov 2012. <https://doi.org/10.1190/geo2012-0045.1>.
- [71] A. Klotzsche, F. Jonard, M. C. Looms, J. van der Kruk, and J. A. Huisman. Measuring Soil Water Content with Ground Penetrating Radar: A Decade of Progress. *Vadose Zone Journal*, 17(1):180052, 2018. <https://doi.org/10.2136/vzj2018.03.0052>.
- [72] A. Kalogeropoulos, J. van der Kruk, J. Hugenschmidt, S. Busch, and K. Merz. Chlorides and moisture assessment in concrete by GPR full waveform inversion. *Near Surface Geophysics*, 9(3):277–286, nov 2011. <https://doi.org/10.3997/1873-0604.2010064>.
- [73] A. Kalogeropoulos, J. van der Kruk, J. Hugenschmidt, J. Bikowski, and E. Brühwiler. Full-waveform GPR inversion to assess chloride gradients in concrete. *NDT&E International*, 57:74–84, jul 2013. <https://doi.org/10.1016/j.ndteint.2013.03.003>.
- [74] J. van der Kruk. Properties of surface waveguides derived from inversion of fundamental and higher mode dispersive GPR data. *IEEE Transactions on Geoscience and Remote Sensing*, 44(10):2908–2915, oct 2006. <https://doi.org/10.1109/TGRS.2006.877286>.
- [75] J. van der Kruk, S. A. Arcone, and L. Liu. Fundamental and higher mode inversion of dispersed GPR waves propagating in an ice layer. *IEEE Transactions on Geoscience and Remote Sensing*, 45(8):2483–2491, aug 2007. <https://doi.org/10.1109/TGRS.2007.900685>.
- [76] J. van der Kruk, R. W. Jacob, and H. Vereecken. Properties of precipitation-induced multilayer surface waveguides derived from inversion of dispersive TE and TM GPR data. *Geophysics*, 75(4):WA263–WA273, jul 2010. <https://doi.org/10.1190/1.3467444>.
- [77] X. Xiao, A. Ihamouten, G. Villain, and X. Dérobert. Use of electromagnetic two-layer wave-guided propagation in the GPR frequency range to characterize water transfer in concrete. *NDT&E International*, 86:164–174, mar 2017. <https://doi.org/10.1016/j.ndteint.2016.08.001>.
- [78] X. Xiao, A. Ihamouten, G. Villain, X. Derobert, and G. Tian. Modeling of Water Contents in Concrete Using Electromagnetic Guided Waves. *Transactions of Nanjing University of Aeronautics and Astronautics*, 2017.
- [79] W. L. Lai, X. Dérobert, and P. Annan. A review of Ground Penetrating Radar application in civil engineering: A 30-year journey from Locating and Testing to Imaging and Diagnosis. *NDT&E International*, 96:58–78, jun 2018. <https://doi.org/10.1016/j.ndteint.2017.04.002>.

- [80] C. Warren, A. Giannopoulos, and I. Giannakis. gprMax: Open source software to simulate electromagnetic wave propagation for Ground Penetrating Radar. *Computer Physics Communications*, 209:163–170, dec 2016. <https://doi.org/10.1016/j.cpc.2016.08.020>.

Materials and Preliminary Studies

2	Evaluation of Radar Signal Features on Drying Screed Samples	35
2.1	Materials and Methods.	35
2.2	Results and Discussion.	40
2.3	Summary and Conclusion	45
	Bibliography	46

2. Evaluation of Radar Signal Features on Drying Screed Samples

After the general review of GPR applications for moisture measurement in CE, given in A, this section starts to focus on the structure of interest - layered building floors. In practice, the most varying parameters of a floor structure are the used materials for screed and insulation, as well as their installed thicknesses. Therefore, an experimental approach applying these variations is believed to cover a wide range of practical setups. A detailed presentation of this approach is given later in publication B, which deals with the laboratory realization to investigate moisture damage in building floor constructions. In there, the production process of the screed samples is described in only a few sentences, which leaves a wide gap in an important milestone of this thesis. While the production alone is only a small part of this milestone, the subsequent drying process provides an opportunity to investigate the suitability of the previously researched GPR signal features.

These investigations are discussed in the following chapter and were part of a poster presentation held on the DGZfP Jahrestagung 2019 (Appendix II) showing the application of radar and neutron probe to measure the moisture content of screed samples with varying thickness, binder and strength over a time period of 90 days after casting. The gravimetric Darr and chemical calcium-carbide method served as references for determining the moisture loss during drying. With the moisture reference obtained, a special focus was placed on the combination of radar signal features and the neutron probe to analyze the potential of a multivariate evaluation. This also allowed conclusions to be drawn about the strengths and weaknesses of individual features.

2.1 Materials and Methods

2.1.1 Casting of Screed Samples

In order to perform laboratory tests on building floors, a modular approach is followed, which allows the efficient setup of many different configurations. While the insulation materials required for this are available in many different varieties, the screed test specimens (TS) must be specially cast. In practice, the most common types of screed are either based on cement or calcium sulphate and are installed with an average thickness of 4 cm to 7 cm. In addition to the binder type and thickness, different strengths (compressive and bending tensile strength) are used, depending on the application. With regard to these three variables, a set of 12 screed specimens was cast in accordance to Table 2.1. Due to the risk of breakage when handling thin screed plates, no screed specimens below 5 cm thickness were prepared for the experiments. Concerning the strength, two variations (normal and solid) were chosen for both binder types. The edge length of 800 mm was based on the spherical measuring volume of the neutron probe with a diameter of approx.

560 mm. The sufficiently large extension is intended to avoid possible edge effects, also for the radar measurements, which require a distance to outer boundaries from the depth to be measured.

When measuring moisture damage, the amount of liquid water contained in the medium is the relevant variable. After a screed has been produced, this liquid water content changes drastically within the first 90 days, which is why this time is particularly interesting for evaluating the intended moisture measurement methods. However, this process is not only determined by the drying of the specimen, but is also subject to hydration, in which liquid water is bound to build up the cement matrix. Thus, the moisture content cannot be directly determined by weighing the specimen alone. Therefore, the hydration progress and moisture content is to be observed with the help of nine sister test specimens (STS), which were prepared from the same batch for each specimen (Figure 2.1 left). On defined days after casting, these STS were first examined with the CCM method [1] and then subjected to Darr drying at 105 °C for cement-based screeds and 40 °C for calcium-sulphate-based screeds in accordance with DIN 12570:2000 [2].

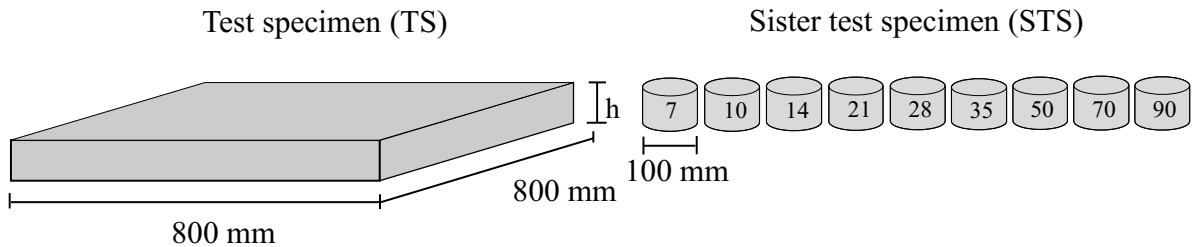


Figure 2.1: Sketch of cast test specimen (TS) and respective sister test samples (STS). The numbering of the STS defines the day after casting, on which the sample is used for referencing moisture methods (Darr and CCM).

Table 2.1: Properties of the different screed types used for test specimens.

Label	Binder	Compressive strength	Bending tensile strength	Water demand
CT1	Cement	25 Nmm ⁻² (C25)	5 Nmm ⁻² (F5)	0.1333 lkg ⁻¹
CT2	Cement	40 Nmm ⁻² (C40)	7 Nmm ⁻² (F7)	0.0875 lkg ⁻¹
CA1	Calcium-sulphate	25 Nmm ⁻² (C25)	5 Nmm ⁻² (F5)	0.15 lkg ⁻¹
CA2	Calcium-sulphate	30 Nmm ⁻² (C30)	7 Nmm ⁻² (F7)	0.15 lkg ⁻¹

Product name of the used screeds in order of the Table: maxit plan 425, maxit plan 435, maxit plan 470, maxit plan 490

Impressions of the casting process are shown in Figure 2.2 a), where a freshly mixed CA screed is poured into the formwork. To ensure a proper handling of the screed samples to be positioned and exchanged on the modular specimen, threaded sleeves were embedded into the four corners of each specimen to allow the flexible use of ring bolts (Figure 2.2 b)). Their use will be visualised later in Figure B.3 within the second publication.

One day after casting, the formworks were removed and all specimens were covered by PE-foil on the bottom and waterproof tape on the shell surfaces to ensure realistic drying from above. Hydration took place in a standard climate with 23 °C and 50 % relative humidity (RH). For this purpose, the screed plates were stored on 600 mm x 600 mm x 280 mm extruded polyethylene insulation (Styrodur) in combination with a euro pallet. These

were placed in two heavy-duty shelves, which were surrounded by a 3 m x 6 m x 2.5 m tent (see Figure 2.3). The desired climate was controlled using appropriate equipment (air conditioning, air humidifier, air dehumidifier, data logger).



Figure 2.2: Casting of screed samples: a) Freshly mixed CA screed gets poured into its formwork. b) Embedding of threaded sleeves into each corner to enable handling with ring bolts.



Figure 2.3: Storage of the samples in a climate controlled tent at 23 °C and 50 % RH.

2.1.2 Hardware and Measurement Procedure

After preparation and taping of the samples, all of them were measured daily during the first seven days using the radar method and the neutron probe. For the radar measurements, two antennas with center frequencies of 2 GHz and 2.6 GHz were used in

common-offset configuration. They were connected to a SIR20 system from GSSI [3]. The two perpendicular 60 cm survey lines investigated, as well as the typical measurement setup are shown in Figure 2.4. With 250 scans/meter, each survey line includes 100 A-scans. An A-scan contains 512 samples covering a 11 ns time window. Data acquisition by the neutron probe was always performed in the screed's center with a time interval of 15 seconds. This was carried out ten times for each specimen and the scalar values obtained were averaged. As a hedge against possible malfunctions, each measurement was carried out with two probes. A floor scale was used to directly observe the weight loss occurring in the TS. This also served as a measure for the successive increase in the time interval between the measurement days, which was carried out individually for each screed type. The observation of the hydration process of all samples lasted a minimum of 90 and a maximum of 98 days. Subsequently, the calcium-sulphate-based screeds were dried at 40 °C and the cement screeds at 105 °C to obtain the respective dry weights.



Figure 2.4: Measurement setup with neutrone probe and radar antenna on screed test specimens. The right graphic shows the perpendicular orientation of the two recorded GPR survey lines on a screed in top view

2.1.3 Feature Extraction and Evaluation

Univariate Analysis

The literature research on moisture measurement with GPR in publication A yielded numerous signal features which show a correlation to the water content of building materials. The most commonly used features in the time [4, 5] and frequency domain [6] were implemented and used to evaluate the measurements performed. An overview of this selection can be found in Figure 2.5.

The automated extraction of this features is mainly based on a local maxima and minima search within the A-scan, by which both the direct wave and the reflection wave can be detected. To avoid possible misinterpretations, irrelevant high and low points, that do not belong to the direct wave or reflection wave must be excluded, which is ensured by a specific threshold based processing. However, these thresholds were chosen according to the collected data set and may cause errors or inconsistencies on completely new or disturbed data. Unusual reflections (which may also be caused by water) or noise can affect this automatic extraction, which must be taken into account when analyzing the features. After extraction, the features are evaluated by examining their correlation to the referenced moisture contents of exemplary screed specimens.

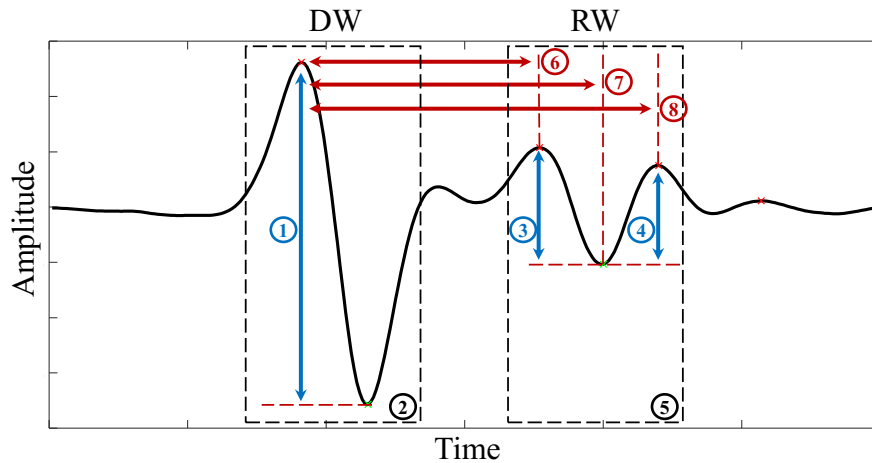


Figure 2.5: Extracted signal features of a radar measurement (A-scan) consisting of direct wave (DW) and reflection wave (RW). **1, 3** and **4**: peak-to-peak amplitudes; **2, 5**: maximum frequencies ; **6, 7** and **8**: two-way travel times.

Multivariate Analysis

To investigate the potential of a multivariate analysis, subsets of features are combined in different configurations, which are used as input parameters for a screed moisture prediction model concerning the whole data set. Here, also the results of the neutron probe measurements are considered, as shown in Figure 2.6. The analysis gives first insights into the neutron probes potential to serve as an independent feature for moisture measurement on building floors. Additionally, the amplitude of DW and RW, as well as the time difference between these two wave types are used as GPR features.

The combination of all four features is evaluated by applying a multiple linear regression (MLiR). The resulting models are then used to predict the referenced moisture contents, whereby the achieved accuracy is represented by the adjusted R^2 measure.

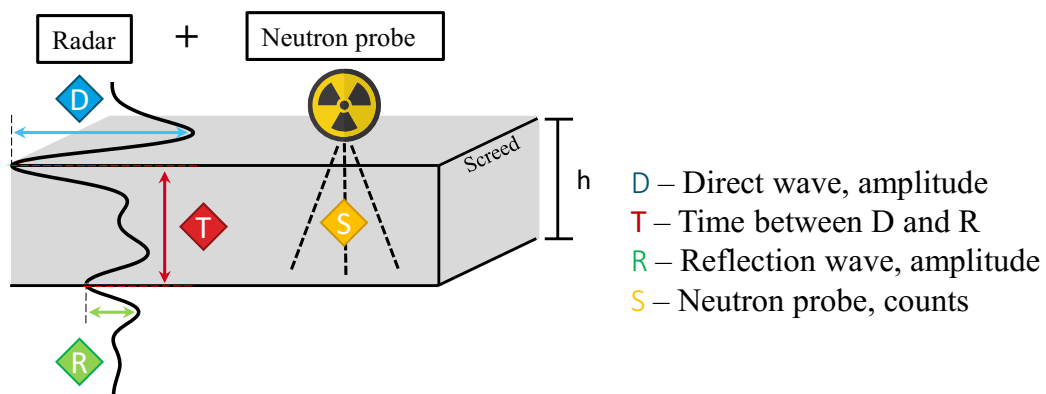


Figure 2.6: Regarded features of radar and neutron probe for the multivariate analysis of screed moisture.

2.2 Results and Discussion

2.2.1 Moisture Reference

For a better understanding of the recorded radar signals, the moisture contents measured with the different reference methods will be briefly discussed. Figure 2.7 shows an exemplary comparison of the screed types used. Here, only the 6 cm thick TS and STS are shown with regard to a better overview. The other specimens show similar moisture developments.

First of all, a clearly higher weight loss of the CA samples can be recognized, which dry out almost completely to less than 0.2 mass percent (wt%). In comparison, the CT screeds show a moisture content above 4 wt% after 90 days. This is related to the developed pore structure of both screed types. While large pores in CA screeds accelerate drying, CT screeds show predominantly very small pores with pore radii below $0.1 \mu\text{m}$ [7]. These small pores physically bind liquid water and make it immobile. Thus, the equilibrium moisture content of CA screeds is less than 0.3 wt%, while CT screeds normally contain values between 2.5 wt% and 3.5 wt%. Given that, the measured moisture contents are in line with expectations [8], although especially CT2 shows only a very low water loss. In addition to the increased strength, this type is also listed as a 'rapid screed', which also has the lowest water requirement according to the manufacturer's specifications listed in Table 2.1. Attempts to explain the measured values are omitted here, since it is not the subject of this study. However, it should be noted that the very low moisture dynamics over the time period of 90 days are not suitable for the investigation of moisture measurement methods, which is why CT2 is excluded from the evaluation.

Systematic deviations of approximately 1.5 wt% between the CCM and Darr method are generally known for CT screeds [9]. On the one hand, this is due to the dissolution of chemically bound water during drying at $105 \text{ }^\circ\text{C}$. On the other hand, the liquid water is probably not completely released when the pressure bottle is shaken during the CCM measurement procedure, which could explain in particular the larger error of approx. 2 wt% for the more solid cement screed CT2.

A more detailed analysis of the moisture contents measured with the Darr method and CCM is given in the publication of Strangfeld and Klewe [10], which can be found in Appendix I. In there it is also shown that the normalized dry weight of the sister samples is close to constant for the measured time period (Figure I.6 and I.7). This indicates that the hydration process is already completed before the first measurement on the seventh day and proves that the entire solid matrix was completely formed within one week. In conclusion, the moisture curves measured on TS CT1, CA1, and CA2 turn out to be good references to investigate the suitability of selected signal features, since they show the actual decrease of liquid water within the samples.

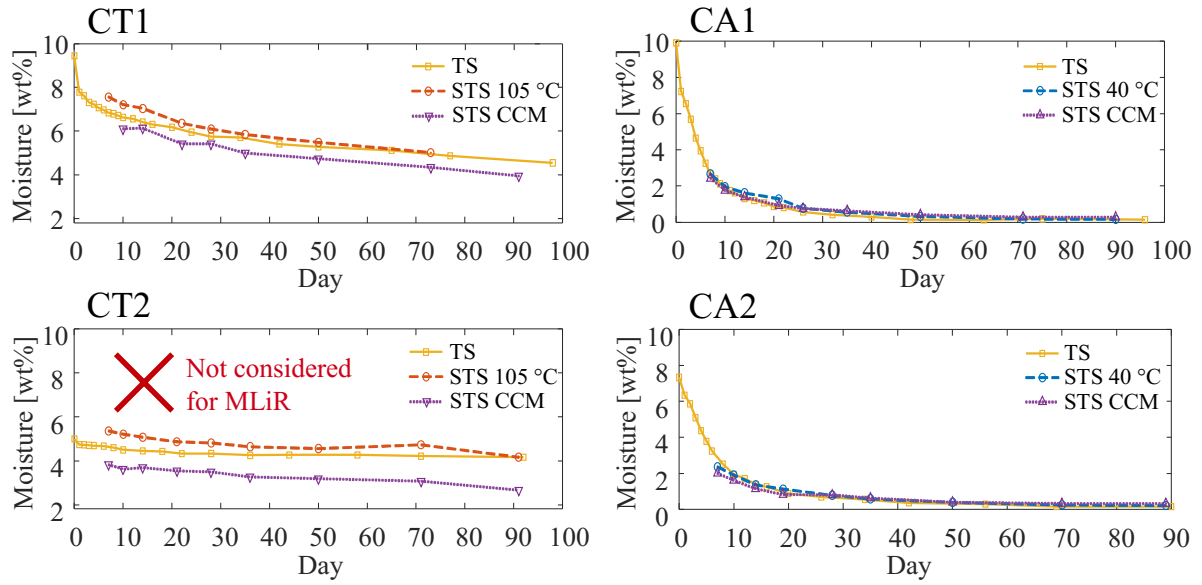


Figure 2.7: Moisture contents of all screed types with 6 cm thickness measured on TS and STS by Darr (yellow, red) and CCM method (purple)

2.2.2 Univariate Analysis on Exemplary Screed Samples

The influence of the hydration process and the associated moisture loss on the recorded radar signals is shown exemplarily on the 6 cm CT1 screed in Figure 2.8. As expected, the reflection wave, which travels through the medium twice, shows the greatest sensitivity to the contained water. However, the direct wave, which partially travels through the screed, also reveals minor changes in amplitude and frequency. The quantitative behaviour of all extracted signal features over the test period is shown in Figure 2.9.

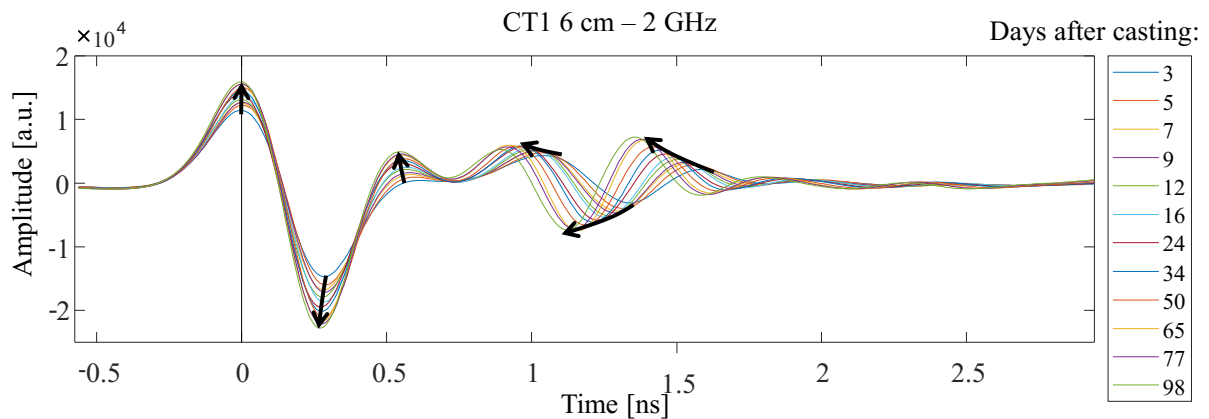


Figure 2.8: Influence of moisture on the radar signal: Mean A-scans of the 6 cm CT1 screed recorded on different days after casting.

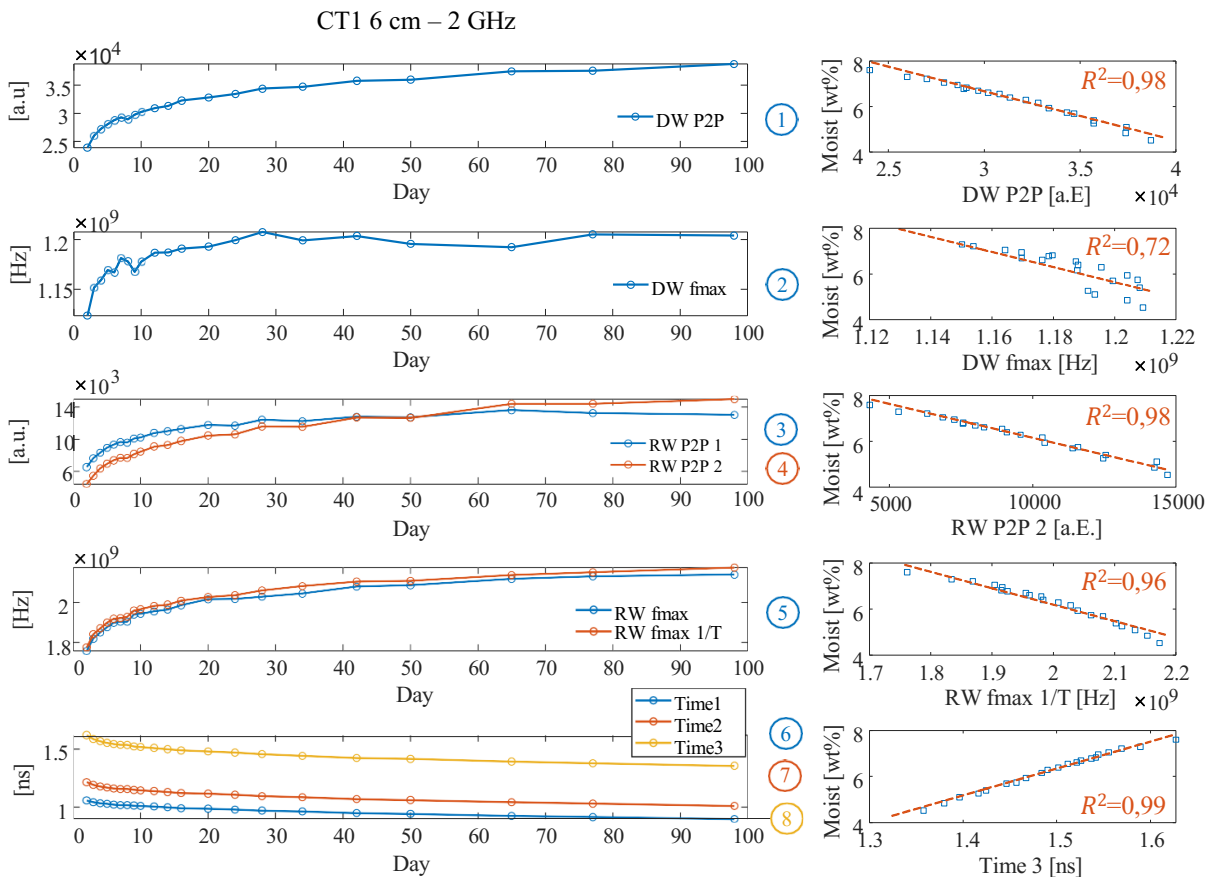


Figure 2.9: Extracted signal features of 6 cm CT1 screed with corresponding numbering in the legend (see Figure 2.5) and their correlation to the measured TS moisture profile from Fig. 2.7

In general, the water dependent attenuation of the amplitude and frequency can be seen on all related signal features. This is confirmed by the negative correlations on the right hand side. In contrast, the travel-time related features show a positive correlation, which can be explained by Eq. A.1. Since a higher water content leads to a higher permittivity, the travel-time time increases as the drying progresses.

While the results shown for the 6 cm CT1 screed serve as a positive example for the majority of the recorded data set, problems of the automated evaluation will also be discussed in the following. Here, the correct separation of DW and RW is the most error-prone aspect. A strict separation is partly hindered by smaller specimen thicknesses or very dry samples, causing both waves to interfere with each other. This leads to erroneous curves especially for the frequency feature 5, as well as for the amplitude and time features 3 and 6, since the influence of the described effect is greatest here. To illustrate this problem, Figure 2.10 shows the development of the recorded radar signals of a fast drying CA screed (see Figure 2.7) with the disturbed signal features mentioned. While up to day 8 the correct first maximum of the reflection wave can still be detected and assigned, from day 10 onward both waves interfere. This results in a more dominant maximum about 0.25 ns earlier, which is subsequently used for all further calculations of the features on later measurement days. The recognizable deviations in the frequency feature and time feature clearly show this, while the influence on the amplitude feature is already noticeable from day 6.

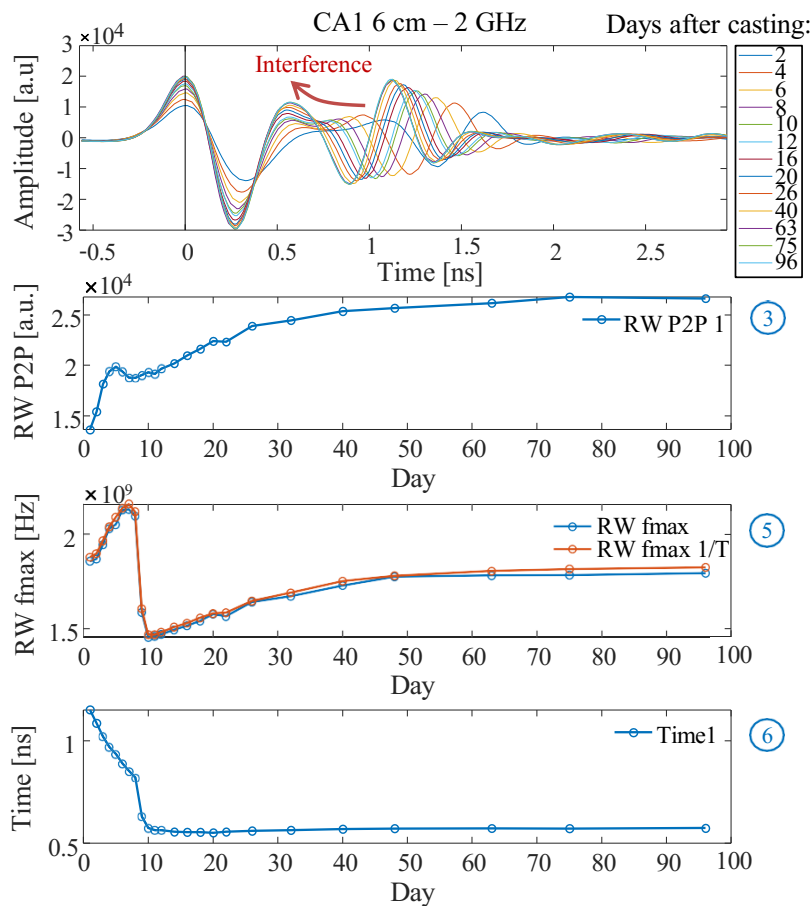


Figure 2.10: Mean A-Scans of the 6 cm CA1 screed on different days after casting and the extracted signal features that are influenced by the interference between DW and RW.

Based on the successes and problems described in Figure 2.9 and 2.10, the peak-to-peak amplitude and travel time features generally turned out to be the most robust for moisture measurements on screeds. However, this is only true if they are picked outside the transition range between DW and RW, which lies between the second maximum of DW (at approx. 0.5 ns) and the first maximum of RW. Concerning this, the features 1, 4, 7, and 8 show consistently good correlations with the recorded moisture contents. Features 3, 5, and 6, on the other hand, may be influenced by an interference between DW and RW. Feature 2, the maximum frequency of DW is only slightly influenced by the moisture content (compare the slightly sloped arrow at the minimum of the DW in Figure 2.8), and shows a therefore more inaccurate correlation.

2.2.3 Multivariate Analysis on Entire Dataset

After investigating the behaviour of specific signal features on exemplary screeds, all test specimens are now included for the prediction of their moisture contents, regardless of their material type and thickness. Figure 2.11 shows the actual versus the (fitted and) predicted moisture content by MLiR models with different combinations of input features (visualized by the diamond shaped symbols as used in Figure 2.6). In each plot, the screed’s material type and thickness are coded by the marker type and

color, respectively. Knowing that, the governing parameter in the travel time feature (T) in b) becomes obvious. As expected, the screed thickness naturally has an influence on this feature, which makes it difficult to make a uniform moisture prediction for the entire dataset. Also the neutron probe (S) in d) shows an expected dependence on the material type as well as on the thickness, which results in the poorest accuracy of all models. The reflection wave (R) in c) also reveals a visible separation by color, indicating an influence by the screed thickness. Here, longer travel distances of the reflection wave lead to a higher attenuation, which causes an overestimation of the screed moisture. The direct wave (D) in a) only penetrated the specimens superficially. Consequently, it is not influenced by the thickness. However, the slight separation of CT1 suggests an influence of the screed material.

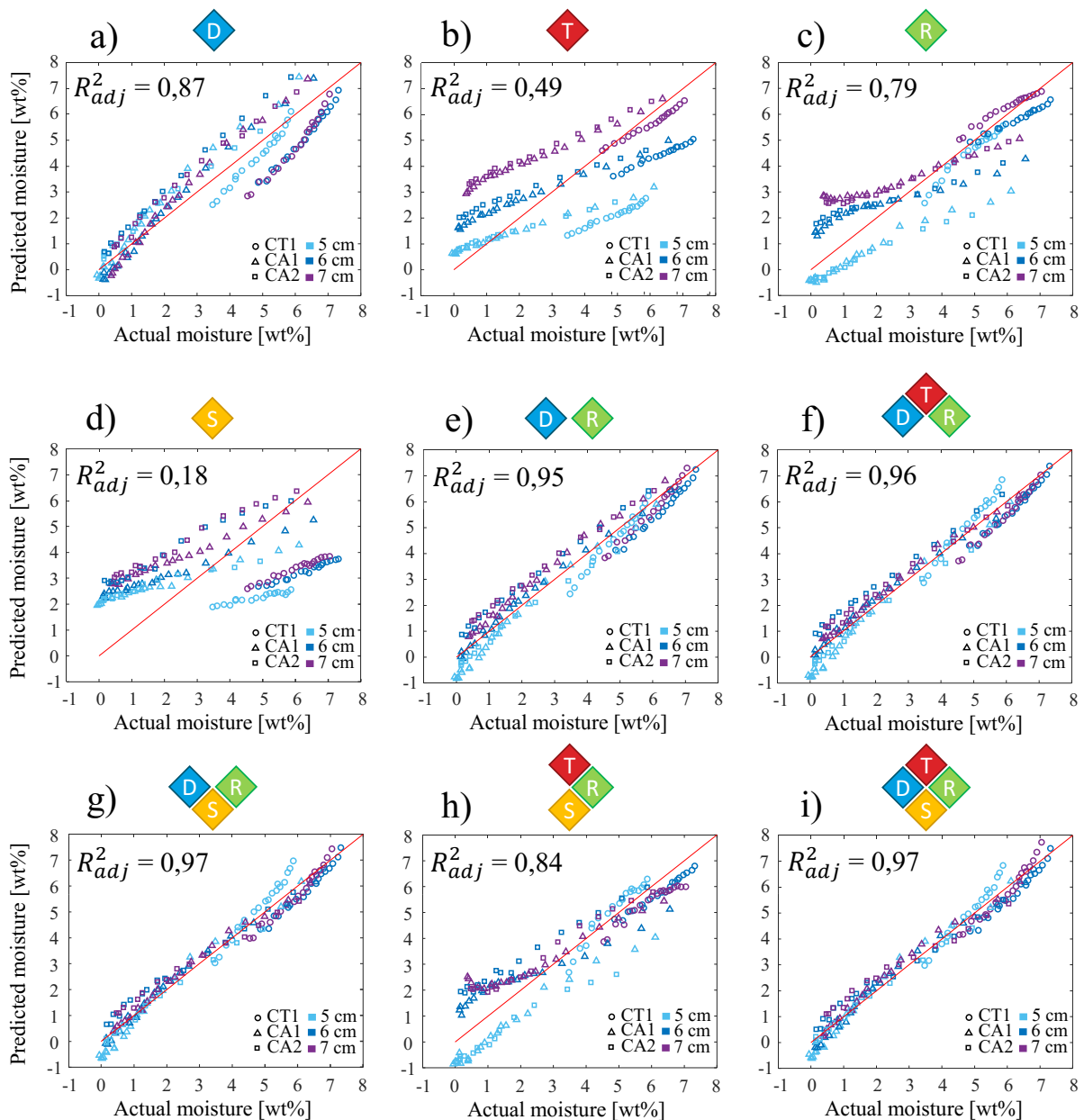


Figure 2.11: Actual vs. predicted moisture of MLiR models with different combinations of input features (see also Figure 2.6)

While the consideration of, once again, single signal features revealed interesting characteristics when used for the whole data set, the multivariate approach provides consistently good result. Except the combination of T, R, and S in h), all other models achieved high adjusted R^2 values above 0.95. It shows that the direct wave delivers an indispensable value to a joint use of multiple features. Among all other features, it's ability to provide thickness independent moisture information is unique and therefore an advantageous addition. However, also in general the use of more than one feature proves to be advantageous for the prediction of screed moisture contents.

2.3 Summary and Conclusion

The generated reference for the observed drying process of each TS enabled to closely investigate the suitability of GPR signal features and the neutron probe to measure the moisture contents of screeds. The univariate analysis of GPR features from the literature review revealed clear correlations to the screed's moisture. Problems occurred for especially thin or dry specimens, which showed an interference of DW and RW. This mainly affects all features related to the first maximum of the reflection wave (feature 3, 5, and 6 in Figure B.7). The second maximum of the reflection wave proved as robust against possible interference, which is why its amplitude and travel time (feature 4 and 8) were further investigated in an multivariate analysis together with the direct waves amplitude (feature 1) and the scalar results of the neutron probe. Used as differently combined input parameters for MLiR models to predict the moisture content regardless of the underlying screed material or thickness, the features revealed specific characteristics and limitations. Here, the direct wave turned out as a valuable information source to overcome the strong dependence on the specimens thicknesses, which affects all other features. Nevertheless, the use of more than one feature generally showed promising results with regard to an sufficient sensitivity to the moisture content in screeds with unknown material parameters.

The presented investigations and results provided the basic knowledge for the subsequent investigations about moisture measurements on layered floor constructions. These will be presented in two publications. The first deals with the laboratory measurements and the subsequent methodology development to classify moisture damage cases on unknown floor constructions. The second then deals with the validation of the developed methods on five real on-site damage cases.

Bibliography

- [1] F. Radtke. *Schnellbestimmung der Feuchtigkeit beliebiger Materialien mit der Carbid-Methode*. [https://www.radtke-messtechnik.com/wp-content/uploads/2021/06/Anleitung-CM-Ger2.05 edition](https://www.radtke-messtechnik.com/wp-content/uploads/2021/06/Anleitung-CM-Ger2.05%20edition%2C%202021), 2021.
- [2] DIN EN ISO 12570:2000. Wärme- und feuchtetechnisches Verhalten von Baustoffen und Bauprodukten, Bestimmung des Feuchtegehalts durch Trocknen bei erhöhter Temperatur. 2000.
- [3] Geophysical Survey Systems, Inc. *SIR 20 Manual*. <https://www.geophysical.com/wp-content/uploads/2017/11/GSSI-SIR-20-Manual.pdf>, mn92-078 rev f edition, 2003-2017.
- [4] S. F. Senin and R. Hamid. Ground penetrating radar wave attenuation models for estimation of moisture and chloride content in concrete slab. *Construction and Building Materials*, 106:659–669, mar 2016. <https://doi.org/10.1016/j.conbuildmat.2015.12.156>.
- [5] A. Benedetto, F. Tosti, B. Ortuani, M. Giudici, and M. Mele. Soil moisture mapping using GPR for pavement applications. *7th International Workshop on Advanced Ground Penetrating Radar*, jul 2013. <https://doi.org/10.1109/iwagpr.2013.6601550>.
- [6] W. L. Lai, T. Kind, and H. Wiggerhauser. A Study of Concrete Hydration and Dielectric Relaxation Mechanism Using Ground Penetrating Radar and Short-Time Fourier Transform. *EURASIP Journal on Advances in Signal Processing*, 2010(1), jul 2010.
- [7] H. Epple. Austrocknungsverhalten von Calciumsulfat-Fliessestrichen. *Applica*, Vol. 23-24, 2006.
- [8] F. Kurz and H. Sgarz. Measurement of Moisture Content in Building Materials using Radar Technology. *International Symposium Non-Destructive Testing in Civil Engineering (NDT-CE)*, 2015.
- [9] W. Schnell. Zur Ermittlung von Belegreife und Ausgleichsfeuchte von mineralisch gebundenen Estrichen. *boden wand decke, Heft 1*, 1985.
- [10] C. Strangfeld and T. Klewe. Comparison of the Calcium Carbide Method and Darr Drying to Quantify the Amount of Chemically Bound Water in Early Age Concrete. *Materials*, 15(23):8422, nov 2022.

Results

B	Combining Signal Features of Ground-Penetrating Radar to Classify Moisture Damage in Layered Building Floors.....	49
B.1	Introduction.....	51
B.2	Materials and Methods.....	53
B.3	Results.....	60
B.4	Discussion.....	66
	Bibliography.....	68
C	Classification of On-Site Floor Moisture Damage with GPR - Limitations and Chances.....	71
C.1	Introduction.....	73
C.2	Methods.....	74
C.3	Results.....	78
C.4	Discussion.....	83
C.5	Summary and Conclusion.....	87
	Bibliography.....	89

B. Combining Signal Features of Ground-Penetrating Radar to Classify Moisture Damage in Layered Building Floors

Abstract

To date the destructive extraction of drilling cores is the only possibility to obtain depth information about damaging water ingress in building floors. The time- and cost-intensive procedure constitutes an additional burden for building insurances, that already list piped water damage as their largest item. With its high sensitivity for water, ground penetrating radar (GPR) could provide an important support to approach this problem in a non-destructive way. In this ongoing research project we study the influence of moisture damage on GPR signals at different floor constructions. For this purpose, a modular specimen with interchangeable layers is developed to vary the screed and insulation material as well as the respective layer thickness. The obtained data set is then used to investigate suitable signal features to classify three scenarios: dry, damaged insulation and damaged screed. It was found that analyzing statistical distributions of A-scan features inside one B-scan allows an accurate classification on unknown floor constructions. Combining the features with multivariate data analysis and machine learning was the key to achieve satisfying results. The developed method lies the basis for upcoming validations on real damage cases.

Bibliographic Information

T. Klewe, C. Strangfeld, T. Ritzer, S. Kruschwitz (2021, September). Combining Signal Features of Ground-Penetrating Radar to Classify Moisture Damage in Layered Building Floors. Applied Sciences, 11(19), 8820, <https://doi.org/10.3390/app11198820>.

Author's contribution

Conceptualization, T.K., C.S., T.R. and S.K.; methodology, T.K., C.S., T.R. and S.K.; software, T.K.; validation, T.K.; formal analysis, T.K.; investigation, T.K.; resources, C.S., T.R. and S.K.; data curation, T.K.; writing—original draft preparation, T.K.; writing—review and editing, C.S. and S.K.; visualization, T.K.; supervision, C.S. and

S.K.; project administration, C.S.; funding acquisition, C.S. and S.K.

Copyright Notice

This is a published article accessible by <https://doi.org/10.3390/app11198820>. It is licensed under an open access Creative Commons CC BY 4.0 license.

B.1 Introduction

More than half of the building insurance claims in Germany (53%) are caused by piped water damage, which entailed costs of over 3 billion Euro in 2019 alone [1]. One reason for this, apart from generally ageing pipe systems, is that water leakage often remains unrecognized until signs of degradation become noticeable. At that point the extent of damage is already critical, which underlines the demand of an accurate determination and localization of water ingress.

Neutron probes [2] are already successfully applied on building floors to localize the source of damage and to identify affected areas. The radiated fast neutrons lose most of their kinetic energy when colliding with low-mass atoms. This is especially true for hydrogen. As a result, the fast neutrons are transformed into slow (thermal) neutrons, which are then detected by a counter tube inside the probe. Given that, the method is highly sensitive to moisture, however it cannot distinguish between chemically bound or fluid water. Therefore, a calibration must be done by the destructive extraction of drilling cores. These cores are also the only possibility to obtain additional information about the depth of moisture penetration. This is a time- and cost-intensive procedure, especially for building floors, where knowledge about the affected layer is essential to plan and perform efficient renovations. Here, ground-penetrating radar (GPR) can serve as a suitable addition to the neutron probe in order to classify common moisture damages in layered building floors in a non-destructive way.

The sensitivity of GPR for water has already been proven in many publications, especially in geophysics [3, 4]. However, in civil engineering (CE), GPR is also increasingly being applied for non-destructive moisture measurements on building materials like asphalt, concrete, and screed [5, 6, 7, 8, 9, 10]. Here, various methods have already been established. However, their adequate use and suitability highly depends on the particular case. Due to numerous possible uncertainties, like the given structure, installed materials, and layer thicknesses, interpreting GPR results is not straightforward and requires the expertise of trained personnel. These uncertainties often influence the same signal features that are used for moisture measurements (see section B.1.1). Here, relying on only one feature, as it is done in most of the related publications [11], can lead to high uncertainty. In contrast, this work pursues the strategy of combining different features, which allows the use of multivariate data analysis. It aims to achieve an automated classification of three scenarios: (1) the dry state, (2) damaged insulation, and (3) a damaged screed, all of them on unknown floor constructions. This is accomplished by a machine learning approach trained with novel radargram features that consider the spatial continuity of the present damage. The features are extracted from an experimentally measured data set, including varying materials and layer thicknesses. Before discussing the methodology in section B.2, a short introduction to moisture measurements with GPR is given.

B.1.1 Moisture Measurement with GPR

Besides the mostly negligible conductivity and magnetic permeability, the electric permittivity ε is the governing material parameter for moisture measurements with GPR [12, 13]. This gets particularly clear by comparing ε for dry concrete and water. Whereas the former lies between 2 to 9 [14], the latter shows values around 81. This difference causes a significant rise for wet concrete (between 10 to 20), which influences various propagation characteristics of the electromagnetic (EM) waves. By analyzing specific time-

amplitude-, or frequency-based features of the received signals, these water-related influences become measurable. A detailed review of those features typically used for moisture measurement with GPR in CE is presented in [11]. However, a short overview is given in the following.

First, the velocity v of an EM wave is directly related to ε . For non-magnetic conditions, as it is usually the case in building materials, it can simply be calculated as follows [15, 14]:

$$v = \frac{c}{\sqrt{\varepsilon}} = \frac{2D}{T}, \quad (\text{B.1})$$

where c is the velocity of EM waves in free space, and T the two-way travel time in a material with the thickness D . Comparing the dry state of a material, sent and reflected pulses are received later for rising moisture content. Furthermore, the intensities and thus the measured amplitudes are reduced due to higher attenuations, caused by generally increased conductivity and more frequently occurring scattering events on water-filled pores. Filled pores also lead to Rayleigh scattering [16], which is one way to explain the observable shift of the received signals to lower frequencies for higher moisture content. Another explanation is given with the presence of dielectric dispersion, presented in the popular models of Debye [17] and Cole–Cole [18]. It describes the rising imaginary part of ε and the resulting absorption of higher-frequency components close to the relaxation frequency, which is 10 GHz to 20 GHz for free water [15, 19], but can be smaller for porous materials.

Another important characteristic of EM waves is the occurrence of reflection and transmission on material boundaries with different permittivities. With ε_1 and ε_2 of two mediums, an EM wave travelling from medium 1 to medium 2 is reflected by the amount of the reflection coefficient $r \in [-1, 1]$, which is calculated as follows [20]:

$$r = \frac{\sqrt{\varepsilon_1} - \sqrt{\varepsilon_2}}{\sqrt{\varepsilon_1} + \sqrt{\varepsilon_2}} \quad (\text{B.2})$$

Therefore, the amplitude of a reflection wave (RW) is highly influenced by the boundary's permittivity contrast, from which it originates. Figure B.1 shows this simplified ray-based principle with an exemplary screed plate above air, forming such a permittivity contrast. It also presents the usually performed collection of multiple reflection signals (A-scans) along a survey line, whereas the offset between the transmitter (T) and receiver (R) stays constant (common-offset configuration). The recorded A-scans can then be combined in a radargram (B-scan) that offers the opportunity to visualize spatial deviations caused by inhomogeneities, like the presence of reinforcements or water-damaged areas.

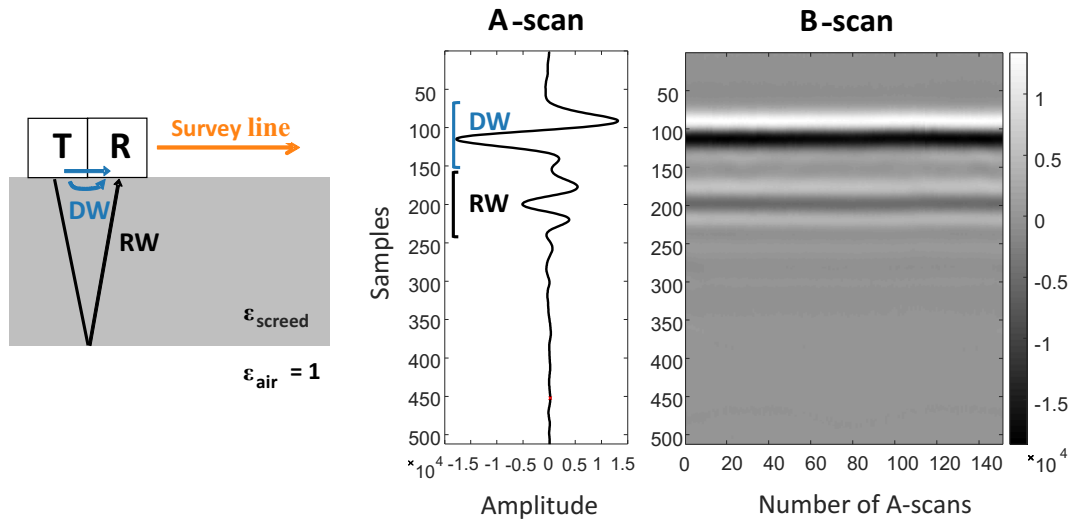


Figure B.1: Principle of GPR. Multiple A-scans collected along a survey line form a B-scan.

The most dominant wave-type in an A-scan is the direct wave (DW), which travels the shortest path between T and R and is therefore recorded first. As shown, it is a superposition of an air and a ground wave and is generally used as a time reference for the following RW, since the moment of emitting the pulse (time zero) is unknown [21]. Typical signals and their respective features measured on layered floor constructions are discussed in section B.2.5.

B.2 Materials and Methods

Figure B.2 shows the general procedure of the work presented in this section. After introducing the designed modular test specimen in section B.2.1, the conducted experiments to obtain a dataset of three damage scenarios are discussed in the sections B.2.1–B.2.4. In section B.2.5, various features are extracted to train and test different classifiers, which are shown in section B.2.6.

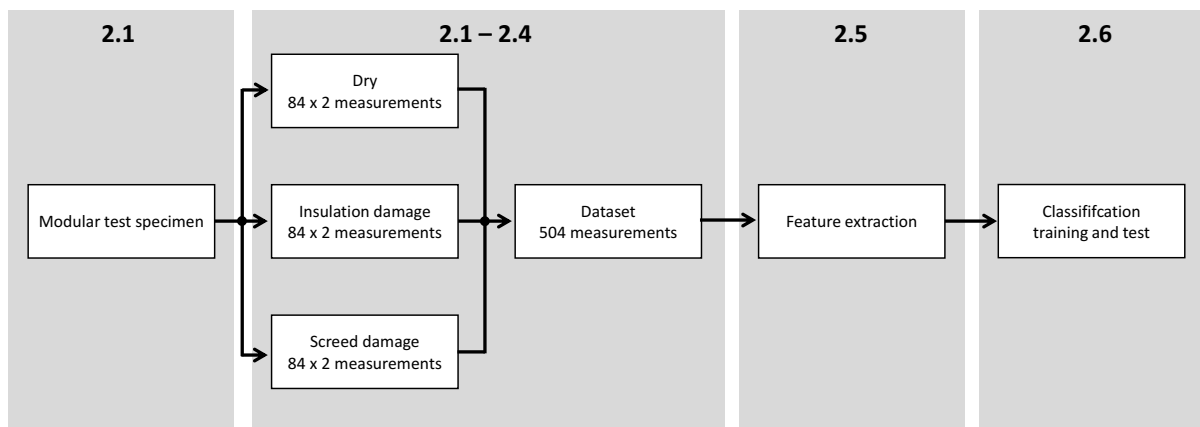


Figure B.2: Schematic of the work steps presented in section 2 divided by their respective subsections.

B.2.1 Modular Test Specimen

To study multiple different floor constructions, we designed a modular specimen (Figure B.3), in which the screed and insulation layer can be exchanged in various ways according to the requirements of the experiment. The inner dimensions of 84 cm length, 84 cm width, and 30 cm height ensure sufficient space for the individual square-shaped parts with an edge length of 80 cm. Table B.1 shows the variations of the chosen materials and their thicknesses that are believed to cover most floor setups in practice. Polyethylene (PE) foil is used to create a moisture barrier above and below the insulation. The influence of the laminate flooring and the concrete base layer on the presented classification method is considered to be negligible compared to the screed and insulation layer. Therefore, and with regard to the experimental effort, the flooring and base layer remained unchanged for the entire test series.

The cement and anhydrite screed were both chosen with the popular compressive strength C25 and the consistency class F5. The production process was carried out as instructed by the manufacturer. To guarantee efficient handling of the 60 kg to 100 kg heavy specimens, threaded sleeves were embedded in each corner. This allowed the temporary use of ring bolts to lift the plates.

The amount of different materials and thicknesses (Table B.1) allows for the simulation of 84 different floor constructions for each of the three scenarios (252 setups in total). The experimental implementation of water damage in the insulation and screed layer is described in the following sections.



Figure B.3: Modular test specimen with screed, insulation, and concrete base layer.

B.2.2 Water Damage in Insulation Layer

To evaluate the resulting damage of added water, HIH-5030 humidity sensors were embedded in the insulation material, as shown in Figure B.4. For EP, XP, and GW, this was accomplished with drilling holes of 3 cm diameter and depths varying from 50% to 75% of the respective insulation thickness. Top sealing was attained with waterproof tape. For the fine-grained PS, drilling holes were not necessary because the sensors could be placed easily.

Table B.1: Used materials and layer thicknesses for the screed (top) and insulation layer (bottom).

Material	Thickness D [cm]	Density [$\text{g}\cdot\text{cm}^{-3}$]	Porosity* [%]
Cement screed (CT)	5, 6, 7	1.92	20.76
Anhydrite screed (CA)	5, 6, 7	2.05	27.18
Expanded polystyrene (EP)	2, 5, 7, 10	0.027	-
Extruded polystyrene (XP)	2, 5, 7, 10	0.037	-
Glass wool (GW)	2, 6, 10	0.061	-
Perlites (PS)	2, 6, 10	0.092	-

* Measured with mercury intrusion porosimetry.

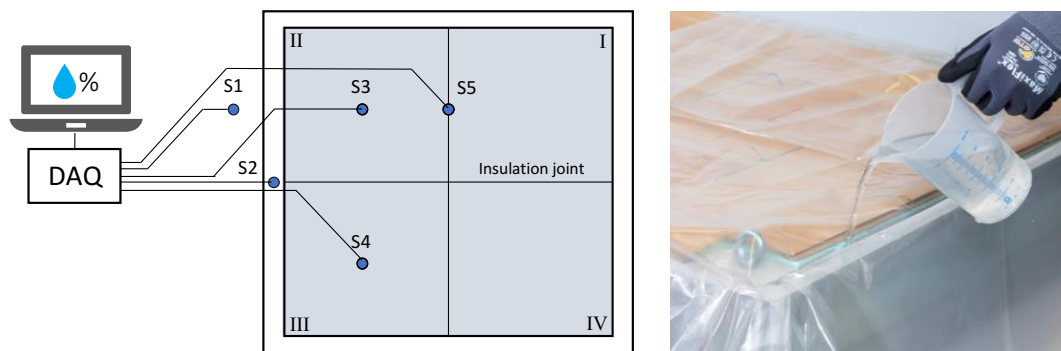


Figure B.4: Evaluation of the resulting insulation damage through the use of embedded humidity sensors.

After adding equal amounts of water in all four sides of the setup, the moisture could spread for at least 12 hours to ensure stable conditions. In practical investigations, a threshold of 80 % relative humidity is often considered as an adequate reason for renovations, since it provides optimum growth conditions for mould [22]. Following that, a setup was labeled as 'damaged' only if all three sensors S3 to S5 exceeded this critical value. Thereafter, the measurement procedure, which is discussed in section B.2.4, was conducted for each of the six screeds.

B.2.3 Water Damage in Screed Layer

The quantification of screed moisture was carried out using the direct Darr method [23], which captures the loss of water by weighing samples before and after an oven-drying procedure. With the wet sample weight W_w and the dry sample weight W_d , the dry basis moisture content M_d is calculated as follows:

$$M_d = \frac{W_w - W_d}{W_d} \quad (\text{B.3})$$

Moisture content above 4 weight percent (wt%) and 0.5 wt% were valued as damage for cement and anhydrite screed, respectively. Due to preliminary investigations of the screed's hydration process, W_d was already known for each sample. Consequently, the sample's moisture content could be obtained by measuring W_w only. With 1.7 wt% to 2.3 wt% for CT and around 0.1 wt% for CA, these were rather low before simulating

the damage. Therefore, we first flooded each sample by submersing them in water for 30 minutes (CT) or 10 minutes (CA). The moisture could then spread and evaporate for at least 2 days before the actual damage was induced. In consideration of practical screed damage that usually occurs after flooding from above, we then constantly poured water on top of the plates for 10 minutes. Besides continually weighing the samples, additional nuclear magnetic resonance (NMR) measurements were performed with the MOUSE [24, 25] to obtain depth-resolved moisture distribution during the described saturation process. Figure B.5 presents the exemplary NMR results with their respective water content measured on the 5 cm thick CT and CA screed.

Compared to CA, the CT screed shows an unbalanced water ingress for the sample's top and bottom side after the submersion. We explain this with a lower porosity of CT, not allowing the air in the bottom to be displaced towards the upper areas. The porosity also allows the water to spread more in CA after two days of rest. Nevertheless, sprinkling the samples resulted in quite a similar moisture distribution for both screed types with sufficiently high moisture content to be labeled as damage. After that, the screed was measured with all 14 insulation setups.

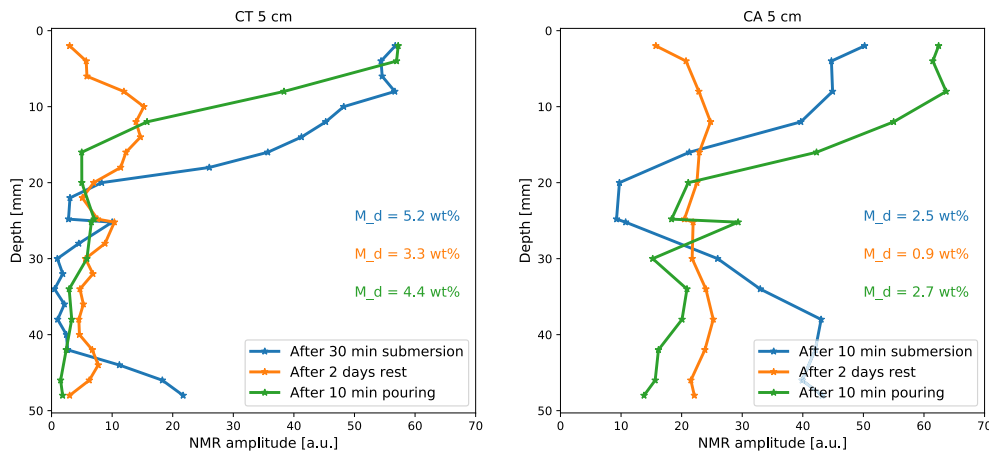


Figure B.5: NMR measurements showing the depth-resolved moisture distribution during the saturation process of the 5 cm CT (**left**) and CA (**right**) screed.

B.2.4 Hardware and Measurement Procedure

The GPR measurements were carried out with the SIR 20 from GSSI and a 2 GHz antenna pair (bandwidth 1 GHz to 3 GHz) in common-offset configuration. As shown in Figure B.6, the ground-coupled antenna pair is moved along two defined 40 cm survey lines that run from quadrant IV to I (1) and along the insulation joint (2). These joints were present for EP, XP, and GW, though not for the fine-grained PS. With 250 scans/meter, each survey line includes 100 A-scans to form one B-scan. An A-scan contains 512 samples covering a 11 ns time window.

Furthermore, each floor construction was investigated with a Troxler neutron probe placed in the setup center. To reduce the influence of individual deviations, 10 successive measurements with a respective time interval of 15 seconds were averaged.

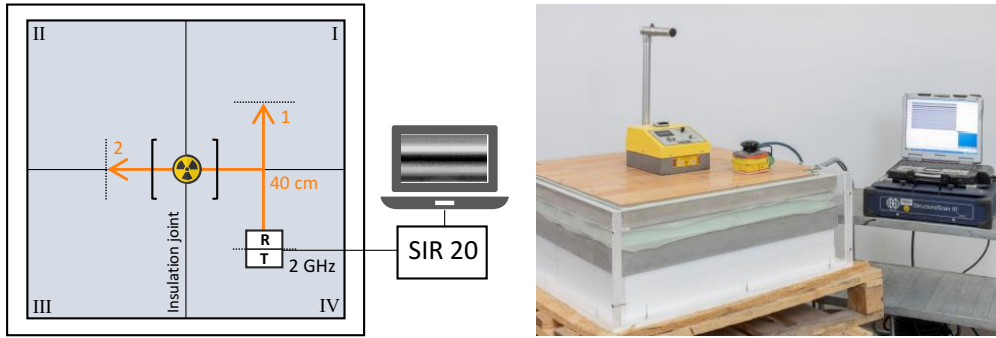


Figure B.6: Measurement procedure with 40 cm long radar survey lines 1 and 2. The neutron probe is placed in the center of the construction.

B.2.5 Feature Extraction

A-Scan Features

As discussed in section B.1.1 previously, there are several signal features enabling the measurement of water with GPR. Before presenting the ones chosen in this work, it is important to understand the typical signal shapes that occur on layered floor constructions. Figure B.7 gives an exemplary A-scan showing three prominent amplitude peaks and their respective origin in the setup. Since the direct wave (A_{DW}) partly travels through the superficial ground, it is influenced by the underlying nearest materials, here by the floor cover and the screed. The first reflection arises from the border between screed and insulation and is mostly recognized in the second dominant amplitude peak A_{RW1} . After that, A_{RW2} shows the second reflection’s amplitude, originating from the insulation-concrete interface below.

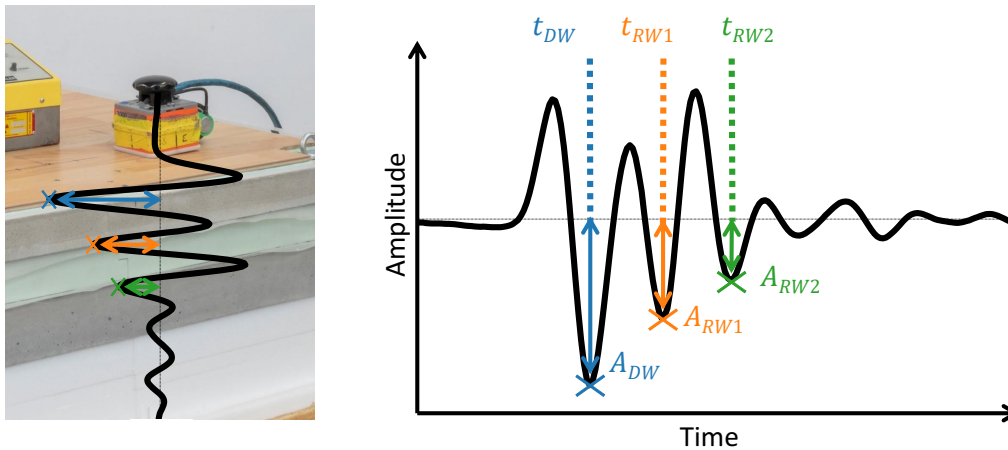


Figure B.7: Exemplary A-scan with three prominent amplitudes influenced by present material interfaces.

All described reflection waves can interfere, especially for dry or thin layers, where resulting higher velocities or short traveling paths impede a clear separation in time. This is also why quantitative statements about actual water content cannot be reliable for such layered floor constructions. However, classifying the investigated scenarios is still possible and will be performed with the following signal features:

- Feature F_1 : A_{DW} - Amplitude of direct wave [7, 6, 8]
- Feature F_2 : A_{RW2} - Amplitude of second reflection [7, 6, 8]
- Feature F_3 : f_{RW2} - Dominant frequency of second reflection (STFT) [26]
- Feature F_4 : A_{RW1}/A_{DW} - Ratio between the amplitudes of first reflection and direct wave [9]
- Feature F_5 : f_{RW1}/f_{DW} - Ratio between the dominant frequencies of first reflection and direct wave

The presented signal features cover all relevant signal parts, with insulation damage mostly influencing the second and first reflection and screed damage causing variations in the first reflection and the direct wave. However, the same features are also influenced by underlying layer thicknesses and different material types. Therefore, another preprocessing step is needed to overcome these construction-specific dependencies, which will be achieved by the B-scan features presented in the following section.

B-Scan Features

To achieve a damage classification independent of the underlying floor construction, we calculate the following scalar statistical values for each 1×100 A-scan feature vector \vec{F}_1 to \vec{F}_5 , each including the respective feature elements F_1 to F_5 for all 100 A-Scans within one B-scan.

- Feature F_A : Standard deviation of \vec{F}_1
- Feature F_B : Standard deviation of \vec{F}_2
- Feature F_C : Span of \vec{F}_3
- Feature F_D : Standard deviation of \vec{F}_4
- Feature F_E : Span of \vec{F}_5

These measures for statistical distributions along a recorded survey line are motivated by the assumption that water damage often shows inhomogeneous deviations inside the respective B-scan. Such deviations can also be suitable to evaluate the spatial continuity of present damage. Both findings were generally recognized during our studies and will be discussed in the results section B.3. For the lower resolved frequency features, the span is expected to achieve better variance compared to the standard deviation, which works well on amplitude features with a higher resolution and range of values.

Figure B.8 summarizes the discussed processing steps including the extraction of A-scan feature vectors out of B-scans and the following reduction to scalar B-scan features. The values shown for F_A to F_E are derived from the depicted A-scan feature plots (normalized by their means). They do not represent the actual values that were used for classification, since those were standardized with the *StandardScaler* function from the Scikit-Learn library. It does a mean removal for all features and scales them to unit variance, which is usually required by the classifiers discussed in section B.2.6. Regarding the magnitudes of amplitude, time, and frequency values, which are widely apart from each other, this step is necessary to avoid a baseless and unwanted dominance of certain features during the training process.

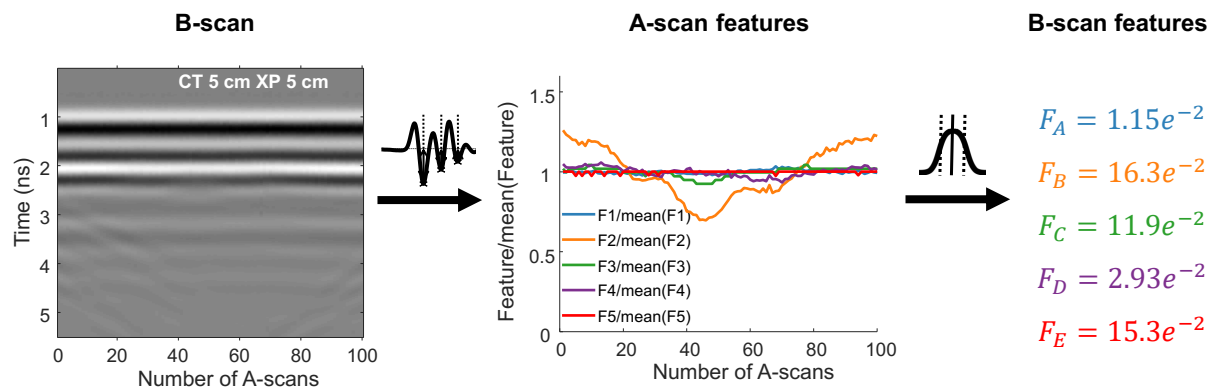


Figure B.8: Processing steps to extract A- and B-scan features.

Feature Selection

The choice of this specific A- and B-scan feature set was made based on the achieved scores using the univariate feature selection method *SelectKBest* from the Scikit-Learn library in Python [27]. Using the *f_classif* scoring function, it estimates the degree of linear dependency between random variables (here, the features and damage scenario) by using the F-test. The five features presented before performed best in a set of 22 potential features including amplitude, time, and frequency values/ratios of each relevant reflection type in Figure B.7. To avoid the use of insufficient input variables, which would impede efficient computation, only these five features were used to train the classifiers (next section), and all others were discarded. The respective scores of the chosen feature set will be shown in section B.3.2.

B.2.6 Classification of Damage Scenarios

With 84 different floor constructions for each of the three scenarios and two survey lines measured, a data set of 504 B-scans was produced, from which the features mentioned above were extracted. With this data, we trained the following four classifiers in standard configuration (default parameters only), which are all included in the Scikit-Learn library. The default parameters can be found in the respective documentation (e.g., default kernel of SVM: radial basis function):

- Multinomial logistic regression (MLR)
- Random forest (RF)
- Support vector machine (SVM)
- Artificial neural network (ANN)

The ANN consisted of two hidden layers with five neurons each (according to the number of features). To get a statistical comparability of the accuracies achieved, a $k = 20$ -fold cross-validation was applied for all classifiers using the *cross_val_score* function from Scikit-Learn. Here, the parameter *cv* (cross-validation generator) was defined with *Shuffle-Split*(*n_splits*=20, *test_size*=0.2, *random_state*=0) which produces 20 random splits of training and test data sets with a size of 80% and 20%, respectively. All classifiers were cross-validated with the same set of splits, which includes 20 consecutive training and

test procedures for each classifier. The results were then statistically evaluated (mean and standard deviation) and are shown in section B.3.2. However, before discussing the classification, an impression of the collected data shall be given with exemplary measurement results from the experiments.

B.3 Results

B.3.1 Measurements at Modular Specimen

Figures B.9 and B.10 show the measurement results of all three scenarios at one respective floor construction. The first covers the configuration of a 7 cm CT screed combined with a 10 cm EPS insulation. The B-scans on top also contain text information about the underlying moisture states of screed and insulation, as well as the performed neutron probe measurement. All exemplary radar results were collected along survey line 1 (see Figure B.6).

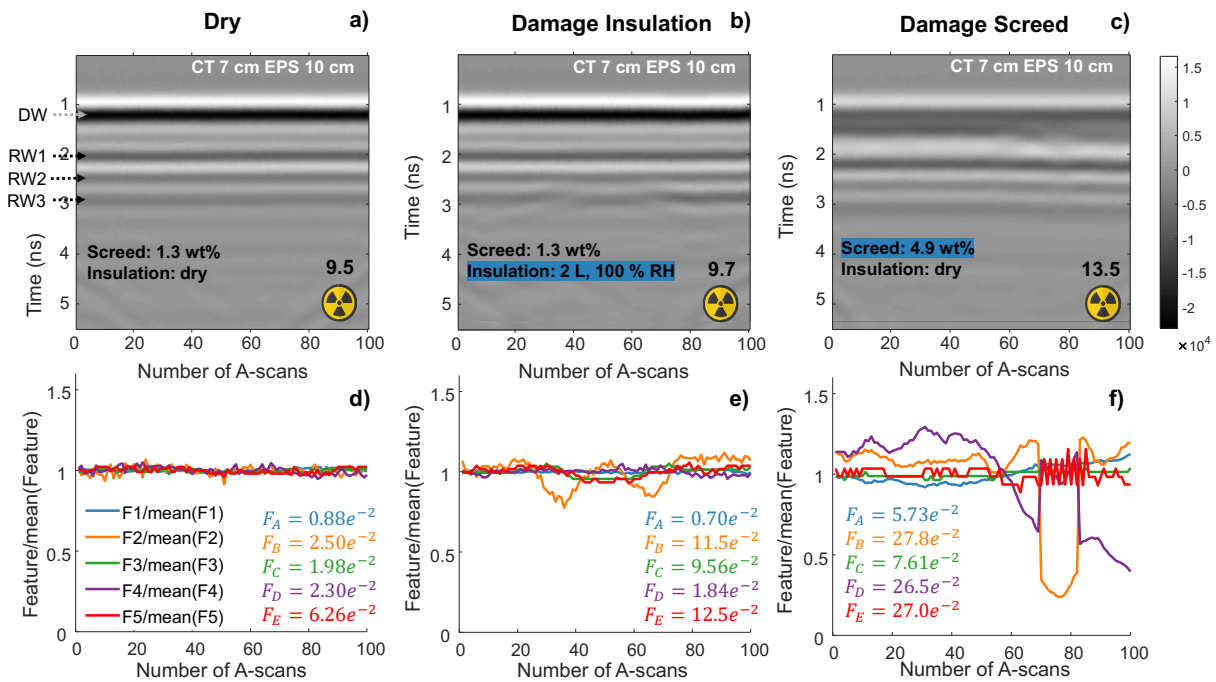


Figure B.9: Measurements at a 7 cm CT and 10 cm EPS floor construction for the scenarios: (a) Dry, (b) damage insulation, and (c) damage screed. The bottom (d-f) shows the respective A-scan vector plots for each B-scan (top).

According to the general assumption mentioned in Section B.2.5, the dry measurement in (a) has a homogeneous reflection pattern, whereas the two damage scenarios in (b) and (c) present clear deviations at specific time-spans. For the insulation damage in (b), we see amplitude changes in the second (RW2) and third (RW3) reflection around 2.5 ns to 3 ns, which come from the affected layer. Water added to EPS usually gathers inside the insulation joints, and from there, it slowly penetrates the material. Therefore, the areas of higher attenuation were located horizontally around the survey line's center, where the joint is crossed. These deviations become even clearer by considering the respective A-scan feature vector plots below each B-scan. Compared to the relatively flat lines for

the dry measurement in (d), F_2 (A_{RW2}) particularly shows significant variations in (e), which is also captured by an increased standard deviation (F_B). These deviations are not immediately recognizable in the B-scan, since the third reflection RW3 shows a more significant variance. Insulation of 10 cm thickness usually developed two reflections, whereby the latter and therefore third reflection was not covered by the used feature set. However, due to their interference, RW2 also experienced a change in amplitude and is therefore suitable for recognizing damage. Since the neutron probe is more sensitive to moisture closer to its radiation source, a small amount of water inside the insulation is not sufficient to cause a significant increase.

In the case of screed damage in (c), the water induces deviations which appear in earlier time-spans, like in the direct wave DW or the first reflection RW1. As shown in Figure B.5, all screed samples were poured from above, which is why the DW experiences a significant drop in its amplitude compared to other scenarios. A_{DW} is especially sensitive to superficial material properties and is therefore an appropriate feature to recognize flooding damage. In this case, F_4 being the ratio of A_{RW1} and A_{DW} shows a high dynamic in (f). This is also because an unexpected reflection occurs at around 1.4 ns right after the direct wave, which was not present in other scenarios. The reason could be a steep water gradient providing a strong permittivity contrast and therefore a new reflector. This assumption is supported by the highest NMR amplitude measured for the 7 cm CT among all screeds, which was around 90 at the sample's surface. The other screeds had values of around 60 and did not show an extra reflection (compare Figure B.10). Here, the new reflection at around 1.4 ns is interpreted as RW1, whereby the former RW1, originating from the screed bottom, is then seen as RW2. After a decrease of A_{RW1} between A-scans 50 and 65, it completely disappears between 70 and 80, causing a shift in reflection-counting. This leads to dominant jumps for F_2 and F_4 , which cause an increased standard deviation and support the feature's sensitivity for water-induced deviations. The neutron probe is also capable of recognizing the increased moisture content with a difference of 4 digits compared to the dry measurement.

Figure B.10 gives another example of a 5 cm CA screed and 6 cm GW floor construction. As before, the dry scenario in (a) shows a flat reflection pattern compared to notable deviations in the second reflection caused by a damaged insulation (b). Like with EPS, the water tended to accumulate in the joints between the GW plates and was slowly absorbed by the material. In this case, it formed a stronger permittivity contrast on the insulation's bottom, which resulted in an increased reflection amplitude in the survey line's center (see Equation (B.2)). This gets especially clear by considering Figure B.11, in which parts of the GW insulation (measured by survey line 1) are shown. As all three plates were flipped by 90 degrees, the bottom edge belongs to the insulation joint between quadrants IV and I. The fact that only the first and lowest plate 1 shows marks of water ingress at this specific edge underlines the explanation of a strong permittivity contrast, which forms a thin reflector above the concrete plate. In this case, the neutron probe measures a slight increase due to an overall lower depth of the setup.

Another interesting difference to the example before can be seen in the damaged screed scenario (c), which is even more representative for the whole measured data set. Like with all other screeds (except the 7 cm CT) the induced moisture damages appear comparatively homogeneous and do not show the expected deviations. This can be explained by an evenly distributed moisture gradient throughout the whole sample. The most dominant influence is the overall reduced amplitude for DW, RW1, and RW2, which becomes

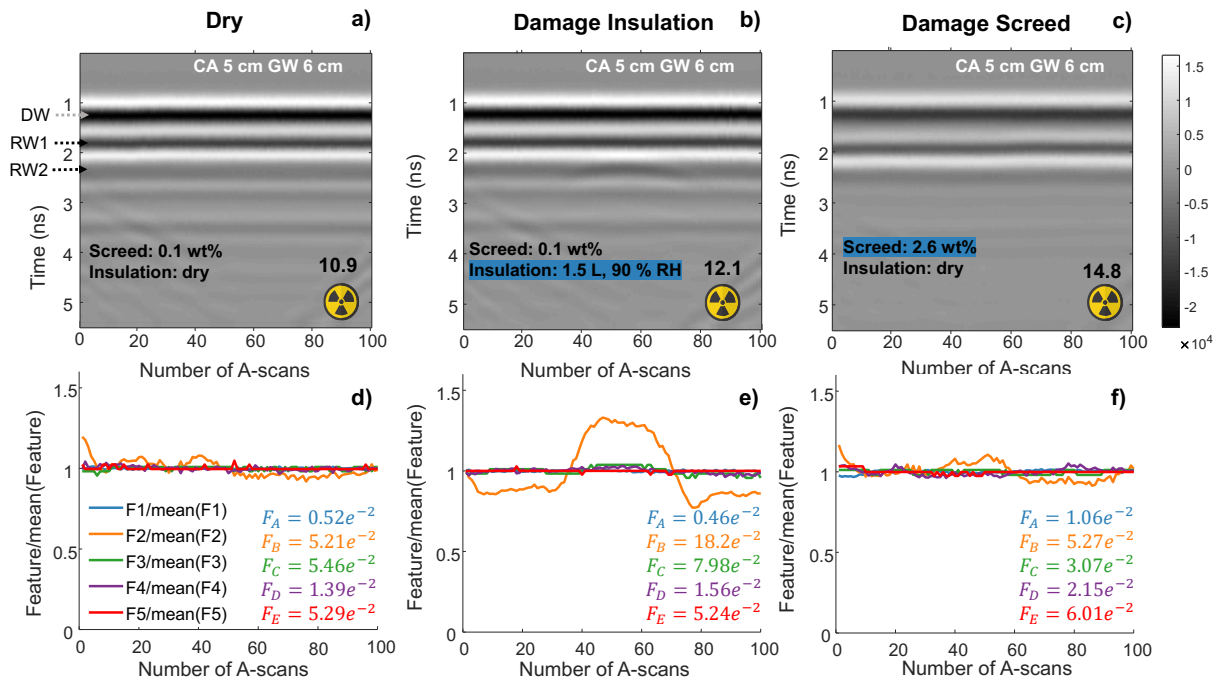


Figure B.10: Measurements at an 7 cm CA and 6 cm GW floor construction for the scenarios: (a) dry, (b) damage insulation and (c) damage screed. The bottom (d-f) shows the respective A-scan vector plots for each B-scan (top).

clear by comparing the dry scenario. However, it is not a clear indication for water without this prior knowledge. Nevertheless, by considering the values of F_A , F_D and F_E in (f), small increases can be registered, which might be sufficient to recognize the damage by trained classifiers. The validity of this statement shall be reviewed in the following section. Again, the screed damage is more visible for the neutron probe than moisture in the insulation layer.

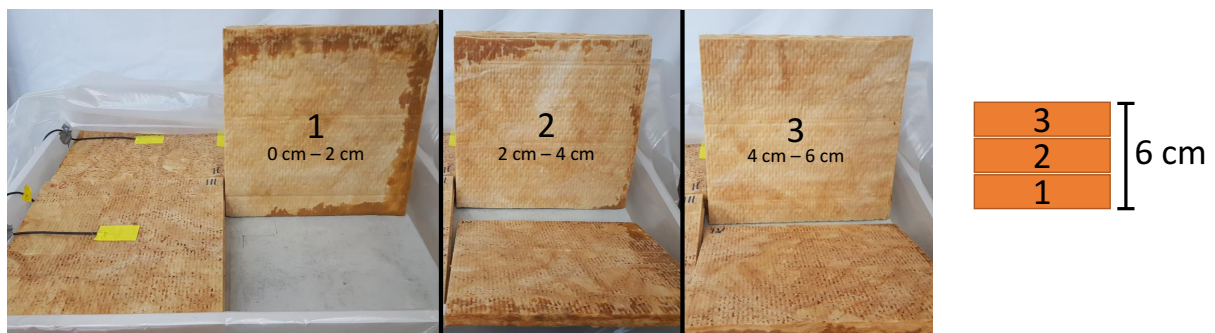


Figure B.11: Water ingress (dark dyeing) in the 6 cm GW insulation. The pictures show the respective bottom of each used insulation plate (40 cm x 40 cm x 2 cm) in quadrant IV.

B.3.2 Damage Scenario Classification

Table B.2 shows the achieved mean accuracies with the standard deviation of all trained classifiers mentioned in section B.2.6. By using the features presented in section B.2.5, all algorithms were capable of correctly recognizing 84.3% to 88.3% of the considered damage scenarios, without further knowledge about the underlying material or layer thickness. With regard to the broad variations considered in this data set, these accuracies are quite satisfying. To provide a better understanding of the presented results, Figure B.12 shows confusion matrices containing each used classifier for the individual layer thicknesses of insulation and screed.

For a perfect classification with 100% accuracy, all confusion matrix cells (entries) except the main diagonal would be zero, which means that every scenario would have been classified correctly. Knowing that, the highest deviation of that perfect case gets immediately visible in Figure B.12, which lies in the mid column of the top left matrix. It shows that more than half of the measured scenarios with a damaged insulation of 2 cm thickness were classified as dry. This can be explained by the low amount of water (around 0.5 L), that was necessary to cause relative humidities above 80%. Especially for GW and PS, the inserted water was absorbed by the outer edges and did not penetrate into measured areas. As a reference, Figure B.13 again shows the flipped GW plate after the measurement with no signs of water ingress on the bottom edge (insulation joint between quadrant IV and I). Due to the significant number of unaffected B-scans, the classification results in Table B.2 also show the accuracies for the excluded 2 cm insulation. All classifiers achieved a higher score and comparable standard deviations.

Table B.2: Statistical comparison ($k = 20$ -fold cross-validation) of the achieved accuracies for all trained classifiers.

Classifier	Accuracy (%)		Accuracy* (%)	
	Mean	Std	Mean	Std
MLR	86.4	3.0	89,7	3.1
RF	88.3	3.7	92.2	2.6
SVM	84.3	3.3	86.6	3.9
ANN	88.2	3.6	93.5	2.5

* Cases with insulation depth of $D = 2$ cm excluded.

Additionally, for insulations of 6 cm thickness which only included GW and PS, the respective confusion matrix contains 8.3% to 37.5% false-negatives for damaged insulations. Since the GW of 6 cm already showed a measurable influence in Figures B.10 and B.11, the wrongly classified scenarios are located in the PS data set. In fact, survey line 1 for PS of 6 cm thickness presents a smooth reflection pattern, which is exemplarily shown in Figure B.14 b). Unfortunately, the structure of PS did not allow referencing pictures like for GW; however, the similarity between dry and damaged insulation suggests that no water penetrated in the measured area.

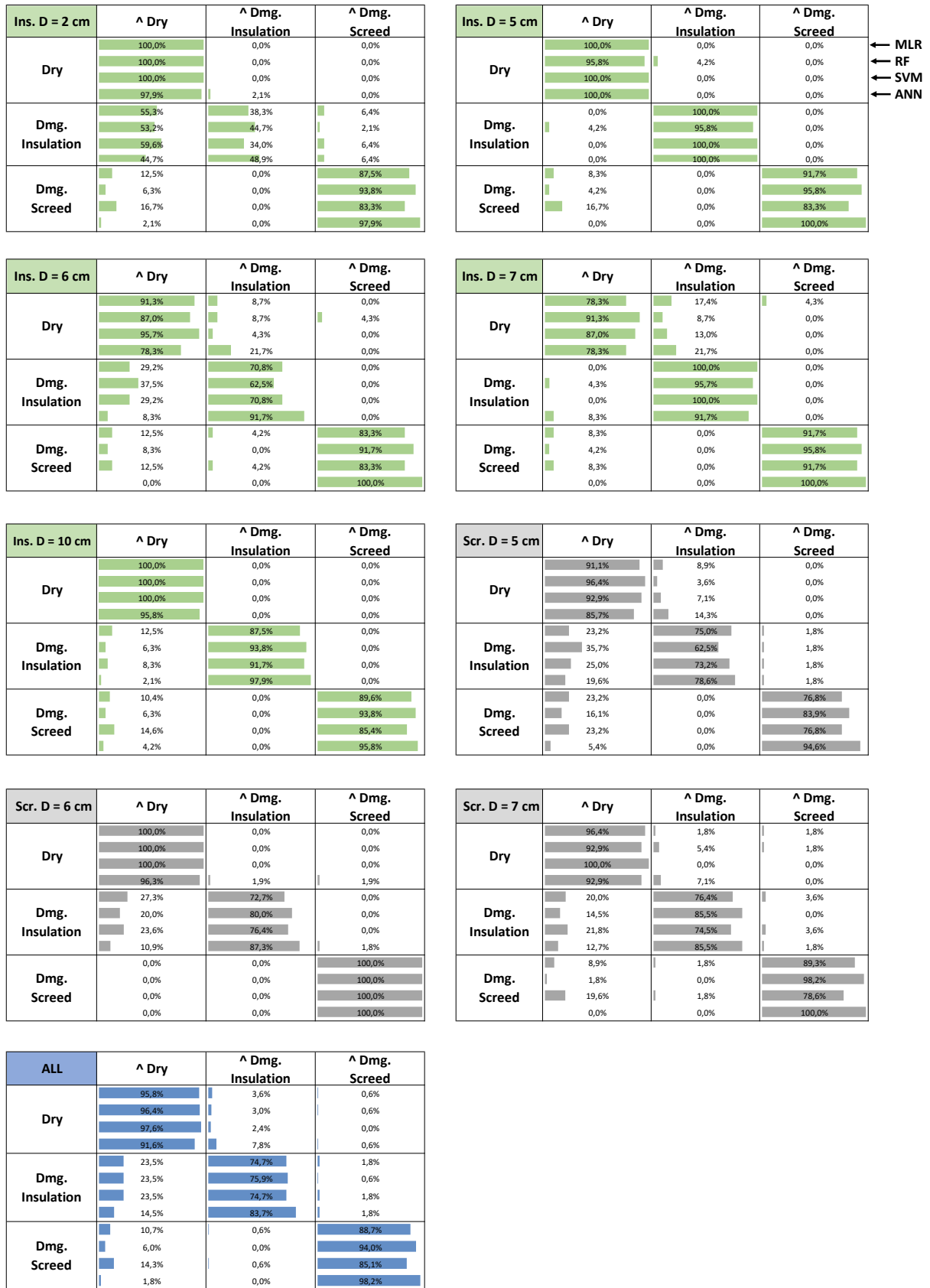


Figure B.12: Combined confusion matrices for the individual insulation (green) and screed (gray) thicknesses considered in the experiment. The classifier’s accuracies within one cell are presented in the same order as in Table B.2. Rows and columns include the actual and the predicted ($\hat{\text{}}$) scenario, respectively. The blue confusion matrix summarizes the overall accuracies for each scenario.

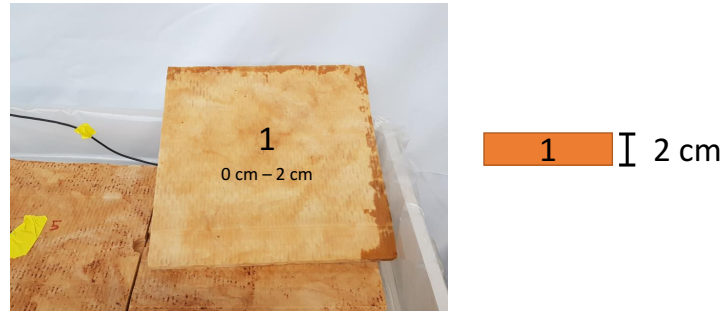


Figure B.13: Water ingress (dark dyeing) in the 2 cm GW insulation. The picture shows the bottom of the used insulation plate (40 cm × 40 cm × 2 cm) in quadrant IV.

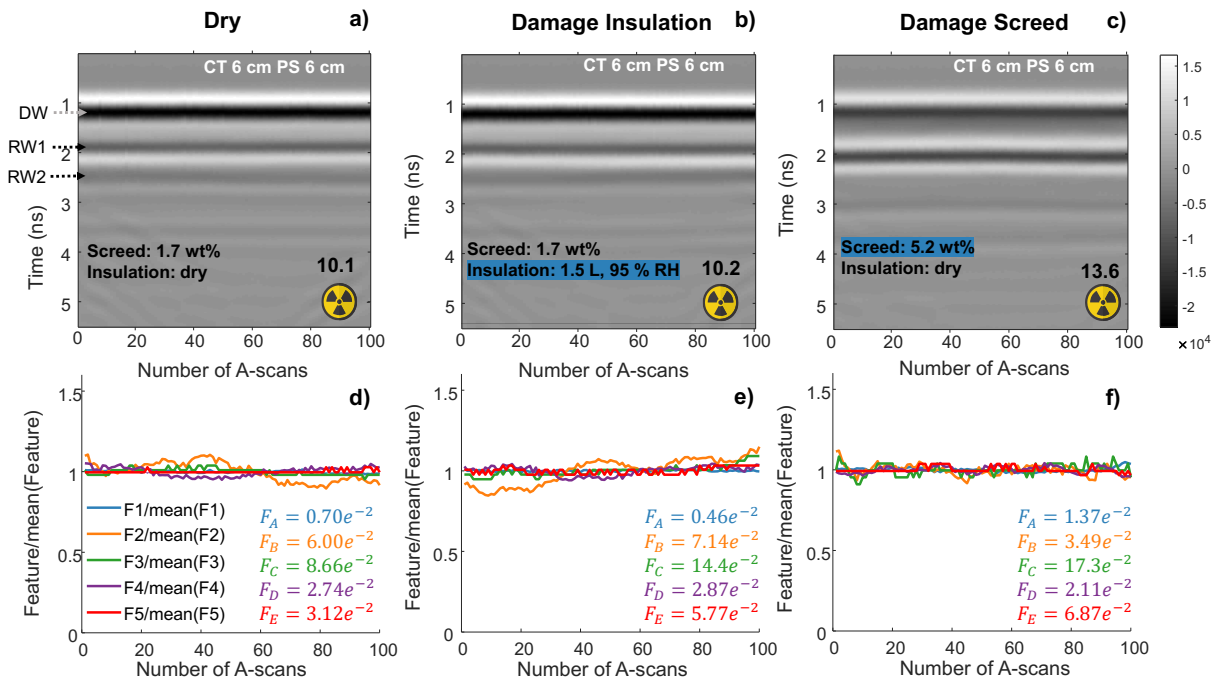


Figure B.14: Measurements at a 6 cm CT and 6 cm PS floor construction for the scenarios: (a) dry, (b) damaged insulation, and (c) damaged screed. The bottom (d–f) shows the respective A-scan vector plots for each B-scan (top).

In general, most of the wrong classifications are false-negatives, which are represented by entries left of the main diagonals. Besides the mentioned reasons for damaged insulations, the damaged screed scenario also shows around 5% to 20% of measurements that were classified as dry in nearly every confusion matrix. With regard to the mostly homogeneous reflection patterns shown in Figures B.10 and B.14, these results are rather satisfying. It shows that even the slight deviations in F_A , F_D and F_E , as discussed in the previous section, are mostly sufficient to recognize the considered screed damages.

Overall, the four used classifiers achieved similar accuracies in all matrix entries. Only the damaged screed scenario reveals a more significant trend with a comparatively poorly-performing SVM, while ANN shows the best results.

Looking at the achieved scores of each extracted feature can give a better insight into the data’s structure and their decisive components. Table B.3 points out F_B as the best-performing feature, followed by F_C and F_A .

Table B.3: Achieved scores of the applied B-scan features.

Feature	Origin in A-Scan	Score
F_A	A_{DW}	0.61
F_B	A_{RW2}	1.0
F_C	f_{RW2}	0.95
F_D	A_{RW1}/A_{DW}	0.48
F_E	f_{RW1}/f_{DW}	0.41

The reasons for these scores become clearer by considering the selected scatter plots in Figure B.15 with standardized values. Combining the best-performing, RW2-related features F_B and F_C shows a good separation of the damaged insulation scenario with a broad distribution of possible values. However, due to the discussed appearance of smooth reflection patterns, the damaged screed is mostly indistinguishable from the dry scenario. In this case, features regarding DW and RW1 are obviously more decisive, which can be seen by a better separation in the middle and left scatter plot. However, the separation is not that clear as for the damaged insulation with F_B and F_C , which explains the comparatively lower scores. The blue outliers belong to the 7 cm CT screed shown in Figure B.9, where the extra reflector caused an unusually strong deviation in F_D .

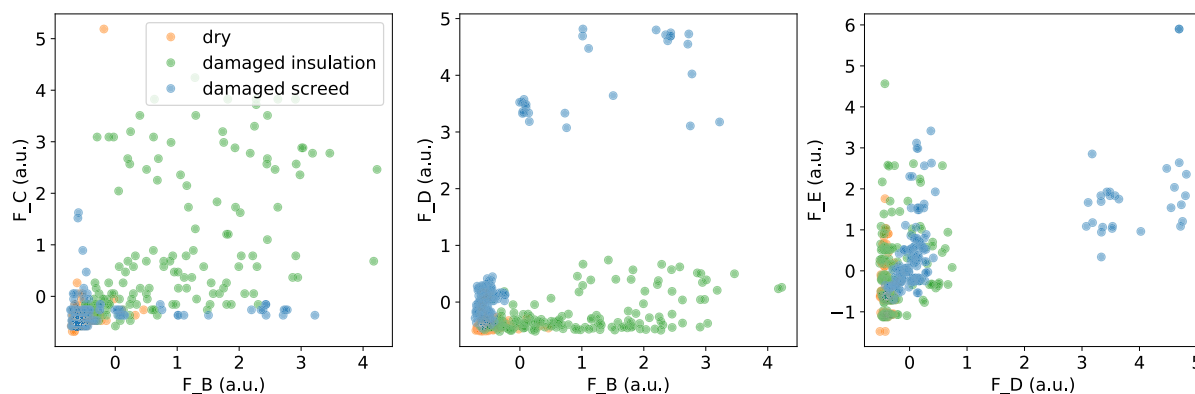


Figure B.15: Scatter plots showing the feature combination of F_B & F_C (**left**), F_B & F_D (**middle**) and F_D & F_E (**right**).

B.4 Discussion

The results show that the proposed method regarding the horizontal distribution of specific A-scan features in one B-scan is suitable to classify moisture damages in unknown floor constructions. In a data set of 504 B-scans covering 252 different experimental setups, 84.3% to 88.3% of the scenario's dry, damaged insulation, and damaged screed were recognized correctly by the trained classifiers. A closer investigation of the produced false-negatives often revealed the measurement of undamaged areas which underlines the method's sensitivity and suggest even higher accuracies. In particular, the combination of amplitude and frequency features covering all relevant reflections in the GPR signal contributed to the successful results. Therefore, this study generally proposes an enhanced

use of multivariate data analysis when performing moisture measurements with GPR. The presented method also worked well as a supporting procedure for the neutron probe. In particular, moisture inside the insulation layer was mostly undetected by the sole use of the radiation measurement, whereas GPR achieved a satisfying sensitivity.

Since the data set only contained laboratory measurements under controlled conditions, the method still needs to be validated in practical on-site investigations of real damage cases. Here, unknown parameters like an unstable layer thickness or obstructive floor heating pipes could lead to misinterpretations which might produce an increased number of false-positive classifications. Upcoming works by the authors will address these questions. If satisfying accuracies can be achieved, the method will be capable of significantly reducing the need for destructive drilling cores to classify underlying damage scenarios, and therefore cut the costs of renovations.

Further, potential optimizations could be investigated regarding the classifiers' configurations, since only default parameters have been used so far. In addition, the use of deep learning (ANN) to automatically extract novel, relevant features out of radargrams (b-scans as input parameter) can be examined with the obtained dataset.

Bibliography

- [1] GDV. Annual of Gesamtverband der Deutschen Versicherungswirtschaft e.V. <https://www.gdv.de/de/zahlen-und-fakten/versicherungsgebiete/wohngebaeude-24080>, 2019. Accessed on 20/07/2021.
- [2] D. S. Chanasky and M. A. Naeth. Field measurement of soil moisture using neutron probes. *Canadian Journal of Soil Science*, 76(3):317–323, aug 1996.
- [3] J. A. Huisman, S. S. Hubbard, J. D. Redman, and A. P. Annan. Measuring Soil Water Content with Ground Penetrating Radar: A Review. *Vadose Zone Journal*, 2(4):476–491, nov 2003.
- [4] L. Slater and X. Comas. The Contribution of Ground Penetrating Radar to Water Resource Research. In *Ground Penetrating Radar: Theory and Applications*. Elsevier, 2009.
- [5] T. Saarenketo and T. Scullion. Road evaluation with ground penetrating radar. *Journal of Applied Geophysics*, 43(2-4):119–138, mar 2000.
- [6] G. Klysz and J.-P. Balayssac. Determination of volumetric water content of concrete using ground-penetrating radar. *Cement and Concrete Research*, 37(8):1164–1171, aug 2007.
- [7] K. Grote, S. Hubbard, J. Harvey, and Y. Rubin. Evaluation of infiltration in layered pavements using surface GPR reflection techniques. *Journal of Applied Geophysics* 57, 57(2):129–153, feb 2005.
- [8] S. Laurens, J. P. Balayssac, J. Rhazi, G. Klysz, and G. Arliguie. Non-destructive evaluation of concrete moisture by GPR: experimental study and direct modeling. *Materials and Structures* 38, 38(9):827–832, nov 2005.
- [9] W. L. Lai, S. C. Kou, W. F. Tsang, and C. S. Poon. Characterization of concrete properties from dielectric properties using ground penetrating radar. *Cement and Concrete Research*, 39(8):687–695, aug 2009.
- [10] F. Kurz and H. Sgarz. Measurement of Moisture Content in Building Materials using Radar Technology. *International Symposium Non-Destructive Testing in Civil Engineering (NDT-CE)*, 2015.
- [11] T. Klewe, C. Strangfeld, and S. Kruschwitz. Review of moisture measurements in civil engineering with ground penetrating radar – applied methods and signal features. *Construction and Building Materials*, 278:122250, apr 2021.
- [12] J. L. Davis and A. P. Annan. Electromagnetic Detection of Soil Moisture: Progress Report I. *Canadian Journal of Remote Sensing*, 3(1):76–86, dec 1977.
- [13] M. N. Soutsos, J. H. Bungey, S. G. Millard, M. R. Shaw, and A. Patterson. Dielectric properties of concrete and their influence on radar testing. *NDT&E International*, 34(6):419–425, sep 2001.
- [14] D. J. Daniels. *Ground Penetrating Radar - 2nd Edition*. The Institution of Engineering and Technology, 2007.

- [15] A. P. Annan. Electromagnetic Principles of Ground Penetrating Radar. In Harry M. Jol, editor, *Ground Penetrating Radar: Theory and Applications*, chapter 1, pages 4–38. Elsevier, 2009.
- [16] C. Bohren and D. Huffman. *Absorption and Scattering of Light by Small Particles*. Wiley, 1983.
- [17] P. J. W. Debye. Polar molecules. *Journal of the Society of Chemical Industry*, 48(43):1036–1037, oct 1929.
- [18] K. S. Cole and R. H. Cole. Dispersion and Absorption in Dielectrics I. Alternating Current Characteristics. *The Journal of Chemical Physics*, 9(4):341–351, apr 1941.
- [19] U. Kaatze. Complex permittivity of water as a function of frequency and temperature. *Journal of Chemical & Engineering Data*, 34(4):371–374, oct 1989.
- [20] C. A. Balanis. *Advanced engineering electromagnetics*. John Wiley & Sons, 2nd edition, 2012.
- [21] R. Yelf. Where is true time zero? *Proceedings of the Tenth International Conference on Ground Penetrating Radar*, 2004.
- [22] J. B. M. Coppock and E. D. Cookson. The effect of humidity on mould growth on constructional materials. *Journal of the Science of Food and Agriculture*, 2(12):534–537, dec 1951.
- [23] ASTM D2216-19. Standard Test Methods for Laboratory Determination of Water (Moisture) Content of Soil and Rock by Mass. *ASTM Vol. 04.08*, 2019.
- [24] B. Blümich, P. Blümli, G. Eidmann, A. Guthausen, R. Haken, U. Schmitz, K. Saito, and G. Zimmer. The NMR-mouse: construction, excitation, and applications. *Magnetic Resonance Imaging*, 16(5-6):479–484, jun 1998.
- [25] B. Blümich, J. Perlo, and F. Casanova. Mobile single-sided NMR. *Progress in Nuclear Magnetic Resonance Spectroscopy*, 52(4):197–269, may 2008.
- [26] W. L. Lai, T. Kind, S. Kruschwitz, J. Wöstmann, and H. Wiggenhauser. Spectral absorption of spatial and temporal ground penetrating radar signals by water in construction materials. *NDT & E International*, 67:55–63, oct 2014.
- [27] F. Pedregosa, G. Varoquaux, A. Gramfort, V. Michel, B. Thirion, O. Grisel, M. Blondel, P. Prettenhofer, R. Weiss, V. Dubourg, J. Vanderplas, A. Passos, D. Cournapeau, M. Brucher, M. Perrot, and E. Duchesnay. Scikit-learn: Machine Learning in Python. *Journal of Machine Learning Research*, 12:2825–2830, 2011.

C. Classification of On-Site Floor Moisture Damage with GPR - Limitations and Chances

Abstract

Machine learning in non-destructive testing (NDT) offers a significant potential to efficiently perform daily data analysis or to reveal yet unknown relationships in persisting problems. However, the successful application highly relies on a diverse and labeled training data base. In most cases, this is not guaranteed, which often questions the transferability of trained algorithms on new data.

To closely investigate this problem, the authors apply classifiers, which were trained by laboratory Ground Penetrating Radar (GPR) data to categorize on-site moisture damage cases in layered building floors. Investigations were carried out at five different locations in Germany. As a reference, drilling cores were extracted for each measurement point. They were labeled as (i) dry, (ii) with insulation damage, or (iii) with screed damage. Compared to the accuracies of 84 % to 90 % within the laboratory training data (504 B-Scans), the classifiers achieved only a poor overall accuracy of 53 % for the investigated on-site data (72 B-Scans). The main problems were caused by overfitting small deviations between laboratory measurements on dry floors and screed damages. For this reason, the generally more heterogeneous and dynamic on-site data was falsely classified in most of the cases. Nevertheless, this study still demonstrates a promising sensitivity of the applied signal features for each individual damage case. Especially the results showing insulation damage, which cannot be detected by any other non-destructive method, revealed characteristic patterns. The accurate interpretation of such results still relies on trained personnel, whereby fully automatized approaches require a much bigger and diverse on-site data basis. Until then, the findings of this work contribute to a more reliable analysis of moisture damage in building floors by the use of GPR and give practical insight into the application of machine learning within non-destructive testing in civil engineering (NDT-CE).

Bibliographic Information

T. Klewe, C. Strangfeld, T. Ritzer, S. Kruschwitz (Manuscript of 2022, August) Classification of On-Site Floor Moisture Damage with GPR - Limitations and Chances

Author's contribution

Conceptualization, T.K., C.S., T.R. and S.K.; methodology, T.K., C.S., T.R. and S.K.; software, T.K.; validation, T.K.; formal analysis, T.K.; investigation, T.K.; resources, C.S., T.R. and S.K.; data curation, T.K.; writing—original draft preparation, T.K.; writing—review and editing, T.K., C.S. and S.K.; visualization, T.K.; supervision, C.S. and S.K.; project administration, C.S. and S.K.; funding acquisition, C.S. and S.K.

Copyright Notice

This article was submitted to the Journal of 'Construction and Building Materials' in August 2022. It will be resubmitted to the Journal of 'NDT & E International' in late 2023 with further changes in the summary and conclusion.

C.1 Introduction

Non-destructive testing in civil engineering (NDT-CE) often deals with the investigation of large areas, including various, local events of damage. Such examinations produce a large amount of data that require an extensive analysis by experienced personnel. Applying machine learning methods could help to not only accelerate these processes but may also provide further insight into the data structure and into yet unknown relationships within NDT-CE. However, the successful use of these emerging techniques requires a profound and diverse training data base. Compared to the popular and successful examples within computer vision applications like autonomous driving or facial recognition, the availability of labeled non-destructive testing (NDT) data is often limited, which implies the risk of an insufficient representation of the space of possibility [1]. Unfortunately, referencing training data for machine learning is not always straight forward for NDT-CE. This work approaches these problems and questions by producing referenced training data within laboratory conditions to classify new, also referenced on-site measurements. The validation and its results shall give practical insight into the application of machine learning in NDT-CE. The study was conducted on moisture damage in layered building floors, which present a relevant research question.

Between 2000 and 2020, the annual costs of pipe water damage in Germany increased by 165 % to the latest amount of 3.3 billion Euro [2]. In the event of a moisture damage, the actual extend often remains unrecognized, causing a costly deterioration of building structures. The additionally increased risk of mould threatens the health of residents [3, 4], which underlines the importance of a fast and precise damage diagnosis.

For pipe water damage, building floors are the most affected structure, since they either include the broken pipe system within their insulation, or are flooded from above. This results in two primary damage cases: a wet insulation or a wet screed. Moisture barriers in form of polyethylene foils generally prevent the water transfer between both layers. However, in the rare case of a poor functionality, also both layers may be damaged simultaneously. Knowledge about the presence and distribution of these different damage cases is of high importance to perform an efficient and effective repair.

Most of the common, non-destructive moisture measurement techniques [5, 6], like resistivity-based, capacitive, or thermal methods, are not suitable for a comprehensive investigation of building floors. They only obtain moisture information about superficial areas or may be impeded by the layered structure. Furthermore, floor structures often include a flooring on top of screed and insulation, which may disturb the informative value of the applied method. Especially the moisture state of the insulation, which lies deepest, is unrecognized by most methods and presents a particular challenge when performing moisture investigations on building floors.

A suitable exception are Neutron probes [7], as they are capable to achieve penetration depths of close to 30 cm. However, they only deliver integral measurements of the investigated area and cannot provide depth-resolved information. Further, it is not possible to distinguish between chemically bound and liquid water, which is why the time and cost intensive extraction of drilling cores is necessary to calibrate the data.

So far, Ground Penetrating Radar (GPR) is the most promising non-destructive method to enable the valuable depth information that is necessary to classify moisture damage in building floors. Commonly used in geophysics [8, 9], it is increasingly applied in civil engineering (CE) [10, 11], also to perform moisture measurements on building materials like asphalt, concrete, bricks, and screed [12, 13, 14, 15, 16, 17, 18, 19, 20]. A short overview

about the principle of moisture measurements with GPR is given in the following.

C.1.1 Moisture Measurement with GPR

By transmitting and receiving electromagnetic (EM) waves, GPR represents a suitable and sensitive method for material moisture measurement. Here, the electric permittivity ε is the considerable material parameter [21, 22], which is highly influenced by the amount of water present within an investigated area. This is explained by the high contrast of ε between a dry building material like concrete and water, lying between 2 to 9 [23] and 81 [24], respectively. An increased moisture content therefore causes higher electric permittivities of a medium, rising up to 10 to 20 for wet concrete. This has a significant influence on the propagation characteristics of EM waves, causing measurable lower amplitudes, longer travel times and lower frequencies of the received signals. When analyzing the measured data, extracting these features can therefore be used to give statements about underlying moisture contents. A specific review is given in [25], providing further literature about various applications of GPR for moisture measurements in CE.

C.1.2 Preceding Laboratory Study

To investigate common damage cases in floor constructions with GPR, a laboratory study was conducted and presented in the former publication of Klewe et al. [26]. Here, a modular specimen, shown in Figure C.1, was used to enable an interchangeable test setup. With that, the diverse practice of real floor construction was modeled by varying the layer thicknesses and materials of the screed and insulation layer, as listed in Table C.1.

The experimental program included the simulation of the three scenarios to be classified: (i) dry, (ii) insulation damage, and (iii) screed damage. Each scenario was investigated on 84 different floor constructions, which resulted in a data set of 252 measurements or 504 B-scans (each measurement included two orthogonal survey lines). The obtained data set then provided the basis to develop an identification strategy by extracting significant features, by which different classifiers were trained. The same features and classifiers are also used in this work and will be shortly presented later in C.2.2.

In the preceding study, high classification accuracies of 84 % to 88 % were achieved, which showed the general potential and suitable sensitivity of GPR to identify different moisture damage scenarios in building floors. Whether the developed methods and further findings can be directly applied on real damage cases is yet to be answered and therefore the key question of the following on-site study.

C.2 Methods

C.2.1 On-Site Measurements

The investigations on real floor damages were conducted on five different on-site locations in Germany during the period from December 2019 to March 2021. The affected buildings and their conditions varied widely and involved a recreation center, a restaurant, a community center, a student residence, and a parking garage. In the following, the different measurements are labeled according to their cities, in which they were performed: (i) Berlin, (ii) Grossenseebach, (iii) Nürnberg, (iv) Pegnitz and (v) Wunsiedel.



Figure C.1: Modular test specimen with screed, insulation, and concrete base layer (left, middle) and the simulation of an insulation damage by adding water to the setup (right).

Table C.1: Used materials and layer thicknesses for the screed (top) and insulation layer (bottom).

Material	Thickness D [cm]
Cement screed (CT)	5, 6, 7
Anhydrite screed (CA)	5, 6, 7
Expanded polystyrene (EP)	2, 5, 7, 10
Extruded polystyrene (XP)	2, 5, 7, 10
Glass wool (GW)	2, 6, 10
Perlites (PS)	2, 6, 10

The general procedure of an investigation was the same for each case. Before conducting the data acquisition, a grid was established in all rooms of interest by marking numbered measurement points (MP). The spacing between neighbouring points ranged from approximately 1.5 m to 3 m, depending on the respective room design. As shown in Figure C.2, an MP (generally) defined the center of two 50 cm, orthogonal survey lines, on which a 2 GHz antenna pair was moved along in common-offset configuration. The antenna was connected to a SIR 20 from GSSI, recording 250 scans/meter. Therefore, an MP was investigated with two B-scans consisting of 125 A-scans each. Each A-scan covered the time window of 11 ns, sampled by 512 data points.

After conducting the GPR measurement, a drilling core of 6.8 cm diameter ranging from the floor surface to the insulation bottom was extracted at the MP (Figure C.2, right). The screed and insulation material were immediately separated and sealed in two plastic bags to avoid water evaporation. Later, the moisture content of each sample was determined by oven drying and weighing according to the Darr method [27]. The obtained values in wt% serve as a reference for the conducted GPR surveys. Here, values above 4 wt% and 0.5 wt% for cement- and anhydrite screed, respectively, and above 15 wt% for the insulation indicate a damage in the respective layer. This reference is used to label each survey line (or B-scan) with its respective real damage case. If both layers reveal a damage, which is not included in the laboratory study, the measurement is labeled as screed damage, since it is the top and therefore first layer influencing the emitted EM waves.

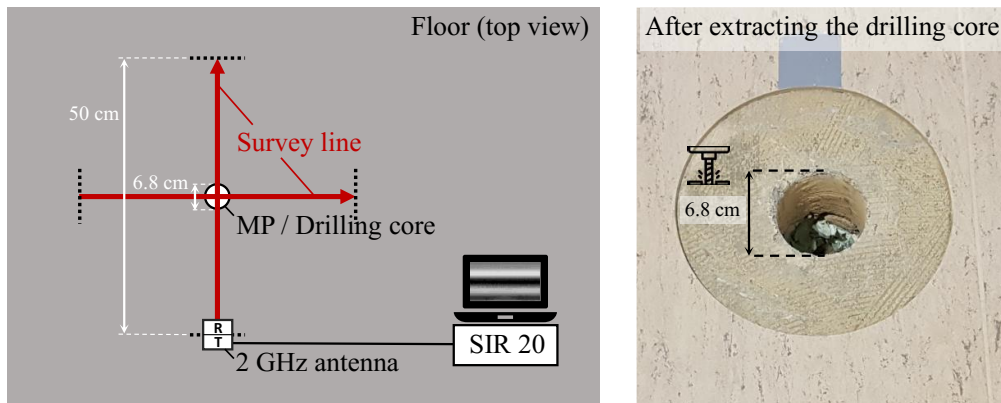


Figure C.2: GPR procedure (left) around a measurement point from which the reference drilling core is extracted (example right). It is covered by two 50 cm radar survey lines measured with the SIR 20 from GSSI and a 2 GHz antenna pair.

C.2.2 Feature Extraction

Since this work aims at validating a laboratory method by applying it on real damage cases, the same features as presented in the work of Klewe et al. [26] are used. However, the following description shall give a short overview of the underlying strategy.

GPR measurements on building floors usually show three prominent wave types, originating from certain areas within the construction. Box II in Figure C.3 gives an exemplary A-scan. The direct wave (DW) travels the shortest path between transmitter and receiver and is therefore measured first. It transmits partly over air and partly over the surface and is therefore sensitive to superficial screed moisture. The first reflection wave (RW1) originates from the transition between screed and insulation, whereas the second (RW2) forms between insulation and the underlying concrete layer. The former is sensitive to both, screed and insulation damages, whereas the second is mostly influenced by moisture in the insulation layer. The laboratory study [26] summarized in C.1.2, presented the following five A-scan features to classify moisture damage cases in building floors:

- Feature F_1 : A_{DW} - Amplitude of direct wave [14, 13, 15]
- Feature F_2 : A_{RW2} - Amplitude of 2nd reflection [14, 13, 15]
- Feature F_3 : f_{RW2} - Dominant frequency of 2nd reflection (STFT) [17]
- Feature F_4 : A_{RW1}/A_{DW} - Ratio between the amplitudes of 1st reflection and direct wave [16]
- Feature F_5 : f_{RW1}/f_{DW} - Ratio between the dominant frequencies of 1st reflection and direct wave

All these features are not only influenced by moisture, but also by parameters like the layer thicknesses of screed and insulation as well as their respective material. For on-site investigations, these parameters are usually unknown, which is why decisions based on pure thresholds regarding these features would not be applicable. Therefore, the A-scan features are further processed in terms of their variation within one survey line (or

B-scan), as shown in Figure C.3. The laboratory investigation revealed that dry floor constructions show no deviations for a specific feature when looking at a whole B-scan. However, a present damage influences the concerned reflection waves and causes variations, as shown with an exemplary insulation damage in box III of Figure C.3. Therefore, statistical measures like the standard deviation and the span were used to transform the vectorial A-scan features into scalar B-scan features (box IV), which worked well to distinguish damage cases within the laboratory data set. This was achieved by training different classifiers, which shall now be tested on the collected on-site data.

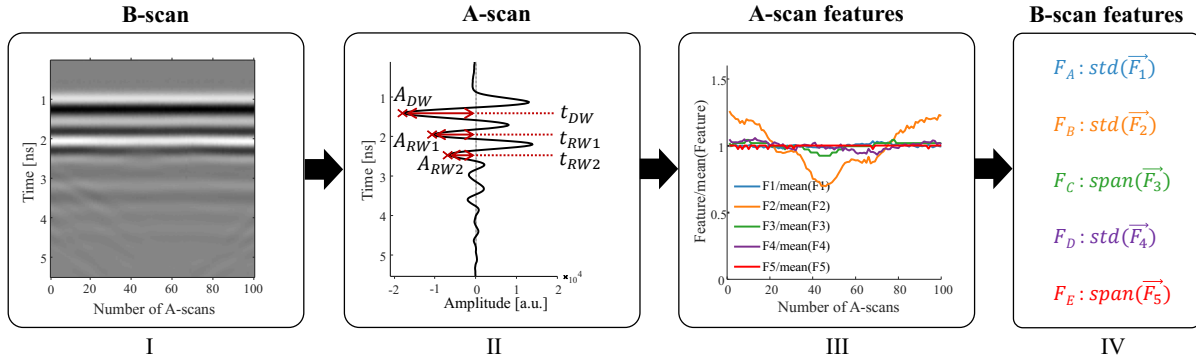


Figure C.3: Processing to extract A- and B-scan features.

C.2.3 Classification

To investigate the transferability of the introduced method into practice, the classifiers applied in this work are trained with the laboratory data obtained in the preceding study mentioned in C.1.2. Like there, from the python scikit-learn library [28] a multinomial logistic regression (MLR), random forest (RF), support vector machine (SVM), and artificial neural network (ANN) were used in standard configuration (default parameters only). However, the training process is slightly adjusted.

Instead of randomly splitting the data into training and test samples, groups of likely dependent measurements were defined to be used as separate test data. Therefore, the presence of a specific material (screed or insulation) with a certain thickness defines a particular group. For example, all measurements with a 5 cm EP insulation, or all measurements with a 7 cm CA screed, are separated from the training data to be used as test data. With the given variations in Table C.1, this leads to a total number of 20 groups. However, in the laboratory study, excluding all measurements with 2 cm insulation achieved higher accuracies, which is why this is also done here. Consequently, subsets of 16 groups were used to train and test each of the four classifiers, resulting in 64 trained models. Before performing the training, the data was standardized using the *StandardScaler* from the scikit-learn library for mean removal and a unit variance. This is done to avoid unwanted dominance of certain features with higher magnitudes.

The achieved mean accuracies of 84 % to 90 % by the classifiers were comparable to those from the preceding study, which suggests a sufficient independence of test and training data when performing random splits. However, the whole data set was still obtained in a single experimental program, which might lead to an overall dependence and overfitting. Applying trained classifiers to completely new data is always challenging, since

their ability to extrapolate is limited and governed by the training sample’s capability to represent the whole space of possibilities. To meet these problems, new data obtained from on-site measurements will be evaluated by all of the 64 classifiers, where each type (MLR, RF, SVM, and ANN) forms a voting group of 16 decisions. The voting group which is most certain with its decision (highest number of the same predicted class) sets the final classification. This method of generating multiple versions of a classifier by using different training sets is generally referred as bootstrap aggregating (or bagging) [29]. Here, it is applied to achieve more stable and accurate classifications of unknown on-site data. Again, before the classification, the on-site data is standardized by the same *StandardScaler* that was fitted and used on the laboratory training data.

C.3 Results

In total, 186 MPs (372 B-Scans) were collected over all five on-site locations in Germany (Berlin = 29; Grossenseebach = 33; Nürnberg = 44; Pegnitz = 48; Wunsiedel = 32). According to the extracted drilling cores, 50 MPs were labeled as dry, 45 MPs as insulation damage, and 93 MPs as screed damage. First, this section gives insights into overall characteristics of the measured data, followed by a detailed analysis of the achieved classification results.

C.3.1 On-Site Measurements

Figure C.4, C.5, and C.6 show exemplary and representative on-site measurements of building floors with the three regarded damage scenarios dry, insulation damage, and screed damage, respectively. Each figure contains two collected B-scans and their extracted A-scan features. Since a drilling core was extracted for each MP, the obtained layer thickness and moisture content for screed and insulation are provided in the bottom right corner of each B-scan. The transparent-white, vertical bars mark the position of the extracted drilling cores within the survey lines

Example a) in Figure C.4 presents a dry-labeled measurement comparable to those collected in the laboratory study (also shown later in Figure C.11). The B-scan barely shows horizontal deviations for DW, RW1 and RW2, which can indicate the absence of water within the investigated area. Nevertheless, the extracted A-scan features reveal dynamics in F_2 , F_4 , and F_5 , including all regarded wave types from section C.2.2. Compared to the significantly calmer and flatter shapes obtained in the laboratory study, this might suggest a generally higher heterogeneity of underlying material parameters like layer thickness or moisture content within an on-site survey line. This assumption is further underlined by the second dry example in Figure C.4 b). Here, already the B-scan shows clear horizontal deviations, which are also captured by the respective A-scan features. The increased travel time in the survey line’s second half could either result from a rising screed thickness or a higher screed moisture. However, the likewise decreasing amplitude of DW (represented by the blue F_1) rather indicates a rising moisture content, since this feature is especially sensitive to superficial screed moisture and is not influenced by the underlying layer thickness.

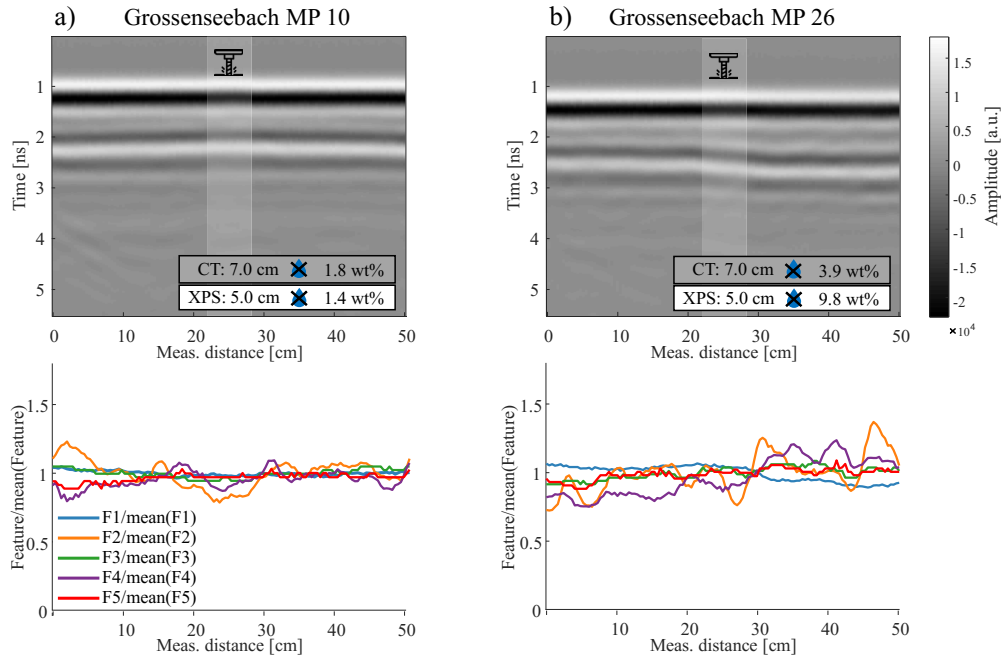


Figure C.4: Two exemplary B-scans (top) and their respective A-scan features (bottom) of dry on-site floors in Grossenseebach. The transparent-white, vertical bars mark the position of the extracted drilling cores within the survey lines. The obtained thickness and moisture content of screed and insulation are given in the B-scan’s bottom right corner.

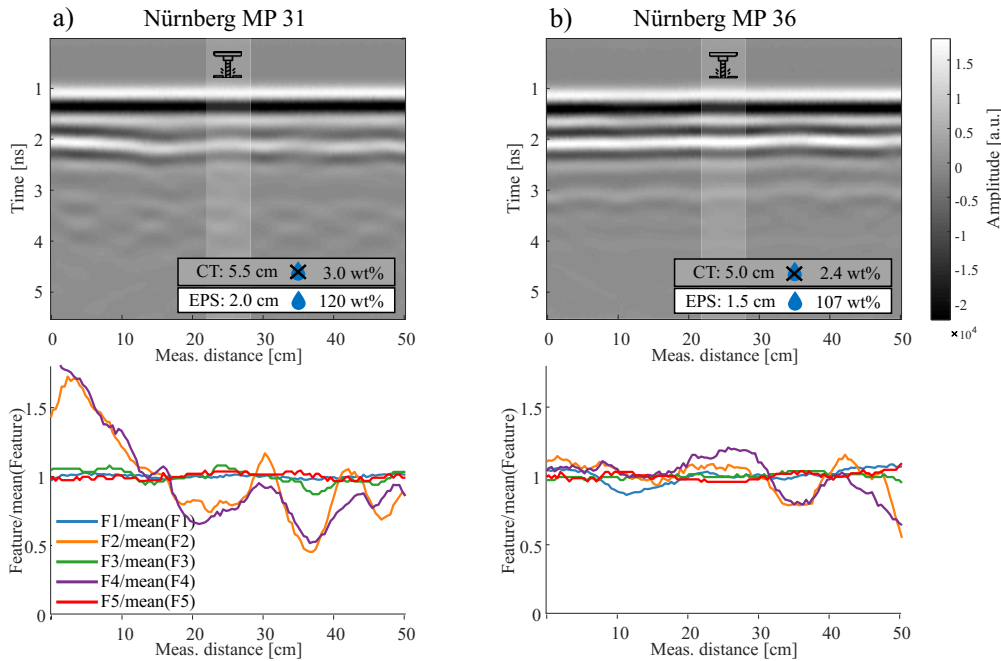


Figure C.5: Two exemplary B-scans (top) and their respective A-scan features (bottom) of on-site floors with insulation damage in Nürnberg. The transparent-white, vertical bars mark the position of the extracted drilling cores within the survey lines. The obtained thickness and moisture content of screed and insulation are given in the B-scan’s bottom right corner.

The drilling core extracted on MP 31 in Nürnberg, shown in Figure C.5 a), clearly enabled the location of a damaged insulation with 120 wt%. Also the respective GPR measurement presents significant amplitude deviations for RW1 and RW2, while DW remains rather constant. Such attenuation patterns of RW1 and RW2 are quite common for water inside the insulation layer and could be also observed within the laboratory study. Similar influences can be seen in MP 36, however they appear not that distinct as in MP 31. Besides RW1 and RW2, also DW shows slight deviations. This impedes a clear interpretation, since the obtained radar data could be mistaken for both a dry setup or a damaged screed. However, the increased dynamic of F_2 and F_4 between 20 cm to 50 cm, where F_1 remains comparably calm, rather indicates an insulation damage.

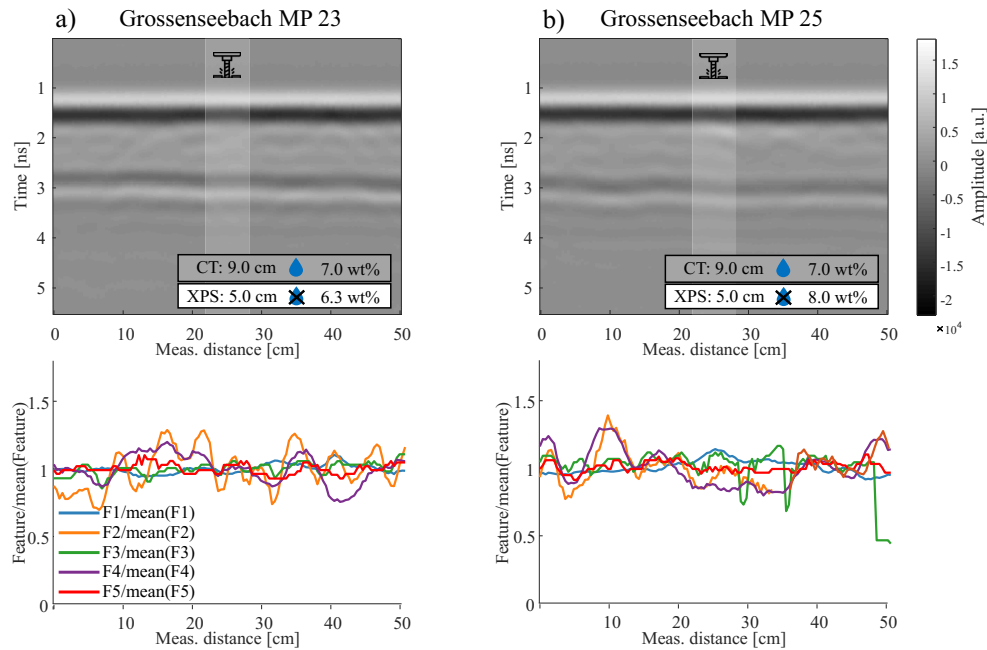


Figure C.6: Two exemplary B-scans (top) and their respective A-scan features (bottom) of on-site floors with screed damage in Grossenseebach. The transparent-white, vertical bars mark the position of the extracted drilling cores within the survey lines. The obtained thickness and moisture content of screed and insulation are given in the B-scan’s bottom right corner.

Figure C.6 shows two typical measurements on floors with screed damage, both containing quite high moisture contents of 7 wt%. The most obvious indication is the highly attenuated DW, shown by a lower contrast between 1 ns and 2 ns in both B-scans. However, such a threshold-based amplitude feature is not captured by the applied extraction strategy, since statistical measures along the horizontal space axis are considered. Only by comparing the measurements with other MPs like those from Figure C.4, the difference becomes clear. Without dry references, such patterns could also be caused by a more attenuating floor cover or a generally lower gain within the GPR system. However, the integral measuring principle of GPR reflections enables screed damages to influence all considered wave types. Therefore, variations in every feature, as they are present in both examples of Figure C.6, tend to suggest a measured screed damage.

Besides the general presence of multiple unknown parameters when performing on-site moisture measurements with GPR, also other obstacles occurred during the investigations. One of the most common problems was the presence of floor heating, which can be

exemplary seen in Figure C.7. Positioned directly below the screed, the reflection patterns occur before the expected RW1 and impede an application of the presented strategy. Therefore, all measurements containing clear indications of a present floor heating were discarded from the data set. Unfortunately, this was the case for nearly every measurement point in Pegnitz, Wunsiedel, and Berlin, which is why these data sets will not be considered in the following application of classification models. However, it shall be noted that in the example of Wunsiedel, the clearly visible rising attenuation with higher moisture contents could enable a closer investigation of screed damages.

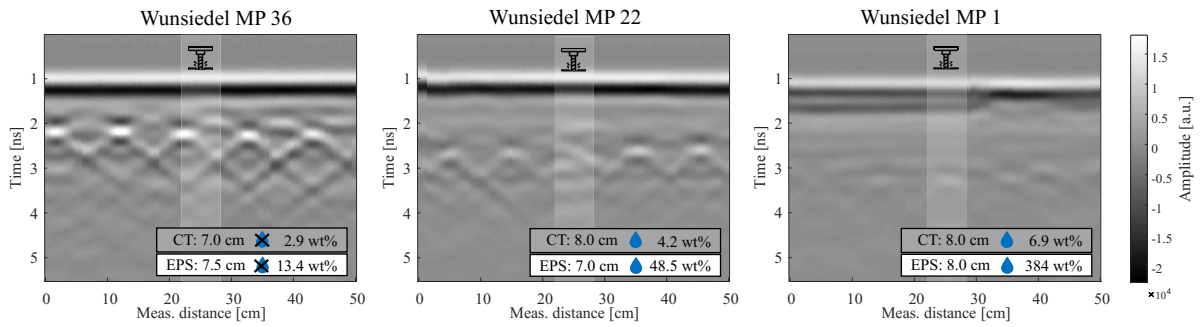


Figure C.7: Disturbing floor heating exemplary shown by three measurements from Wunsiedel. The moisture contents for both, screed and insulation, rise from left to right.

Another problem occurred within eight measurements in Grossenseebach, where a screed reinforcement mesh also hindered the application of the presented classification strategy. As it can be seen in Figure C.8, these structures appear like floor heating, however with much smaller spacing. Again, all measurements affected were discarded from the Grossenseebach data set.

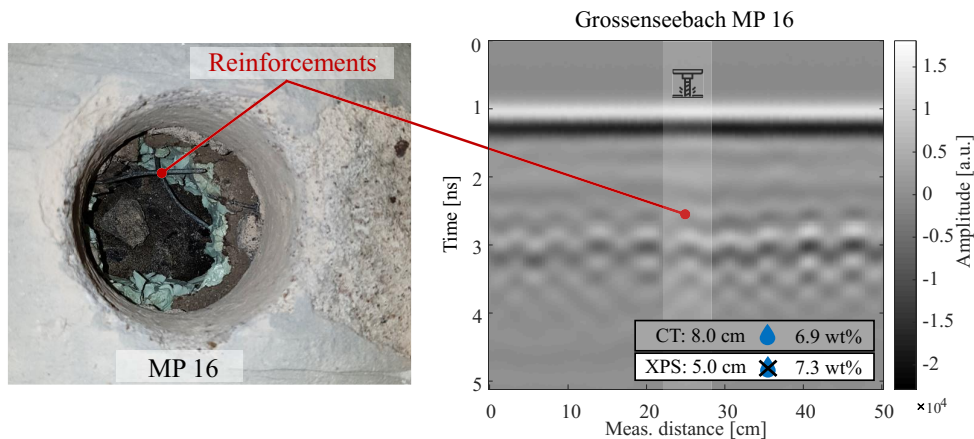


Figure C.8: Screed reinforcement mesh visible inside the drilling hole of MP 16 (left) and in the respective B-scan (right).

In Nürnberg, a steel beam within the survey line affected the B-scans of seven MPs, as shown in Figure C.9. Furthermore, it was located in a room with no insulation inside the floor structure. Since such a scenario was not part of the laboratory study, the twelve MPs collected in that area were discarded.

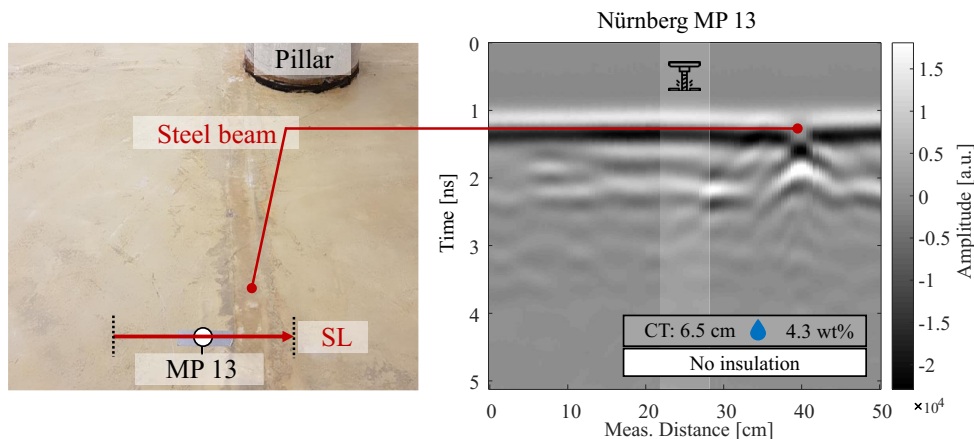


Figure C.9: Steel beam within the survey line (SL) of MP 13 in Nürnberg (left) and the respective B-scan (right).

C.3.2 Classification of On-Site Measurements

As discussed above, only on-site measurements from Grossenseebach and Nürnberg are considered for classification. After removing the data disturbed by screed reinforcement, a steel beam, and the absence of an insulation layer, both data sets contained 50 and 62 B-scans from 25 and 31 MPs, respectively. On these data sets, the feature extraction described in C.2.2 was performed. Here, the processing was not able to always detect all five features for each measurement. In some B-scans, highly attenuated or interfered wave types impeded a clear separation or recognition of those, which resulted in NaN-values for the affected features. Due to that, another 24 B-Scans from Grossenseebach and 16 B-Scans from Nürnberg had to be discarded. As a result, 26 and 46 B-scans remained for both data sets, respectively.

The described narrowing of usable data already points out some clear limitations when performing automated classification approaches on on-site GPR measurements. Nevertheless, the remaining measurements were classified by means of their extracted features. Figure C.10 shows the achieved accuracies and confusion matrices for both data sets. The overall accuracies of 46.2 % for Grossenseebach and 56.5 % for Nürnberg are significantly below those achieved on the laboratory data, laying between 84 % and 90 %. Such a difference often indicates a problem with overfitting [30]. Looking at the confusion matrices reveals that most of the measurements in both data sets were classified as screed damage. This especially questions the significance of the already low accuracies. It does not get clear whether the classification shows good sensitivity for screed damage or if the higher hit rate is a coincidence due to the amount of such cases within the data set. As stated in C.2.1, on-site measurements with damage in both layers were labeled as screed damage. Removing these samples would discard all 28 screed damage samples from the Nürnberg data, (which showed a damaged insulation in each MP), resulting in an overall accuracy based on the remaining 3 out of 15 correctly classified insulation damages.

Applied on new on-site data the automatic classification trained on laboratory data failed to reach the laboratory accuracy. The reasons for this performance shall be discussed in the following section by presenting a deeper analysis of the underlying data sets, focusing on their limitations, pitfalls, however also on their chances for further investigations of moisture damage in building floors with GPR.

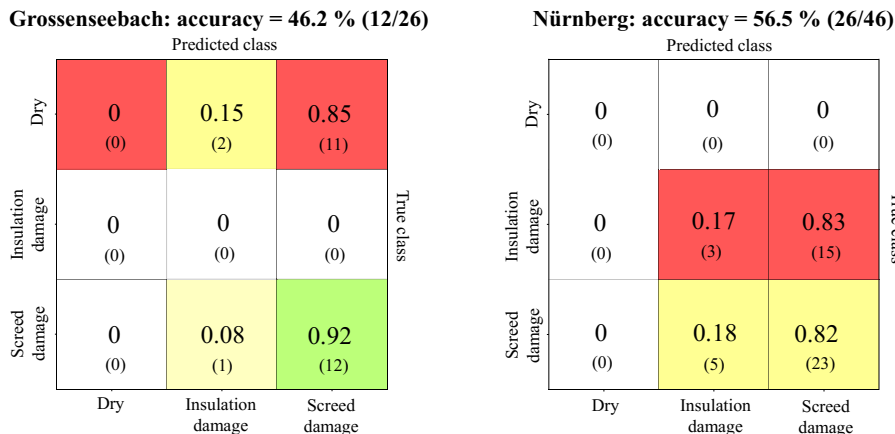


Figure C.10: Classification results of the data sets Grossenseebach and Nürnberg represented by their individual overall accuracy and confusion matrices. Each cell includes the relative (decimal number) and numerical (natural number in brackets) amount of classified cases.

C.4 Discussion

Like already stated, the classification of on-site data based on training data from laboratory revealed poor accuracies. The authors postulate that this is an indication for overfitting. Therefore, looking at representative examples from the laboratory training data should give insight into the classifier’s basis of decision-making when applied on new on-site data.

Figure C.11 presents typical measurements on the cases dry, insulation damage and screed damage within the laboratory experiments. While the B-scans show clear differences between each other, the horizontal A-scan feature distributions below reveal a remarking similarity for the dry measurement and the screed damage measurement. As already discussed in the laboratory study [26], the homogeneous screed damages resulted due to an evenly spread moisture ingress over the entire screed sample. Therefore, all features remain comparatively constant throughout the whole measuring distance. Such a similarity and the consequential danger of confusion between a dry floor and a screed damage was also observed and discussed within the on-site data (section C.3.1), whereas the A-scan features generally show higher dynamics for both damage cases (Figure C.4 and C.6). For such similar distributions, also the B-scan features resemble one another, since they capture occurring deviations by the standard deviation and span. Concerning the laboratory training data, the classifiers had to separate closely situated data points within the feature space to achieve a successful recognition of all damage scenarios. The good accuracies of 84 % to 90 % on the laboratory test data verify such an effective, however narrow decision boundary. By keeping in mind, that such small deviations, as they can be seen for the A-scan feature distributions of laboratory screed damages, are sufficient to separate the laboratory data, it becomes clear that the more dynamic on-site data is mostly categorized as screed damage.

However, the question remains why the on-site data generally shows rather unsteady B-scans compared to the laboratory experiments, especially for dry floors and screed damage. As already addressed in section C.3.1, an overall higher heterogeneity of underlying material parameters like layer thickness or moisture content within one survey line could explain this observation.

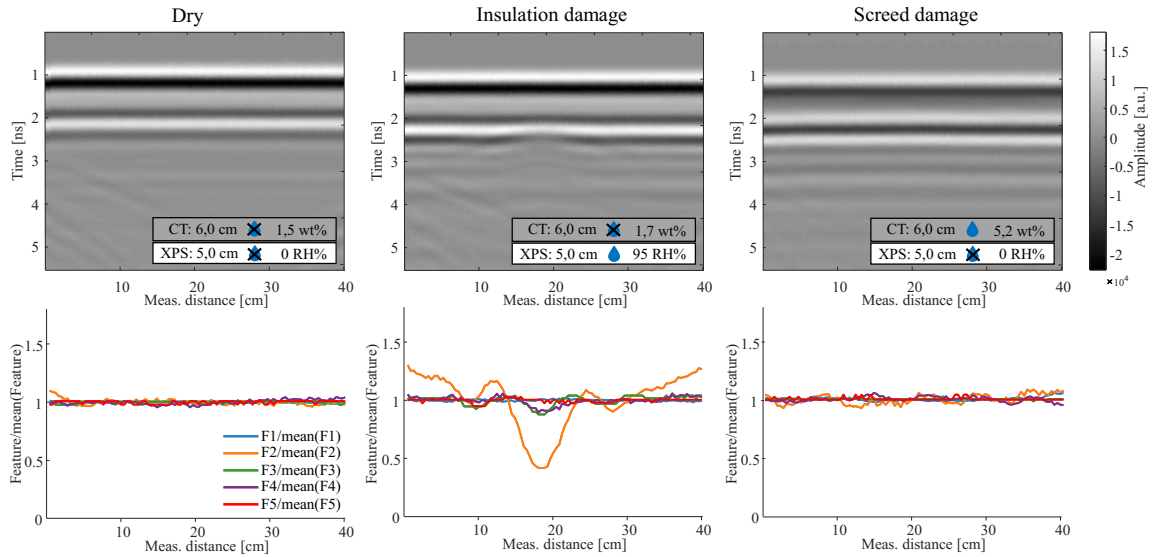


Figure C.11: Exemplary laboratory B-scans (top) and their respective A-scan features (bottom) at an 6 cm CT and 5 cm XPS floor construction for the scenarios: dry, damage insulation, and damage screed.

One indication arises by looking at the layer thicknesses obtained from all the drilling cores extracted throughout the investigations. Figure C.12 and C.13 summarize these values for each of the considered and discarded on-site investigations, respectively. Changing rooms within the buildings are marked by a different background color, grey or white. It shows that even within one room, the thicknesses of screed and insulation can vary drastically, which is why a survey line of 50 cm length is likely to be influenced by these variations. In practice, screed or insulation are sometimes used to level uneven heights within the floor construction, which causes thickness variations. In contrast to the controlled laboratory experiments, where most parameters (and especially the layer thickness) were kept constant, on-site investigations may include considerably more unknown influences. Such circumstances obviously disturb the underlying assumption, that deviating features within a B-scan indicate the presence of moisture.

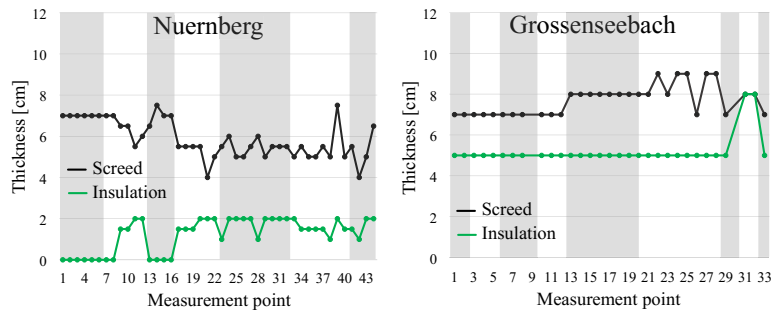


Figure C.12: Layer thicknesses of screed (black) and insulation (green) for every MP in the classified data sets of Nürnberg and Grossenseebach. The alternating background of white and grey signalizes changing rooms.

Another unknown influence is caused by the spacial limitation of extracted drilling cores, which are used as a reference. This becomes particularly clear by considering the relatively small section a drilling core (6.8 cm diameter) covers of a whole survey line (50 cm). The

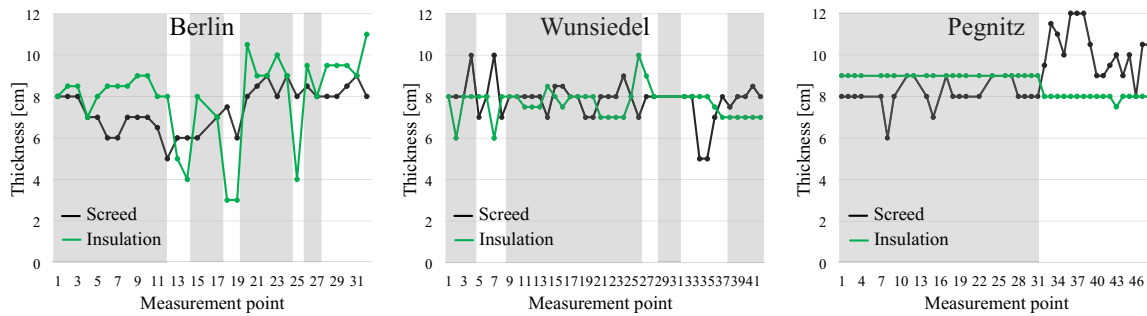


Figure C.13: Layer thicknesses of screed (black) and insulation (green) for every MP in the discarded data sets of Berlin, Wunsiedel, and Pegnitz. Points within one background bar (white or grey) were located in the same room.

transparent white bar in every on-site B-scan within this work visualizes this relation. The resulting difficulties were already mentioned in the discussion of Figure C.4 b), where the decreasing amplitude of the direct wave indicated a rising screed moisture content within the B-scan. Such indications shall further be analyzed by looking at neighboring MPs, as it was the case for MP 40 and MP 34 in Nürnberg (see Figure C.14). The former MP, measured by survey line a) shows a referenced moisture damage for both, screed and insulation, whereas the latter MP, measured by survey line b), revealed an insulation damage. Between MP 40 and MP 34, the screed moisture decreased from 4.8 wt% to 3.0 wt%. In the considered survey line of MP 34, the antenna was moved away from MP 40. Apparently, the transition from a moist to a dryer screed gets visible in the respective B-scan between 15 cm and 25 cm measuring distance. The drilling core was positioned off center around 32 cm due to a room wall limiting the survey line's expansion. It is therefore located in the right half of the B-scan where a decreasing travel time and increasing amplitudes of all wave types suggest a dryer floor setup. The whole survey line seems to include two damage cases, a screed and insulation damage (like in MP 40) in the left half, and a sole insulation damage (like referenced for MP 34) in the right half. Another example of such a transition within a B-scan is given in Figure C.15, showing the neighbouring MPs 2 and 3 in Grossenseebach. Here again, the referenced screed moisture content decreases from the former MP (5.1 wt%) to the latter (3.0 wt%), whereas the insulation's state stays dry for both measurements (5.2 wt% and 3.8 wt%, respectively). Likewise, the increasing amplitude of the DW and the decreasing travel time of RW1 and RW2 in survey line b) seem to display the changing scenario from a screed damage to a dry floor setup. While these observations speak for a satisfying resolution and information depth when applying GPR for moisture measurements, they tend to disturb the evaluation of the applied classification strategy. In contrast to the laboratory, multiple damage scenarios within one measurement are a realistic incident and pose a significant uncertainty when classifying an entire B-scan.

Although the application of the automatized classification approach achieved poor results, the general sensitivity of the extracted features for the considered damage cases got clear throughout the investigations. Especially screed damages showed strong indications by influencing every regarded wave type. In case of an observed transition to or from a moist screed, the DW emerged as a valuable source of information, since it is not affected by the underlying layer thickness. If there is no transition visible, a general danger of confusion

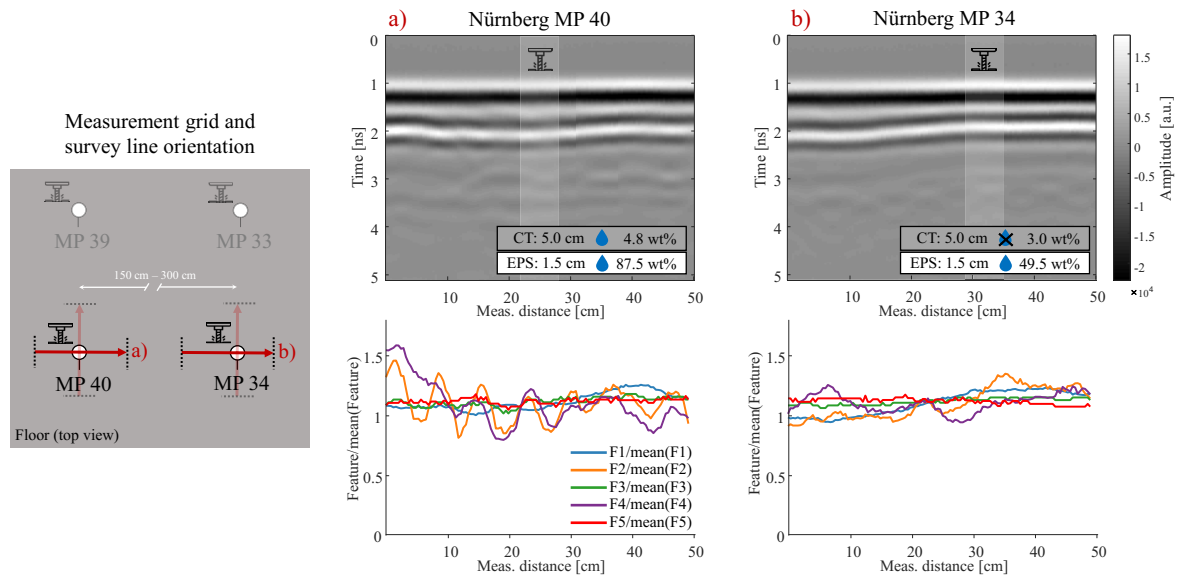


Figure C.14: B-scans and extracted A-scan features of the two neighbouring MPs 40 and 34 in Nürnberg. Their orientation within the room is shown by the measurement grid on the left.

to a dry floor setup remains. Here, comparing different MPs within one on-site investigation might allow the detection of attenuated DWs to narrow down affected areas.

In practice, the identification of an insulation damage is even more important, as there are no other sensitive NDT methods available. Also here, the gathered information within the laboratory and the on-site study revealed valuable findings. In addition to the given examples in Figure C.5 and C.11, Figure C.16 shows measurements from Nürnberg (MP 17 and MP 24) and from the laboratory setup on similar floor setups. The prominent deviations of RW1 and RW2, captured by F_2 , F_3 and F_4 with an concurrently constant DW, captured by F_1 , give good indications for moisture in the insulation layer. The slightly visible reflection hyperbolas might result from small areas with high water content, like in fully filled insulation joints. This was already observed in the laboratory study.

The last example shows, that despite the significant differences between on-site and laboratory investigations, there are still valuable similarities that can be used to analyze new, practical data. With the increased number of unknown parameters for on-site investigations, a solid base of knowledge of how to interpret given results, becomes more important. Here, the considered and extracted features deliver a profound support to tackle this challenge.

Applying automatized classification approaches solely trained by laboratory data clearly emerged as unprofitable. However, including on-site data into the training process might help to adjust the decision boundaries within the feature space to achieve a robust detection of all scenarios. For this purpose, a significantly bigger data basis would be necessary.

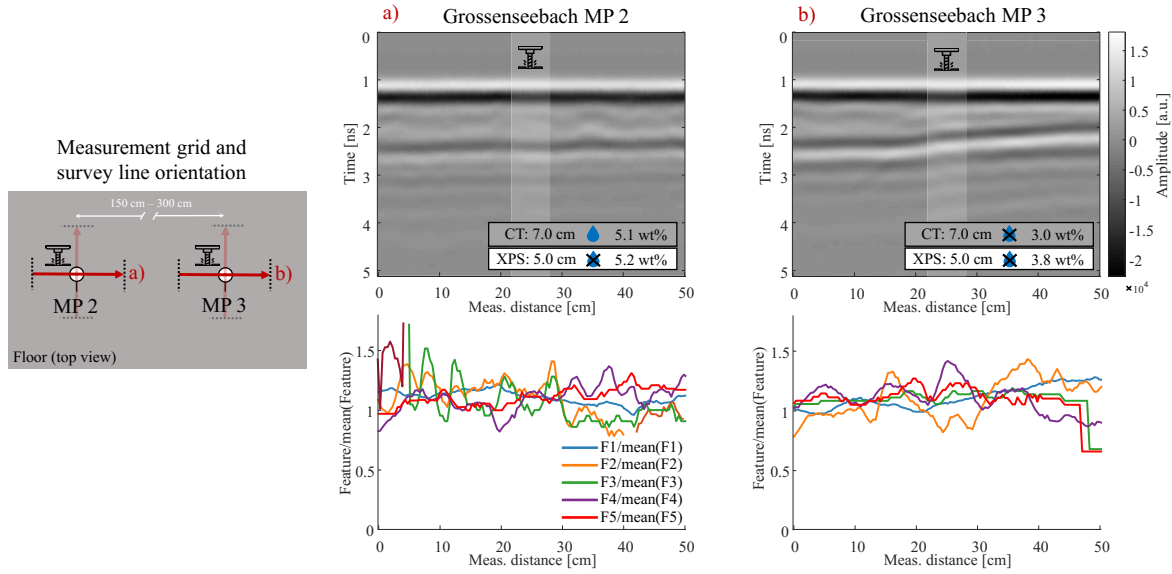


Figure C.15: B-scans and extracted A-scan features of the two neighbouring MPs 2 (a) and 3 (b) in Grossenseebach. Their orientation within the room is shown by the measurement grid on the left.

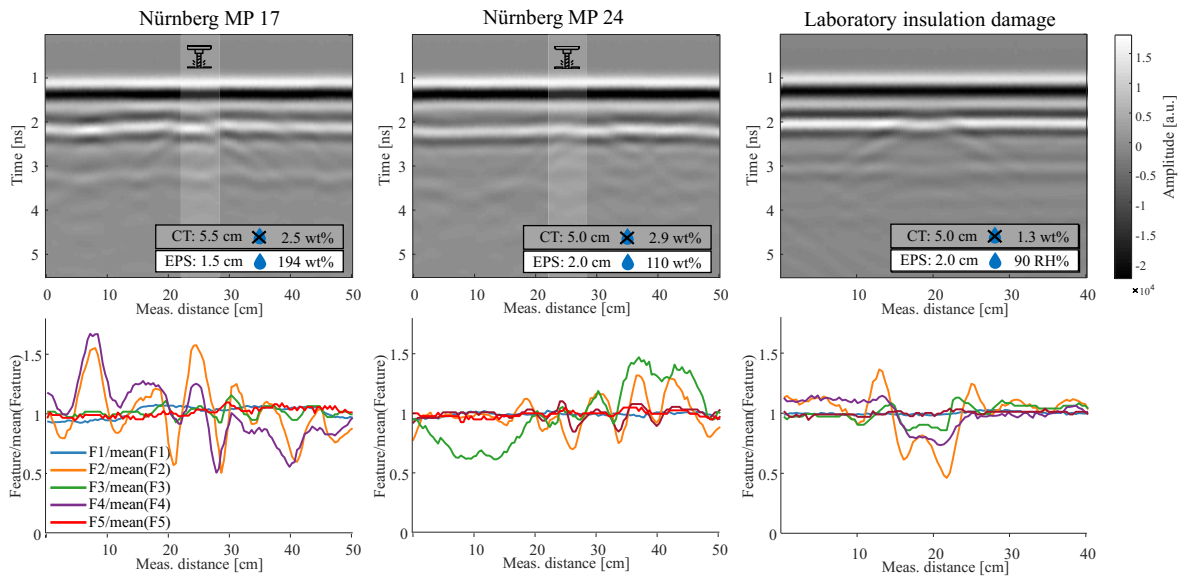


Figure C.16: Exemplary B-scans and A-scan feature distribution of two on-site insulation damages from Nürnberg (MP 17 and MP 24) compared to a laboratory insulation damage with similar floor setup.

C.5 Summary and Conclusion

This work presented the application of classifiers trained by GPR data obtained in a preceding laboratory study to categorize on-site moisture damage scenarios in layered building floors. Five differently affected buildings, all located in Germany, had been investigated for this purpose. The extraction of drilling cores for each MP served as a reference by obtaining the screed’s and insulation’s material type, layer thickness, and moisture content. Thereby, each on-site measurement was labeled with its respective da-

mage scenario, which allowed a quantitative evaluation of the classifier's performance. Already before conducting the classification, numerous MPs had to be discarded when there was floor heating, screed reinforcements, steel beams or no insulation layer within the investigated area. Furthermore, some measurements with highly attenuated or disturbed reflections impeded the extraction of all relevant features and had to be removed from the data sets. The classification of the remaining measurements achieved poor accuracies. Analyzing the well classified laboratory data led to an overfitting problem due to small deviations between measurements on dry floors and measurements on screed damages, which resulted in a narrow decision boundary within the feature space. Therefore, the generally more heterogeneous and dynamic on-site B-scans were commonly interpreted as screed damages.

Reasons for the more unsteady reflection patterns of practical floor setups were identified by varying material parameters within one survey line. Significantly changing layer thicknesses and damages of screed and insulation within one survey line caused frequent misinterpretations of the respective B-scans. This is worsened by the general spatial limitation of extracted drilling cores and their generated reference that cannot eliminate all the unknown parameters that real setups in on-site investigations include.

However, closely analyzing the obtained data allowed to demonstrate the feature's sensitivity for different damage scenarios. Still, for successful interpretations a lot of expert knowledge about the application of GPR on building floors is required. To a certain extent, that knowledge could be provided by the results of this work. Especially insulation damages, which are rarely recognized by all other NDT methods, showed characteristic patterns within the obtained results. This highlights the uniqueness of GPR for moisture measurements on layered structures. In order to efficiently support the analysis of trained personnel, fully automatized approaches with machine learning still require a much bigger and diverse data basis. Consequently, realistic on-site data should definitely be included into the training process to achieve robust and valid decision boundaries that allow a reliable classification of moisture damage scenarios in building floors. Additionally, more labeled examples of different on-site measurements would help to cover the wide range of possibilities, that occur in practice. This could either be achieved by an extensive research program or the establishment of an open data repository for GPR and other NDT investigations. The latter is seen as a key element, which would enable machine learning to develop its promising potential within NDT-CE.

Bibliography

- [1] J. B. Harley and D. Sparkman. Machine learning and NDE: Past, present, and future. 2019.
- [2] GDV. Annual of Gesamtverband der Deutschen Versicherungswirtschaft e.V. <https://www.gdv.de/de/zahlen-und-fakten/versicherungsgebiete/wohngebaeude-24080>, 2019. Accessed on 20/07/2021.
- [3] M. J. Mendell, J. M. Macher, and K. Kumagai. Measured moisture in buildings and adverse health effects: A review. *Indoor Air*, 28(4):488–499, may 2018.
- [4] P. J. Annala, M. Hellemaa, T. A. Pakkala, J. Lahdensivu, J. Suonketo, and M. Pentti. Extent of moisture and mould damage in structures of public buildings. *Case Studies in Construction Materials*, 6:103–108, jun 2017.
- [5] S. Kruschwitz. Feuchtemessung im Bauwesen - ein Überblick. *Fachtagung Bauwerksdiagnose, Vortrag 5*, 2014.
- [6] L.-O. Nilsson, editor. *Methods of Measuring Moisture in Building Materials and Structures*. Springer International Publishing, <https://doi.org/10.1007/978-3-319-74231-1> 2018.
- [7] D. S. Chanasky and M. A. Naeth. Field measurement of soil moisture using neutron probes. *Canadian Journal of Soil Science*, 76(3):317–323, aug 1996.
- [8] J. A. Huisman, S. S. Hubbard, J. D. Redman, and A. P. Annan. Measuring Soil Water Content with Ground Penetrating Radar: A Review. *Vadose Zone Journal*, 2(4):476–491, nov 2003.
- [9] L. Slater and X. Comas. The Contribution of Ground Penetrating Radar to Water Resource Research. In *Ground Penetrating Radar: Theory and Applications*. Elsevier, 2009.
- [10] F. Lombardi, F. Podd, and M. Solla. From Its Core to the Niche: Insights from GPR Applications. *Remote Sensing*, 14(13):3033, jun 2022.
- [11] W. L. Lai, X. Dérobert, and P. Annan. A review of Ground Penetrating Radar application in civil engineering: A 30-year journey from Locating and Testing to Imaging and Diagnosis. *NDT&E International*, 96:58–78, jun 2018.
- [12] T. Saarenketo and T. Scullion. Road evaluation with ground penetrating radar. *Journal of Applied Geophysics*, 43(2-4):119–138, mar 2000.
- [13] G. Klysz and J.-P. Balayssac. Determination of volumetric water content of concrete using ground-penetrating radar. *Cement and Concrete Research*, 37(8):1164–1171, aug 2007.
- [14] K. Grote, S. Hubbard, J. Harvey, and Y. Rubin. Evaluation of infiltration in layered pavements using surface GPR reflection techniques. *Journal of Applied Geophysics* 57, 57(2):129–153, feb 2005.

- [15] S. Laurens, J. P. Balayssac, J. Rhazi, G. Klysz, and G. Arliguie. Non-destructive evaluation of concrete moisture by GPR: experimental study and direct modeling. *Materials and Structures* 38, 38(9):827–832, nov 2005.
- [16] W. L. Lai, S. C. Kou, W. F. Tsang, and C. S. Poon. Characterization of concrete properties from dielectric properties using ground penetrating radar. *Cement and Concrete Research*, 39(8):687–695, aug 2009.
- [17] W. L. Lai, T. Kind, S. Kruschwitz, J. Wöstmann, and H. Wiggenhauser. Spectral absorption of spatial and temporal ground penetrating radar signals by water in construction materials. *NDT & E International*, 67:55–63, oct 2014.
- [18] F. Kurz and H. Sgarz. Measurement of Moisture Content in Building Materials using Radar Technology. *International Symposium Non-Destructive Testing in Civil Engineering (NDT-CE)*, 2015.
- [19] A. Hola. Measuring of the moisture content in brick walls of historical buildings – the overview of methods. *IOP Conference Series: Materials Science and Engineering*, 251:012067, oct 2017.
- [20] I. Garrido, M. Solla, S. Lagüela, and N. Fernández. IRT and GPR Techniques for Moisture Detection and Characterisation in Buildings. *Sensors*, 20(22):6421, nov 2020.
- [21] J. L. Davis and A. P. Annan. Electromagnetic Detection of Soil Moisture: Progress Report I. *Canadian Journal of Remote Sensing*, 3(1):76–86, dec 1977.
- [22] M. N. Soutsos, J. H. Bungey, S. G. Millard, M. R. Shaw, and A. Patterson. Dielectric properties of concrete and their influence on radar testing. *NDT&E International*, 34(6):419–425, sep 2001.
- [23] D. J. Daniels. *Ground Penetrating Radar - 2nd Edition*. The Institution of Engineering and Technology, 2007.
- [24] G. C. Topp, J. L. Davis, and A. P. Annan. Electromagnetic Determination of Soil Water Content: Measurements in Coaxial Transmission Lines. *Water Resources Research*, 16(3):574–582, jun 1980. <https://doi.org/10.1029/WR016i003p00574>.
- [25] T. Klewe, C. Strangfeld, and S. Kruschwitz. Review of moisture measurements in civil engineering with ground penetrating radar – applied methods and signal features. *Construction and Building Materials*, 278:122250, apr 2021.
- [26] T. Klewe, C. Strangfeld, T. Ritzer, and S. Kruschwitz. Combining Signal Features of Ground-Penetrating Radar to Classify Moisture Damage in Layered Building Floors. *Applied Sciences*, 11(19):8820, sep 2021.
- [27] ASTM D2216-19. Standard Test Methods for Laboratory Determination of Water (Moisture) Content of Soil and Rock by Mass. *ASTM Vol. 04.08*, 2019.
- [28] F. Pedregosa, G. Varoquaux, A. Gramfort, V. Michel, B. Thirion, O. Grisel, M. Blondel, P. Prettenhofer, R. Weiss, V. Dubourg, J. Vanderplas, A. Passos, D. Cournapeau, M. Brucher, M. Perrot, and E. Duchesnay. Scikit-learn: Machine Learning in Python. *Journal of Machine Learning Research*, 12:2825–2830, 2011.

- [29] L. Breiman. Bagging predictors. *Machine Learning*, 24(2):123–140, aug 1996.
- [30] T. Dietterich. Overfitting and undercomputing in machine learning. *ACM Computing Surveys*, 27(3):326–327, sep 1995.

Synthesis

3	Discussion	95
	3.1 Summary of Results	95
	3.2 Literature Review	96
	3.3 Materials and Preliminary Studies	97
	3.4 Laboratory Investigations	99
	3.5 On-Site Investigations	103
	3.6 Concluding Discussion	106
4	Outlook	109
	Bibliography	110
	List of Tables	111
	List of Figures	113
	Abbreviations	116

3. Discussion

This thesis researched the suitability of the GPR method for automated classification of typical moisture damage on building floors with unknown parameters by the use of machine learning. The three common cases considered were: (i) dry, (ii) damaged insulation and (iii) damaged screed, which were to be investigated using a comprehensive data acquisition in the laboratory and on-site.

In the following synthesis, all findings of the thesis are first summarized and thus brought into a logical context. Thereafter, a comprehensive discussion of these results and the applied methodology is given, which is structured according to the respective chapters and publications. Here, the decisions made and the directions taken to answer the research questions will be elaborated and critically evaluated.

3.1 Summary of Results

The literature review presented in publication A was conducted to work out the theoretical basics and to identify the most common methods for detecting moisture in building materials using radar signals. Here, it especially became clear that all publications only investigated individual time-, amplitude- or frequency features separately, without combining them. This was seen as a potential aspect for innovation, as the multivariate application of several signal features can help to overcome individual weaknesses and limitations. Therefore, this approach was also followed in the further process of the work, whereby the literature review initially provided potential candidates for selection and did not exclude any signal features from the start.

In chapter 2, preliminary investigations carried out on drying screed samples confirmed the profitable use of multivariate evaluations (Figure 2.11). In addition to the general suitability and dependencies of various features, first limitations due to possible interference between DW and RW could be identified (Figure 2.10). This is particularly evident with thin or dry materials, for which the two-way travel times of the reflected radar signals become shorter. Thus, quantitative moisture measurements were excluded and a qualitative evaluation for the detection of damage cases was planned.

In order to develop such a method, an extensive laboratory experiment was carried out to study the effect of water-damaged insulation layers and screed layers on GPR measurements, which was presented in publication B. For this purpose, a modular test specimen was designed, which allowed the variation of the most decisive parameters, the material type and thickness of screed and insulation, as well as the simulation of moisture damages. The data collected revealed clear differences between dry and damaged structures, which were represented by the water-induced deviations within measured B-scans (Figure B.9). These deviations were to be detected with the newly introduced B-scan features, which evaluate the statistical deviation of A-scan features within a survey line. This was to ensure the detection of damage cases independent of the underlying material parameters. In a subsequent training and cross-validation process of different classifiers,

the suitability of the developed B-scan feature strategy was confirmed within the laboratory data set. Accuracies of over 88 % of the 504 recorded measurements (252 different experimental setups) were achieved (Table B.2). False classifications occurred primarily in some cases of damaged insulation, where the small amounts of added water were not sufficient to penetrate the measured area of the radar survey line (Figure B.13). Since only dry parts of the construction were measured in that case, the classification as such shows the good sensitivity of the method. The combination of amplitude and frequency features, which covered all relevant reflections of the radar signals, was particularly beneficial. Thus, again the application of multivariate methods turned out to be a suitable approach. Furthermore, the data set showed only small differences between dry floors and damaged screeds for the B-scan features (Figure B.10), which could be attributed to a homogeneous distribution of the water added in the screeds. However, these small differences were successfully separated by the trained models (Figures C.10 and B.15), raising the suspicion of overfitting. The consequences of this were then examined in more detail by means of a validation with on-site data.

For this purpose, investigations were carried out at five different locations in Germany, which are presented in publication C. To ensure comparability, the measurement method remained identical to the laboratory experiments. By extracting drilling cores, it was possible to determine the damage case for each measurement point and thus generate a corresponding reference. Even before classification, numerous data had to be sorted out, since disturbances due to underfloor heating (Figure C.7), screed reinforcements (Figure C.8), steel beams or missing insulation (Figure C.9) prevented comparability with the laboratory experiments. In some cases, heavily attenuated or disturbed measurements also hindered the extraction of all relevant features from the entire B-scan. Validation of the remaining data (72 B-scans) achieved only low accuracy with 53 % correctly classified damage cases. Here, the previously suspected overfitting of the small decision boundary between dry setups and damaged screeds within the laboratory proved to be a problem. The generally larger deviations within (also dry) on-site B-scans were thus frequently misclassified as screed damage. In addition, there were sometimes strongly varying layer thicknesses or changing cases of damage within a survey line, which caused additional errors due to the local limitation of the drilling core reference. Nevertheless, individual on-site examples (e.g. Figures C.14, C.15, and C.16) also showed the promising potential of the applied signal features and the GPR method in general, which partly allowed a profound interpretation of the measurements. However, this interpretation still requires the experience of trained personnel and could not be automated using machine learning with the available database.

3.2 Literature Review

The research carried out was the first basis on which to decide on the methodological approach of the thesis and should therefore be discussed from this point of view. Here, it was particularly noticeable that no publication had yet dealt with moisture measurements on building floors using GPR. Only one publication on screeds [1] was thematically related, but did not consider layered structures. Other layered structures such as pavement constructions were investigated in publications by Grote et al. [2] and Fernandes et al. [3]. Here, however, the thickness of the individual layers was known for determining the moisture content, which is not transferable to the measurement of unknown

building floors. As already mentioned under A.5.1, the CMP or WARR survey method (also used in [2]) is generally suitable for the measurement of structures with unknown layer thicknesses. However, Cai et al. [4] already pointed out difficulties in evaluating measurements on existing thin layers, as they can also occur in floors, due to interference of individual wave parts or reflections. Van der Kruk et al. [5] also studied shallow layers with high water contents at the surface of layered soil structures (as they can occur after rainfall) and described their effect on radar measurements using inversion-based methods. As stated in A.5.4, these methods require precise models of the applied GPR system and the investigated medium. With regard to the research question of the thesis, the latter was considered a major challenge given the high diversity of floor setups.

Due to the large number of suitable features, which were always applied isolated in all publications, the combination of these turned out to be a promising innovative approach. Mainly these features were related to the common-offset configuration, which is why this survey method was to be used within this work. Since the use of the WARR or CMP method seemed to be at least theoretically suitable, it was also planned for the intended investigations. This could be ensured by placing a second receiving antenna at the starting point of the survey line, which collects the transmitted signals of the moving common-offset antenna pair. It has already become clear from the results presented before, that this data was not examined in the context of this thesis. Here, detectable interference between wave types did not suggest a focus on deeper evaluations.

Another parameter to be selected was the center frequency. Common floor layer thicknesses of 2 cm to 10 cm suggested a rather higher value to allow the resolution of the closely spaced layer boundaries. Two established designs are the 2 GHz and the 2.6 GHz antenna, which were selected for the first investigations. These were also the highest frequencies used among all researched publications shown in Table A.1.

All of the decisions regarding methodology, antenna configuration, and frequencies applied were made based on the literature review conducted and explained accordingly. Thus, in the course of the work through the collection of new knowledge, a critical review of these decisions becomes possible. This will be done at the appropriate sections of the following discussion.

3.3 Materials and Preliminary Studies

3.3.1 Specimens

The first part of the section dealt with the materials needed for an experimental floor construction. This shall shortly be discussed here, since the selection of suitable materials and their parameter configurations is of high importance to sufficiently represent the wide variation in practice. As mentioned before, the literature review yielded only one example of moisture measurements on screeds and none on floor constructions, which is why no information for planning could be obtained there. Thus, the experience of industrial companies can serve as an important reference to approach this task. In cooperation, the governing variables for the experiment could be determined, which included the material type and thickness of screed and insulation specimens (Table B.1). With regard to the manufacturers to be selected, established representatives with high sales volumes were chosen for both screed and insulation in order to represent large shares of the market. With regard to the on-site measurements carried out later, the selection of variations made can be assessed as appropriate. With the exception of a few measurement points with

thicknesses below 2 cm in Nuernberg (Figure C.12), all insulations, also with regard to the material, were within the value range considered. The screeds encountered in practice were exclusively cement-based and often thicker, with values between 8 cm and 12 cm. This was considered as unproblematic, since the fact that layers rather too narrow than too thick could cause problems in measurements on building floors was already evident from the preliminary investigations carried out.

3.3.2 Feature Evaluation

The main purpose of these preliminary tests was to check the previously researched radar signal features with regard to their suitability for moisture measurements, initially on screeds. Here, the moisture references obtained by the Darr and CCM methods allowed the evaluation of given correlations, however also of possible problems and limitations. In the univariate application on exemplary screed samples, all examined features from the time, amplitude and frequency range showed a good sensitivity for the decreasing moisture content of the screeds. Problems occurred whenever the two-way travel time of the reflection waves became so short due to the decreasing permittivities that it interfered with the direct wave. Here, a fundamental difficulty in measurements on buildings floors became apparent early in the project. At this point, the selected center frequencies had to be questioned. However, there was no further flexibility, since no antennas with higher frequencies are offered by GSSI for the measurement system available. Even independent of the manufacturer, antennas above 3 GHz are rather exotic and are not represented in any publications on moisture measurements in civil engineering. This is because higher frequencies are coupled with higher attenuation, which can be even more evident when water is present. In the case of the research question under investigation, however, the resulting trade-off must always be decided in favor of the penetration depth to not lose any information about the insulation. Therefore, interference between DW and RW had to be accepted as possible disturbance. In addition, for the subsequent observation of layered structures, there are further reflections which can also interfere with each other. One consequence of this was the exclusion of quantitative moisture determination and the focus on qualitative statements. While this supposedly more challenging goal of exact moisture values was not completely ruled out at the beginning of the project, the preliminary investigations showed clear limits. In addition, there is the general uncertainty concerning time-zero, the excitation time of the EM wave, which is also discussed in the review paper (section A.5.1). Such inaccuracies become more significant for smaller two-way travel times, such as those to be measured on floors.

Nevertheless, at the end of the preliminary investigations, a quantitative determination of the screed moisture was still to be examined by a multivariate application of features. Here, the risk of possible interference was minimized by excluding the related extrema (second extrema of DW and first extrema of RW) from the feature extraction. The multivariate analysis by applying multiple linear regression was then performed on the entire data set, which simulated a reasonably realistic scenario of unknown material parameters such as screed type and thickness. The results confirmed that the combination of multiple features could compensate for individual weaknesses and was therefore still seen as a promising approach within this research. This can also be stated as the main finding from the investigations. While the further knowledge gained on the properties of certain features also created a valuable basis, a general transferability of the results to the subsequent measurements on layered floors was considered inappropriate. Thus, excluded

extrema within the signal may be unsuitable for quantitative determination, but may provide valuable information about water-related changes in a qualitative observation. Also despite interference. Therefore, no feature was excluded for subsequent studies on layered structures and re-evaluated using the machine learning approach on the new and fundamentally different dataset to be obtained.

3.4 Laboratory Investigations

3.4.1 Experimental Design

In this section, it is appropriate to first discuss the decisions regarding the experimental design for the laboratory investigation. With regard to the casted screed specimens and the insulations to be considered, the modular specimen developed allowed 168 floor configurations. With two antenna frequencies and three damage scenarios to investigate, this results in 1008 measurements. To reduce the extent and keep the experiment within a realistic range, measurements with 2.6 GHz were excluded, as it showed no noticeable advantages over the 2 GHz variant in terms of resolution and avoidance of possible interference in the preliminary tests. Rather, the A-scans of the 2.6 GHz antenna frequently showed unclear reflection patterns, which is exemplarily shown in Figure 3.1. This causes difficulties especially for the automatic extraction of individual minima and maxima, since the reflection waves can sometimes show a strong offset with respect to the baseline (amplitude = 0). The reason for these reflection patterns was not investigated further, since the focus was placed on one antenna anyway. Here, simulations might have provided information about possible characteristic interferences or other explanations. Due to the rather small differences to CT1 and CA1, also the investigation of CT2 and CA2, were completely dispensed with. Thus, the number of different floor setups was reduced to 84, resulting in 256 setups to be measured.

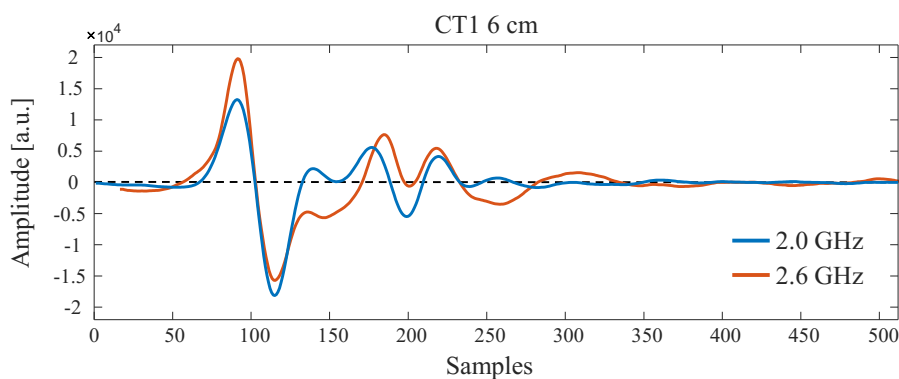


Figure 3.1: Comparison of a 2 GHz and 2.6 GHz A-scan recorded on the 6 cm CT1 screed.

After determining the floor configurations, an elementary component to be planned was the simulation of the various damage scenarios. In this context, 'damage' is not a defined term, which means that there are no uniform thresholds above which a quantity of water contained in screed or insulation can be considered as damage. Therefore, experience values from industrial companies can serve as an orientation, since they reflect thresholds for when they consider repair measures to be necessary in their daily work. The water

content of the insulation materials to be examined, however, appeared to be a difficult threshold value to control, since their structures and compositions differ a lot. While the amount of water added to the setup can be fixed, the time-dependent and quantitative absorption by the insulation materials is not uniform. This would therefore have had to be determined by weighing during the experiment, which on the one hand could provide an influence due to possible water loss, and on the other hand would have resulted in an unmanageable effort in view of the quantity of measurement setups. Instead of the water content, the control of the RH within the insulation layer posed as a threshold value. Here, 80 % RH serves as a suitable limit, since there is a justified risk of mold growth above this value. The laboratory measurements carried out on the scenario of damage insulation showed that even small amounts of water were sufficient to surpass this value. These amounts are summarized in Table 3.1, which was also published in [6]. Here, 3.1 V% to 6.3 V% of added Water (in relation to the insulation volume) resulted in humidity values above 80 %. However, the laboratory experiments carried out did not provide any information about the actual θ_{80} , the water quantities necessary to reach 80 % RH. Therefore, similar tests were carried out on a smaller specimen (as part of a bachelor thesis) to determine the values searched for. The results yielded values of $\theta_{80} < 0.1$ V% for all insulation materials. As a comparison, data on experimentally determined sorption isotherms of EP and XP provided by the Institute for Building Climatology of the Technical University of Dresden were used, which can be seen in Figure 3.2.

Table 3.1: Overview of the resulting humidity values in the insulation material during the laboratory experiments on the modular test specimen.

Insulation type	Material thickness	Water addition	Moisture	Humidity after 12 hours	Humidity at test end
EP	20 mm	0.5 l	3.9 V%	86.8 % RH	94.1 % RH
EP	50 mm	2 l	6.3 V%	97.5 % RH	98.5 % RH
EP	70 mm	2 l	4.5 V%	95.3 % RH	100 % RH
EP	100 mm	2 l	3.1 V%	81.8 % RH	89.3.1 % RH
GW	20 mm	0.5 l	3.9 V%	79.6 % RH	83.8 % RH
GW	60 mm	1.5 l	3.9 V%	87.5 % RH	90.4 % RH
GW	100 mm	4 l	6.3 V%	93.2 % RH	95.4 % RH
PS	20 mm	0.5 l	3.9 V%	86 % RH	89.6 % RH
PS	60 mm	1.5 l	3.9 V%	85.1 % RH	94.5 % RH
PS	100 mm	4 l	6.3 V%	96 % RH	98.9 % RH
XP	20 mm	0.75 l	5.9 V%	58.2 % RH	88.3 % RH
XP	50 mm	2 l	6.3 V%	89.8 % RH	93.7 % RH
XP	70 mm	2 l	4.5 V%	87.3 % RH	94.3 % RH
XP	100 mm	2 l	3.1 V%	96.8 % RH	99.2 % RH

Again, also within the sorption isotherms, θ_{80} for both insulations is at approximately 0.1 V%. The conclusion for the laboratory tests is that higher water quantities were added than necessary for a risk of mold growth. A comparison with the values encountered in practice is shown in Table 3.2. Here, a threshold value of 15 wt% was chosen for classification as insulation damage, which corresponds to about 0.4 V% to 0.5 V% according to the densities of EP and XP given in Table B.1. The water quantities of damaged insulation determined by the drilling cores were on average comparable to the water quantities added in the laboratory measurements, although the former could differ considerably. While values above this average are likely to be less of a problem, insulation damage with less water could potentially be more difficult to detect. These small amounts needed to cause a mold hazard underline the difficulty of moisture measurements in the insulation layer.

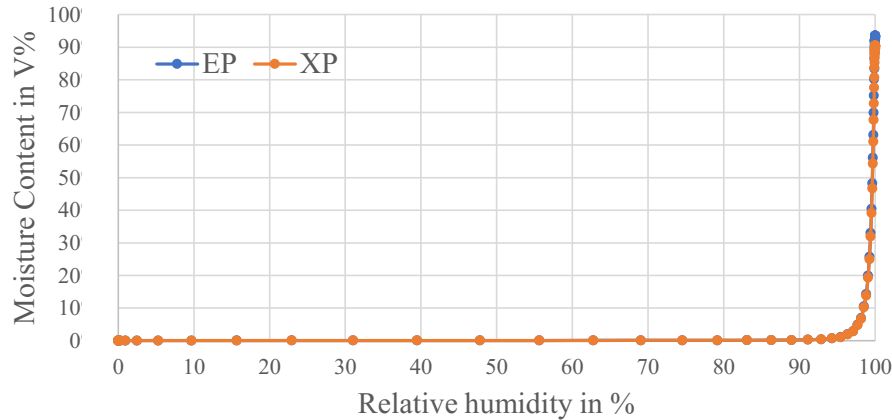


Figure 3.2: Sorption isotherm of EP and XP

Table 3.2: Statistical comparison between the water contents in damaged insulations and screeds for all on-site measurements.

Location	Insulation damage		Screed damage (CT)	
	Mean \pm Std	N	Mean \pm Std	N
Pegnitz	3.4 \pm 3.3 V%	21	6.7 \pm 1.6 wt%	24
Grossenseebach	0.6 \pm n/a V%	1	6.1 \pm 1.0 wt%	18
Wunsiedel	5.8 \pm 7.4 V%	24	5.6 \pm 1.2 wt%	17
Nuernberg	3.2 \pm 1.1 V%	32	5.6 \pm 1.1 wt%	28

Unlike the different insulation materials, the six screeds investigated have a similar structure and handling, which is why the control of water content could be used as a threshold for damage determination. Therefore, values for a damaged cement and anhydrite screed of 4 wt% and 0.5 wt%, respectively, were chosen. The threshold values concerning readiness for covering are in a comparable range with 3.5 wt% for cement screeds and 0.5 wt% for anhydrite screeds [7]. Table 3.2 also shows the water contents encountered in damaged on-site screeds, which on average are slightly higher than the values of 4.4 wt%, 5.2 wt% and 4.9 wt% set in the laboratory for CT screeds of 5 cm, 6 cm, and 7 cm thickness, respectively. However, with regard to the simulated screed damage, it is not so much the amount of water but its (homogeneous) distribution that is seen as an influencing factor on the subsequent evaluation. Therefore, the methods developed to classify the three damage scenarios must first be discussed.

3.4.2 Methodology Development

The results of the laboratory tests showed that a reconsideration of all possible features, regardless of their position in the A-scan, proved to be beneficial. The five most suitable features resulted from the DW, as well as from RW1 and RW2, which all interfere in the case of a layered structure. Nevertheless, they still allow sufficient separation of the screed and the insulation layer to provide information about the presence of water. The selection of these features was not arbitrary, but based on a statistical evaluation of the linear

dependencies to the examined damage scenarios, as described in B.2.5. Accordingly, the features represent the best solution for the corresponding data set, although this does not have to apply to new data. Therefore, this statistical selection method was later repeated for different data sets (only on-site data, or on-site data and laboratory data). These investigations resulted in the exchange of some features, but did not provide a significant improvement in the validation result. Thus, also for comparability, the feature selection determined in the laboratory was retained. However, using these A-scan features alone, as it is performed in all the publications reviewed, would not have been effective by any means. The results of the literature review and preliminary studies already showed that the variations in material type and thickness made in the laboratory experiment have a significant effect on the very signal features used to detect the damage cases. Nevertheless, in order to ensure a classification independent of the underlying floor structure, a new processing step had to be developed that makes use of the spatial dimension of B-scans.

This was done with the introduced B-scan features, that capture water-related deviations by evaluating the statistical distribution of A-scan features within a survey line. This step allows the reduction of an A-scan feature vector to a scalar value, which is particularly suitable as an input parameter for subsequently trained classifiers. The calculation of B-scan features is an innovative and elementary component for the detection of the different damage cases in unknown floor structures. The method allows an evaluation of the A-scan features decoupled from their quantitative values, which strongly depend on the unknown variables such as material type and thickness. However, the advantages gained are subject to the assumption of little to no horizontal deviations of the A-scan features within a 'dry' B-scan, as it was observed within the laboratory data. The extent to which this approach is successful was subsequently considered by training and applying different classifiers on the recorded data set.

Here, four different classifiers (MLR, RF, SVM, and ANN) were trained and cross-validated in their standard configuration from the *Scikit-Learn* library in python, as presented in section B.2.6. Conducted trials showed that the selection of appropriate signal features had a much greater impact on the classifier's performance than the adjustment of certain model parameters. Parameter tuning is usually very expensive in terms of computation and can quickly become ineffective depending on the underlying data set [8]. The models used are already seen as powerful in their default configuration, which is why they were treated as a tool for research and not as a distinctive object of research. Also, the fact that all models always achieved similar accuracy values, as shown in Table B.2 and Figure B.12, gave no indication that the selection of other models could achieve significantly better results. Therefore, this workspace was omitted and the focus was placed on feature selection and the evaluation of achieved accuracies.

The good classification results showed that the newly introduced method of calculating B-scan features is suitable to recognize different moisture damage cases in unknown floor structures. However, the detection rate of insulation damage also showed an influence of the experimental design discussed earlier, since, in some cases, added water did not penetrate the measured area of the survey line. The corresponding 'misclassification' as dry construction again showed the good sensitivity of the method, which, however, could only be determined by the additional information of the corresponding moisture distribution by visual inspection of the insulation (Figures B.11 and B.13). This demonstrated the previously mentioned difficulties in defining and referencing moisture damage, which, depending on the method chosen, can always leave unknown parameters such as the exact

amount of water or its distribution in the measured area.

Another influence of the experimental design was evident in the measurements of damaged screeds. The homogeneous water ingress from the surface often caused small horizontal deviations of the signal features in a B-scan, so that damaged screeds could easily be mistaken for dry structures by visual inspection. However, the classifiers managed to separate these and achieved high recognition rates. Thus, relatively small differences in the B-scan features were learned by the classifiers to distinguish damaged screeds from dry floors. However, since the robustness of the chosen method benefits from larger deviations, there is a risk of overfitting, due to closely located cases within the feature space. It can therefore be considered whether it would have been more effective simulate more heterogeneous moisture damage in the screed by adding water locally. However, results of on-site measurements, as shown in C.6 or C.15 a), indicated that comparatively homogeneously distributed screed damage presents a similarly challenging separation from dry floors. The discussion is therefore difficult to conduct at this point and will be taken up again in the concluding section 3.6 after the validations at on-site measurements have been addressed.

At the end it should be emphasized once again that the high and promising sensitivity of the classifiers was significantly influenced by the combination of several features covering all relevant signal ranges. Due to the higher deviations of the B-scan features in case of insulation damage, especially the RW2-related features achieved high scores, as shown in Table B.3 and Figure B.15. The sensitivity to insulation damage represents a clear unique selling point of GPR over other moisture measurement techniques. As exemplarily shown in Figure B.9 b), the neutron probe often did not show an increase of the measured counts compared to dry setups and was only sensitive to water in screeds. For this case, also the GPR features regarding DW and RW1 had a significant impact on a successful detection and made a valuable contribution to the classification accuracy. Thus, the results again demonstrated the advantages of multivariate data analysis by using multiple features.

3.5 On-Site Investigations

3.5.1 Measurements

The five objects investigated were selected by the industrial project partner within its incoming inquiries and orders. Here, underlying damage cases could only be estimated in advance and were never completely known beforehand. The final determination was made by extracting drilling cores and a subsequent Darr drying individually for each measuring point. Thus, a reference could be generated by assigning a damage case to each measurement. Section C.2 describes the procedure in detail. It also shows that all measurement parameters were chosen to be identical to the laboratory experiments for reasons of comparability. Only the length of the orthogonal survey lines was increased from 40 cm to 50 cm, since here, unlike on the modular test specimen, there was no limitation due to possible edge effects. Therefore, 5 cm on the start and the end were cut before extracting the B-scan features to use the same amount of A-scans. Unfortunately, no floor plans with corresponding positioning of the measuring points were recorded during the investigations. Here, only the relative positions of outstanding measuring points were noted, which allowed meaningful conclusions to be drawn in isolated cases, however still lacked valuable information. This stood out as a clear disadvantage in the evaluation and would be approached differently in future works by conducting comprehensive mapping.

Already during the first on-site investigation, obvious differences to the laboratory measurements were noticed in some cases, which either could not be used for validation or could lead to accuracy problems in the classification. The biggest obstacle here was the presence of floor heating systems, which, with their positioning under the screed, prevent a suitable feature extraction, since the resulting reflections do not allow any conclusions to be drawn about the insulation. At the first three locations, unfortunately, a large number of the measurement points contained such floor heating, which did not allow any meaningful evaluation. While the problem was not yet known for the first practical measurement, in the following two investigations either failed communication or unawareness on the part of the client led to the undesired selection of the objects. For the last two locations, it was then questioned more than once whether underfloor heating was present or not before the object was selected. Thus, at least the data collected there could be used for the planned validation. Nevertheless, valuable experience was gained during the first three investigations, not least because they revealed a major limitation in the application of the developed method. However, the aforementioned unawareness, the lack of knowledge about the underlying floor structure is also representative of the general problem with unknown parameters. This problem was also evident in the validation performed with the two remaining on-site locations.

3.5.2 Methodology Validation

As already indicated, numerous measurements had to be sorted out even before validation since, as in most cases, they contained floor heating, or other obstacles such as screed reinforcements, present steel beams or missing insulation layers, which avoided comparability. Also strongly attenuated or disturbed measurements sometimes did not allow the extraction of all required signal features in the whole B-scan and thus could not be considered either. The application of the classifiers on the remaining new on-site measurements achieved only a low overall accuracy significantly below previously achieved values within the laboratory data. The reasons for this poor performance are identifiable differences between laboratory and practice, which suggested overfitting of the classifiers. In particular, the narrow decision boundary between dry floors and damaged screeds discussed in 3.4.2 proved inappropriate for the generally much more dynamic and heterogeneous B-scans of on-site measurements. Here, dry setups, as well as insulation damage, were thus frequently misclassified as screed damage. The difference between laboratory and practice is well shown in Figure 3.3, a scatter plot of the most indicative features F_B and F_D for the cases insulation damage and screed damage, respectively. The respective separation of cases by the individual feature is particularly evident in the laboratory data set, where, as previously discussed, screed damage is closely located to dry measurements. Therefore, even slightly higher values for F_D are sufficient to predict laboratory screed damage relatively accurately. Unfortunately, all on-site measurements are far above the average F_D distribution of laboratory data, which explains the almost exclusive classification as screed damage for the test data. Although the Figure shows only the scatter plot of 2 out of 5 features, all other feature combinations depict the same. In the entire feature space, the on-site data (test data) lie far away from the laboratory data (training data), which poses an unsolvable problem of generalization for any model applied. This is also evident from Table 3.3, where (except F_C for insulation damage) the mean value of each case-specific feature of the on-site data is significantly higher compared to the laboratory data.

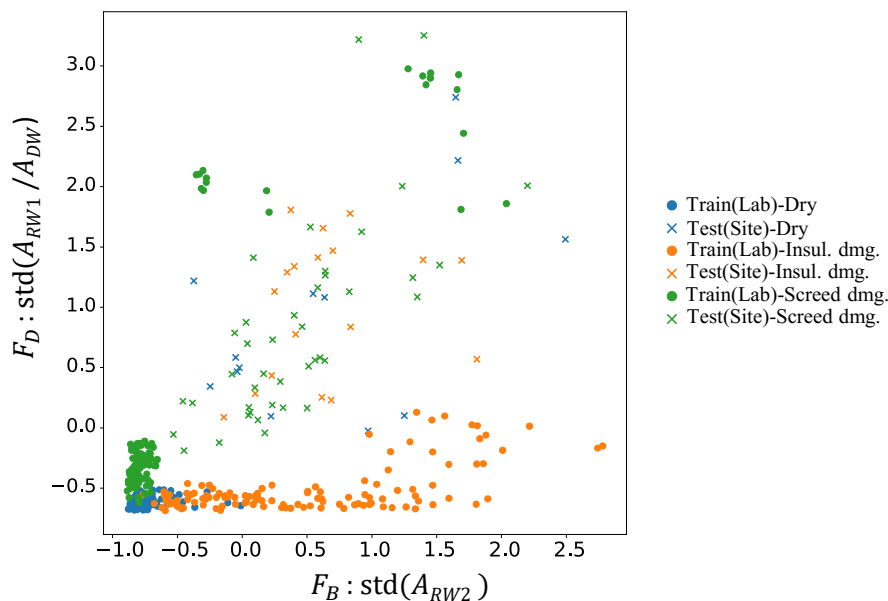


Figure 3.3: Scatter plot of B-scan features F_B and F_D for all damage cases within laboratory data and on-site data.

Table 3.3: Statistical comparison between the features and their standardized distribution for each damage case in the laboratory and on-site

B-scan feature	Dry ($N_{Lab} = 120, N_{Site} = 13$)		Insulation damage ($N_{Lab} = 120, N_{Site} = 18$)		Screed damage ($N_{Lab} = 120, N_{Site} = 41$)	
	Mean \pm Std Lab.	Mean \pm Std On-site	Mean \pm Std Lab.	Mean \pm Std On-site	Mean \pm Std Lab.	Mean \pm Std On-site
F_A	-0.64 \pm 0.11	7.85 \pm 4.52	-0.63 \pm 0.13	10.82 \pm 7.34	-0.38 \pm 0.29	8.45 \pm 6.75
F_B	-0.75 \pm 0.14	0.67 \pm 0.85	0.47 \pm 0.84	0.65 \pm 0.51	-0.53 \pm 0.69	0.43 \pm 0.58
F_C	-0.60 \pm 0.41	0.41 \pm 0.89	0.59 \pm 1.08	-0.01 \pm 0.66	-0.57 \pm 0.26	0.11 \pm 0.74
F_D	-0.62 \pm 0.04	0.92 \pm 0.81	-0.52 \pm 0.19	1.01 \pm 0.56	0.12 \pm 1.03	0.81 \pm 0.79
F_E	-0.55 \pm 0.14	3.70 \pm 3.7	-0.42 \pm 0.25	1.56 \pm 3.00	-0.27 \pm 0.28	1.55 \pm 2.80

The reasons for the unsteady reflection patterns of the practical floor structures were determined by varying material parameters within one measurement. This was shown by significantly changing layer thicknesses (Figures C.12 and C.13) and damages of screed and insulation within one survey line (Figures C.14 and C.15). Here, the general spatial limitation of the extracted drilling cores and their generated reference became especially noticeable. As it has been addressed regarding the laboratory measurements, the many unknown factors are a major problem with moisture measurements, especially when trying to automatize them.

Nevertheless, in some examples (like given in Figures C.14, C.15, and C.16) the B-scan features showed a general sensitivity to the different damage cases. Specifically, screed damage showed strong indicators by influencing each wave type considered. In the case of an observed transition to or from a moist screed, the DW proved to be a valuable source of information, as it is not influenced by the underlying layer thickness. However, also for insulation damage, prominent deviations of RW1 and RW2 with an concurrently constant DW showed to be a good indicator. Unfortunately, these indicators and the resulting potential could not be successfully trained due to the small data base and the previously mentioned problems. Nevertheless, the examples and their findings provide a valuable contribution to the interpretation of moisture measurements with GPR on building floors. At this stage, this interpretation is still dependent on deep expert knowledge and cannot yet be adopted independently by automated classifiers. Nevertheless,

this expert knowledge can be enriched by the findings of this work. In general, especially such observed transitions between the damage cases are a valuable information for the interpretation of the extracted features, even if they caused problems in the automated classification. Such comparisons between the considered cases are often a needed circumstance, especially in on-site investigations, to get an orientation for the evaluation. Unfortunately, such comparisons are never guaranteed, which is a governing uncertainty factor in moisture measurements.

3.6 Concluding Discussion

Now that all publications and additional preliminary studies have been discussed, a critical look will be taken at the entire study and the results achieved. In particular, the question is crucial where, in retrospect, the greatest potential for improvement can be found, to be precise, what could have been done differently? From the author's point of view, three main aspects can be identified, with decreasing relevance and priority for potential improvement: (i) data, (ii) feature extraction, and (iii) applied models.

The most crucial point for the successful automation of a classification task is the underlying database. It must cover the entire space of possibilities with a sufficient number of, in the best case, balanced examples. Within this work, the database was created using the collected measurements, i.e. the performed laboratory experiments and the on-site measurements. The former was used for method development and training of the classifiers, which were then applied to the new on-site data. This revealed a significant gap between the laboratory and the real world, which raises the question of whether this gap could have been closed with a different experimental design. Considering a realistic scope to be maintained, this is seen as rather unlikely. With the chosen approach of the modular test specimen, the most decisive parameters, material type and thickness, could already be varied over a realistic range. Nevertheless, such an experimental design always generates certain dependencies in the data and thus often represents only a special and partly isolated area in the space of possibilities. Even the inclusion of previously unknown difficulties such as underfloor heating or strongly deviating material parameters within a survey line would, regardless of the immense effort, again only have produced special examples that would not have brought any guarantee for improvement. This also applies to the methods used for damage simulation. The ingress of more heterogeneous screed damage in the experiment might have increased the robustness within the laboratory data, however would have not necessarily result in greater accuracy for on-site data. Thus, the gap between laboratory and practice seems insurmountable in the example of moisture measurements on building floors. This leads to the conclusion that, in the best case, a method for on-site problems should be developed with referenced on-site data. Therefore, a broad data base with numerous examples would be necessary. Although even this data set can always be considered limited and as a small representation of reality, this suspicion could at least be successively reduced by a constant extension of at best worldwide distributed users. Here, an open data repository for investigation problems within NDT-CE would be a great opportunity. Such a repository would significantly increase the success and confidence in developed machine learning classifiers and open up a wide range of possibilities. However, this would also require accurate documentation of all available references and metadata. And here, the limitation of the reference, which has been mentioned several times in particular for moisture measurements, remains a challenging problem. As long

as the underlying reference still leaves too many unknown parameters open, machine learning methods, with their strong dependence on the data, will always come up against the same limitations. However, since an open database was not available for this work anyway, the question of a greater focus on on-site measurements may be raised. This is a justified suggestion, as it could at least have enabled the inclusion of on-site data in the training process. This inclusion was also tried with the on-site data collected here, however the amount of suitable examples was not sufficient to improve the accuracy. In this case, further practical measurements might have had a positive effect, however would have limited the extent of the laboratory experiment. But it was the laboratory experiment that made it possible to study the fundamentals of moisture measurements on building floors under controlled conditions, which is particularly valuable for interpreting unknown on-site measurements. For this reason, the question of an adapted focus cannot be answered clearly. Also in retrospect, the collected findings and methods developed from the laboratory are seen as a valuable part of the work. This was especially evident in individual, positive examples within the on-site measurements, as it was discussed in the end of the previous section. Here, the features used showed their sensitivity and potential to correctly interpret the different damage cases. The features were mentioned before as the second most important possibility for improvement and will be discussed critically in the following.

The researched and further developed (B-scan) features proved to be highly suitable within the laboratory data set to identify the different damage cases independent of given variations in floor structures. Here, the success was based on constant B-scans of dry setups, which were significantly different from the water induced variations within the measurements of damaged setups. This observation was also evident in some examples from the on-site measurements, however here the dry structures showed significantly more unsteady B-scans. In most cases, this resulted in false positive classifications (false alarms), since screed damage was often estimated on the basis of the trained decision boundary. It may therefore be assumed that training with a wide range of practical examples would result in more robust decision boundaries within the B-scan feature space. However, this shifts the problem back to the data, which has already been discussed. Thus, the question arises whether other signal features would have been more appropriate for the classification task. Again, this is difficult to evaluate with the results obtained and the available database. The selected A-scan features have been researched from the state of the art and have been found to be the most suitable within a data-based feature selection. This feature selection was also performed again after adding the on-site measurements to the data set, which resulted in the same selection. Nevertheless, other feature combinations were also tested, which did not produce improvements. However, unlike the A-scan features, the introduced B-scan features provided the desired sensitivity to horizontal deviations within a survey line, which were then shown in the validation to be, at this stage, not that robust. In order to compensate at least for the low-frequency deviations, the consideration of shorter survey lines was also investigated. This might have helped for deviations that can occur in the case of a transition between two damage cases, or in the case of changing layer thicknesses. A survey line was thus divided into several sections, which were then considered as independent measurement points both in the training process and in the validation. Unfortunately, no significant improvements could be achieved here. The suitability of the B-scan features for real world damage cases can therefore be questioned. As already mentioned, however, these features showed a promising potential. Nevertheless, at least variations of the proposed approach are con-

ceivable. Here, other statistical operators or other analysis methods could be used. For example, it would be possible to consider the signal derivatives of the A-scan feature vectors to capture the degree of dynamics within a B-scan. In retrospect, greater potential is also seen in the acquisition of C-scans. The recording of a measurement grid, i.e. several parallel measurement lines per measurement point, would result in a higher effort, but would allow the generation of a 3D representation of the measurement area. This would result in a considerable increase in information, possibly enabling the detection of changing material parameters by looking at adjacent areas. Also the introduction of completely new features, which consider whole depth slices would be possible. During the preliminary studies for the laboratory experiments, the acquisition of C-scans was not considered to be profitable in view of the higher effort involved. Only the gained experience and the problems encountered in evaluating the on-site measurements showed the potential value of such measurements. Thus, this results in a clear recommendation for possible improvement.

Finally, it is not ruled out that the use of completely different signal features would be more suitable for the measurement task. With a sufficiently large amount of data, the use of deep learning to extract new features directly from the B-scans would be conceivable. Such approaches from the field of image processing were also briefly considered in this work. However, the time invested in this was not sufficient for a robust assessment of the resulting potential. This approach is based on the application of new machine learning models, which thus introduces the last aspect of this discussion.

As soon as a broad and realistic data set is available and the most suitable features are extracted, the classification models used can be investigated in more depth. This prioritization has been discussed before and is also the reason why only models in their standard configuration have been applied within this work. Nevertheless, this area of optimization shall be briefly addressed. By performing an automated grid search, different model parameters can be chosen iteratively and their effect on the performance of a classifier can be investigated. Depending on the value range of the parameters and the chosen resolution, this can result in an arbitrarily large computational effort, since each iteration contains an independent training and validation process. Whether significant improvements occur as a result is by no means guaranteed. Therefore, it should always be the last step of a study in order to achieve the best possible results if necessary. In the context of this work this step has not yet offered itself. The classification models used performed similarly both in the laboratory and on-site and did not reveal a favorite. An adjustment of the model parameters was only very roughly investigated and did not result in any significant changes. The benefit was therefore considered to be low. Nevertheless, a possible potential for improvement cannot be completely excluded, also by the use of other classification models. As already mentioned, however, suitable data and respective features should first be available for this investigation.

4. Outlook

The essential findings of the study showed limitations but also promising possibilities. There are therefore various tasks for future work.

As already stated at the end of the discussion, the tasks should be subject to a clear prioritization. First of all, a broad data base should be developed, consisting mainly of real on-site data. The establishment of a worldwide used open data repository for NDT-CE applications would be a valuable step to unfold the potential of promising automation solutions with the help of machine learning. This, so far, seems to be the best way to train realistic decision boundaries within the feature space. Also, the inclusion of diverse data, as by conducting additional radar measurement methods, such as WARR/CMP or C-scan measurements, can further increase the information value. In all of this, referencing the data as detailed as possible plays a crucial role. In order to open up the potential for GPR and machine learning, the depth of information would have to be increased considerably at great expense, as by combining many procedures. This is because the findings of this work highlighted the problem of limited local resolution of extracted drilling cores, as material parameters and damage cases can change over small distances. With such a limited reference, considering shorter survey lines by windowing could reduce possible variations, although this may also hinder the potential of the B-scan feature. This is a trade-off that should be investigated in more depth to develop suitable strategies.

After the establishment of a broad and diverse database, respective features can be re-evaluated. Both, adaptations of the method presented here and new approaches may be possible. Also deep learning can be used to process entire B-scan images and to extract distinctive features. This could possibly lead to the discovery of previously unrecognized correlations.

Other obstacles encountered in this work also offer the potential for further studies. An essential aspect here was occurring floor heating, which in view of the recorded measurements at least allows statements about the screed moisture. Here, the characteristic reflection hyperbolas also offer possibilities for further features, as they can allow a more precise evaluation of the radar wave's propagation speed. In this particular case, a preceding laboratory examination would be appropriate to understand governing parameters like the pipe's spacing, their dimensions and materials.

To gain some control over the many unknown parameters in moisture measurements, completely different approaches, such as moisture monitoring, should also be considered. This is because information on the dry condition of a structure greatly simplifies the detection of moisture-induced changes and allows considerably more meaningful statements to be made. Looking a little further into the future, radar antennas in vacuum cleaner robots might be a suitable concept for making an 'Early Warning System' accessible to everyone.

Bibliography

- [1] F. Kurz and H. Sgarz. Measurement of Moisture Content in Building Materials using Radar Technology. *International Symposium Non-Destructive Testing in Civil Engineering (NDT-CE)*, 2015.
- [2] K. Grote, S. Hubbard, J. Harvey, and Y. Rubin. Evaluation of infiltration in layered pavements using surface GPR reflection techniques. *Journal of Applied Geophysics* 57, 57(2):129–153, feb 2005.
- [3] F. M. Fernandes, Andreia Fernandes, and Jorge Pais. Assessment of the density and moisture content of asphalt mixtures of road pavements. *Construction and Building Materials*, 154:1216–1225, nov 2017. <https://doi.org/10.1016/j.conbuildmat.2017.06.119>.
- [4] J. Q. Cai, S. X. Liu, L. Fu, and Y. Q. Feng. Detection of railway subgrade moisture content by GPR. *16th International Conference on Ground Penetrating Radar (GPR)*, jun 2016. <https://doi.org/10.1109/ICGPR.2016.7572613>.
- [5] J. van der Kruk, R. W. Jacob, and H. Vereecken. Properties of precipitation-induced multilayer surface waveguides derived from inversion of dispersive TE and TM GPR data. *Geophysics*, 75(4):WA263–WA273, jul 2010. <https://doi.org/10.1190/1.3467444>.
- [6] C. Strangfeld and T. Klewe. Hygrometric Moisture Measurements Based on Embedded Sensors to Determine the Mass of Moisture in Porous Building Materials and Layered Structures. *European Workshop on Structural Health Monitoring*, pages 213–225, 2021.
- [7] F. Radtke. *Schnellbestimmung der Feuchtigkeit beliebiger Materialien mit der Carbid-Methode*. <https://www.radtke-messtechnik.com/wp-content/uploads/2021/06/Anleitung-CM-Ger2.05> edition, 2021.
- [8] N. Tran, J.-G. Schneider, I. Weber, and A. K. Qin. Hyper-parameter optimization in classification: To-do or not-to-do. *Pattern Recognition*, 103:107245, jul 2020.

List of Tables

A.1	Overview of publications that perform moisture measurements in civil engineering based on signal features of the radar signal. DW - direct wave; RW - reflection wave; CO(al) - common-offset (air-launched); A, B, C - according to Fig. A.5; f_c - applied center frequency	23
2.1	Properties of the different screed types used for test specimens.	36
B.1	Used materials and layer thicknesses for the screed (top) and insulation layer (bottom).	55
B.2	Statistical comparison ($k = 20$ -fold cross-validation) of the achieved accuracies for all trained classifiers.	63
B.3	Achieved scores of the applied B-scan features.	66
C.1	Used materials and layer thicknesses for the screed (top) and insulation layer (bottom).	75
3.1	Overview of the resulting humidity values in the insulation material during the laboratory experiments on the modular test specimen.	100
3.2	Statistical comparison between the water contents in damaged insulations and screeds for all on-site measurements.	101
3.3	Statistical comparison between the features and their standardized distribution for each damage case in the laboratory and on-site	105

List of Figures

1.1	Project plan to classify the two common damage cases on building floors (wet insulation and wet screed) by extracting and combining distinctive signal features of GPR.	6
A.1	Principle of GPR reflection and underlying signal paths	15
A.2	Example of a recorded energy-signal in time domain (A-Scan) including the direct wave (DW) and reflection wave (RW). Basic signal features are the peak-to-peak amplitudes $A_{DW,p-p}$ and $A_{RW,p-p}$ located at the first peaks of DW and RW. The time difference Δt_{RW} between both peaks is often considered as the travel time.	15
A.3	Principle of a line measurement with GPR in common-offset configuration	16
A.4	GPR with multiple offsets: common-midpoint and wide angle reflection and refraction configuration	17
A.5	Principle of signal processing to estimate the moisture content θ by using the reflected energy signal of GPR	19
2.1	Sketch of cast test specimen (TS) and respective sister test samples (STS). The numbering of the STS defines the day after casting, on which the sample is used for referencing moisture methods (Darr and CCM). . . .	36
2.2	Casting of screed samples: a) Freshly mixed CA screed gets poured into its formwork. b) Embedding of threaded sleeves into each corner to enable handling with ring bolts.	37
2.3	Storage of the samples in a climate controlled tent at 23 °C and 50 % RH.	37
2.4	Measurement setup with neutrone probe and radar antenna on screed test specimens. The right graphic shows the perpendicular orientation of the two recorded GPR survey lines on a screed in top view	38
2.5	Extracted signal features of a radar measurement (A-scan) consisting of direct wave (DW) and reflection wave (RW). 1 , 3 and 4 : peak-to-peak amplitudes; 2 , 5 : maximum frequencies ; 6 , 7 and 8 : two-way travel times.	39
2.6	Regarded features of radar and neutron probe for the multivariate analysis of screed moisture.	39
2.7	Moisture contents of all screed types with 6 cm thickness measured on TS and STS by Darr (yellow, red) and CCM method (purple)	41
2.8	Influence of moisture on the radar signal: Mean A-scans of the 6 cm CT1 screed recorded on different days after casting.	41
2.9	Extracted signal features of 6 cm CT1 screed with corresponding numbering in the legend (see Figure 2.5) and their correlation to the measured TS moisture profile from Fig. 2.7	42
2.10	Mean A-Scans of the 6 cm CA1 screed on different days after casting and the extracted signal features that are influenced by the interference between DW and RW.	43
2.11	Actual vs. predicted moisture of MLiR models with different combinations of input features (see also Figure 2.6)	44
B.1	Principle of GPR. Multiple A-scans collected along a survey line form a B-scan.	53

B.2	Schematic of the work steps presented in section 2 divided by their respective subsections.	53
B.3	Modular test specimen with screed, insulation, and concrete base layer. .	54
B.4	Evaluation of the resulting insulation damage through the use of embedded humidity sensors.	55
B.5	NMR measurements showing the depth-resolved moisture distribution during the saturation process of the 5 cm CT (left) and CA (right) screed.	56
B.6	Measurement procedure with 40 cm long radar survey lines 1 and 2. The neutron probe is placed in the center of the construction.	57
B.7	Exemplary A-scan with three prominent amplitudes influenced by present material interfaces.	57
B.8	Processing steps to extract A- and B-scan features.	59
B.9	Measurements at a 7 cm CT and 10 cm EPS floor construction for the scenarios: (a) Dry, (b) damage insulation, and (c) damage screed. The bottom (d–f) shows the respective A-scan vector plots for each B-scan (top).	60
B.10	Measurements at an 7 cm CA and 6 cm GW floor construction for the scenarios: (a) dry, (b) damage insulation and (c) damage screed. The bottom (d–f) shows the respective A-scan vector plots for each B-scan (top).	62
B.11	Water ingress (dark dyeing) in the 6 cm GW insulation. The pictures show the respective bottom of each used insulation plate (40 cm × 40 cm × 2 cm) in quadrant IV.	62
B.12	Combined confusion matrices for the individual insulation (green) and screed (gray) thicknesses considered in the experiment. The classifier’s accuracies within one cell are presented in the same order as in Table B.2. Rows and columns include the actual and the predicted ($\hat{}$) scenario, respectively. The blue confusion matrix summarizes the overall accuracies for each scenario.	64
B.13	Water ingress (dark dyeing) in the 2 cm GW insulation. The picture shows the bottom of the used insulation plate (40 cm × 40 cm × 2 cm) in quadrant IV.	65
B.14	Measurements at a 6 cm CT and 6 cm PS floor construction for the scenarios: (a) dry, (b) damaged insulation, and (c) damaged screed. The bottom (d–f) shows the respective A-scan vector plots for each B-scan (top). . .	65
B.15	Scatter plots showing the feature combination of F_B & F_C (left), F_B & F_D (middle) and F_D & F_E (right).	66
C.1	Modular test specimen with screed, insulation, and concrete base layer (left, middle) and the simulation of an insulation damage by adding water to the setup (right).	75
C.2	GPR procedure (left) around a measurement point from which the reference drilling core is extracted (example right). It is covered by two 50 cm radar survey lines measured with the SIR 20 from GSSI and a 2 GHz antenna pair.	76
C.3	Processing to extract A- and B-scan features.	77

C.4	Two exemplary B-scans (top) and their respective A-scan features (bottom) of dry on-site floors in Grossenseebach. The transparent-white, vertical bars mark the position of the extracted drilling cores within the survey lines. The obtained thickness and moisture content of screed and insulation are given in the B-scan's bottom right corner.	79
C.5	Two exemplary B-scans (top) and their respective A-scan features (bottom) of on-site floors with insulation damage in Nürnberg. The transparent-white, vertical bars mark the position of the extracted drilling cores within the survey lines. The obtained thickness and moisture content of screed and insulation are given in the B-scan's bottom right corner.	79
C.6	Two exemplary B-scans (top) and their respective A-scan features (bottom) of on-site floors with screed damage in Grossenseebach. The transparent-white, vertical bars mark the position of the extracted drilling cores within the survey lines. The obtained thickness and moisture content of screed and insulation are given in the B-scan's bottom right corner.	80
C.7	Disturbing floor heating exemplary shown by three measurements from Wunsiedel. The moisture contents for both, screed and insulation, rise from left to right.	81
C.8	Screed reinforcement mesh visible inside the drilling hole of MP 16 (left) and in the respective B-scan (right).	81
C.9	Steel beam within the survey line (SL) of MP 13 in Nürnberg (left) and the respective B-scan (right).	82
C.10	Classification results of the data sets Grossenseebach and Nürnberg represented by their individual overall accuracy and confusion matrices. Each cell includes the relative (decimal number) and numerical (natural number in brackets) amount of classified cases.	83
C.11	Exemplary laboratory B-scans (top) and their respective A-scan features (bottom) at an 6 cm CT and 5 cm XPS floor construction for the scenarios: dry, damage insulation, and damage screed.	84
C.12	Layer thicknesses of screed (black) and insulation (green) for every MP in the classified data sets of Nürnberg and Grossenseebach. The alternating background of white and grey signalizes changing rooms.	84
C.13	Layer thicknesses of screed (black) and insulation (green) for every MP in the discarded data sets of Berlin, Wunsiedel, and Pegnitz. Points within one background bar (white or grey) were located in the same room. . . .	85
C.14	B-scans and extracted A-scan features of the two neighbouring MPs 40 and 34 in Nürnberg. Their orientation within the room is shown by the measurement grid on the left.	86
C.15	B-scans and extracted A-scan features of the two neighbouring MPs 2 (a) and 3 (b) in Grossenseebach. Their orientation within the room is shown by the measurement grid on the left.	87
C.16	Exemplary B-scans and A-scan feature distribution of two on-site insulation damages from Nürnberg (MP 17 and MP 24) compared to a laboratory insulation damage with similar floor setup.	87
3.1	Comparison of a 2 GHz and 2.6 GHz A-scan recorded on the 6 cm CT1 screed.	99
3.2	Sorption isotherm of EP and XP	101

3.3 Scatter plot of B-scan features F_B and F_D for all damage cases within laboratory data and on-site data. 105

Abbreviations

Δt_{RW}	Time difference between DW and RW
A	Direct air wave
A_{xy}	Amplitude of $xy \in \{\text{DW}, \text{RW1 or RW2}\}$
$A_{xy,p-p}$	Peak-to-peak amplitude of $xy \in \{\text{DW or RW}\}$
A_0	Reflected air-surface amplitude
A_m	Highest possible amplitude (on metallic reflector)
ANN	Artificial neural network
A-scan	Single radar reflection signal in time domain
B-scan	Radargram, series of A-scans
C	Critical refracted wave
c_0	Speed of light
CA	Calcium-sulphate-based screed
CCM	Calcium-carbide method
CE	Civil engineering
CMP	Common-midpoint
CRIM	Complex refractive index model
C-scan	Series of B-scans
CT	Cement-based screed
D	Direct wave feature (amplitude)
d or D	Distance of objects, thickness of layers
DW	Direct wave
e.g.	Exempli gratia (lat.: for example)
EM	Electromagnetic
EPS	Expanded polyethylene
Eq.	Equation
ϵ	Dielectric permittivity
ϵ_0	Dielectric permittivity in vacuum
ϵ_r	Relative dielectric permittivity
F_x	A-scan feature $x \in \{1,2,3,4,5\}$
\vec{F}_x	A-scan feature vector $x \in \{1,2,3,4,5\}$
F_y	B-scan feature $y \in \{A,B,C,D,E\}$
FFT	Fast fourier transformation
f_{xy}	Dominant frequency of $xy \in \{\text{DW}, \text{RW1 or RW2}\}$
G	Direct ground wave
GPR	Ground penetrating radar
GW	Glass wool
M_d	dry basis moisture content (Darr)
MLiR	Multiple linear regression

MLR	Multinomial logistic regression
MP	Measurement point
μ	Magnetic permeability
NDT	Non-destructive testing
NDT-CE	Non-destructive testing in civil engineering
NMR	Nuclear magnetic resonance
PE	Polyethylene
PS	Perlites
R	Refelction wave feature (amplitude)
r	Reflection coefficient
RF	Random forest
RH	Relative Humidity
RMS	Root mean square
RW or R	Reflection wave
Rx	Receiver
S	Neutron probe feature (counts)
s	spacing between Tx and Rx
S1-S5	Humitidy sensors
STFT	Short-time fourier transformation
STS	Sister test specimens
SVM	Support vecotor machine
σ	Electrical conductivity
T	Travel time feature
TS	Test specimens
Tx	Transmitter
Θ	Water content
v	radar wave velocity
WARR	Wide angle reflection and refraction
W_d	Dry sample weight
WT	Wavelet transformation
wt% or M%	Weight percent or Mass percent
W_w	Wet sample weight
XPS	Extruded polyethylene

Appendix

I	Comparison of the Calcium Carbide Method and Darr Drying to Quantify the Amount of Chemically Bound Water in Early Age Concrete	121
II	Poster: Combination of Radar and Neutrone Probe to Determine the Mass Moisture of Screeds	143
	Complete List of Publications	145

I. Comparison of the Calcium Carbide Method and Darr Drying to Quantify the Amount of Chemically Bound Water in Early Age Concrete

Abstract

Hydration is the exothermic reaction between anhydrous cement and water, which forms the solid cement matrix of concrete. Being able to evaluate the hydration is of high interest for the use of both conventional and more climate-friendly building materials. The experimental monitoring is based on temperature or moisture measurements. The first needs adiabatic conditions, which can only be achieved in laboratory. The latter is often measured comparing the weight of the material sample before and after oven drying, which is time-consuming. This study investigates the moisture content of two cement-based and two calcium-sulphate-based mixtures for the first 90 days by using the calcium carbide method and oven drying at 40 °C and 105 °C (Darr method). Thereby, the amount of chemically bound water is determined to derive the degree of hydration. The calcium carbide measurements highly coincide with oven drying at 40 °C. The calcium carbide method is therefore evaluated as a suitable alternative to the time consuming Darr drying. The prompt results are seen as a remarkable advantage and can be obtained easily in laboratory as well as in the field.

Bibliographic Information

Strangfeld, C.; Klewe, T. Comparison of the Calcium Carbide Method and Darr Drying to Quantify the Amount of Chemically Bound Water in Early Age Concrete. *Materials* 2022, 15, 8422. <https://doi.org/10.3390/ma15238422>.

Author's contribution

Conceptualization, C.S.; methodology, C.S. and T.K.; software, C.S. and T.K.; validation, C.S. and T.K.; formal analysis, C.S. and T.K.; experimental setup, T.K.; data recording, T.K.; data curation, C.S. and T.K.; resources, C.S.; writing—original draft preparation, C.S. and T.K.; writing—review and editing, C.S. and T.K.; visualization, C.S.; supervision, C.S.

Copyright Notice

This is an accepted version of the article published in <https://doi.org/10.3390/ma15238422>.
The article is licensed under an open access Creative Commons CC BY 4.0 license.

I.1 Motivation

In 2020, the global human-made mass exceeded all living dry biomass [1] and increases further exponentially [2]. More than 95 % of this anthropogenic mass consists of hydrophilic porous materials and the biggest share is concrete with around 40 % [1]. The cement industry is responsible for around 8 % of the global CO₂ emission [3], which is estimated to grow by 12 % - 23 % until 2050 [4]. But concrete does not last forever. High investments in maintenance of modern transport infrastructure are required. For example, around 13 billion euro are needed in Germany every year [5]. Furthermore, new structures have to sustain much higher loads due to an almost permanent increase of freight transport during the last decades [6]. This is also reflected in an increase of assumed traffic loads to be considered for the design and evaluation of the load-bearing capacity of new bridges [7]. Therefore, the application of specialised concrete mixtures such as ultra-high performance concrete or high-strength concrete comes into question. Nevertheless, these maintenance and building activities generate negative impacts on the environment as well. Per tonne cement, around 580 kg of CO₂ are emitted, mainly due to the chemical process of decarbonation [8, 9]. Thus, as a substitute for cement, “alternative clinkers”, which have a lower chemical CO₂ emission, are promoted nowadays [8, 10, 11]. Furthermore, the demolition of existing structures generates huge amounts of waste. For example 36.4 % of the overall waste (by weight) of the EU comes from the construction sector [12]. This clearly shows the saving potentials if recycled building materials are used. Modern concrete structures should sustain higher loads with simultaneous reduction of CO₂ and usage of recycled construction material.

New binders, new mixtures, use of recycled materials or aggregates, they all represent very promising approaches. Creating confidence in these new materials requires reliable in situ characterisation. In construction, one crucial parameter is the degree of hydration (DoH). For instance, on this parameter the current and final compressive strength are estimated or concrete post-treatment actions are scheduled and optimised. Therefore, this study discusses an approach for quantifying the DoH which works in the field as well.

I.2 Theory to chemisorption of water in early age mixtures

Although concrete is designed to last for several decades, its essential properties are determined during the first hours, days, and weeks after concreting. As soon as the dry bulk material comes into contact with mixing water, the hydration process starts immediately [13]. During this chemical reaction, the resulting micro-structure is developed. Within this process, the liquid mixing water undergoes a change of state. A significant part of it is hydrated, i.e. the liquid water is absorbed by the solid matrix and remains chemically bounded [14]. In addition, physisorption occurs, i.e. liquid water is adsorbed at the fringe of the emitting pore network [15]. Although this water interacts with the surface of the solid cement matrix, its binding energy is much lower compared to chemically bound water, even in the case of mono-layer adsorption [16]. Thus, in distinction to chemically bound water, adsorbed liquid water is also called physically bound water. In most cases, more mixing water is present in the pore network as it would be required for absorption and adsorption. This water is transported to the boundary of the solid structure by hydraulic conductivity or diffusion within the pore network and evaporates

at the outer surface [17]. This part of the mixing water is also called evaporable, mobile, or free water. Nonetheless, absorption and adsorption of mixing water are always closely linked [18]. The hydration generates a fine pore structure with an increasing inner surface at which physisorption takes place [19]. These two processes are jointly responsible for self-desiccation of concrete [18]. If there is not enough liquid water available, the hydration process is unintentionally decelerated or even stops entirely [20]. This has probably strong negative effects on concrete strength, durability and other properties, leading to a significantly reduced lifetime of the entire structure. A precise modelling and quantification of the entire hydration process at an early state is important to ensure a high level of long-term concrete performance [13, 21].

Figure I.1 shows a schematic sketch of the evolution of water and its different states of matter during the hydration process. In the beginning, the dry bulk material in solid state and the mixing water in liquid state are separated. In this sketch all quantities are given in weight. The sum of the initial weight of dry bulk material and mixing water gives the maximum reachable weight of the hydrated sample. During concreting, both are mixed together, and the hydration starts immediately [13]. In the considered scenario, evaporation is taken into account as well. The mixing water takes all three states of matter. A large portion of the mixing water is used for the hydration of the bulk material. In this process, several hydration products are formed and the mixing water is bound into the material matrix [22, 23, 24]. Although all bound water could be re-extracted at very high temperatures of more than 1000 °C [25], at normal ambient conditions the water becomes part of the solid phase and remains there. This leads to an increase of the dry sample weight over time, because the hydrated water is assigned to the dry material matrix. A portion of the mixing water evaporates at the outer surface of the sample. This water in gaseous phase is adsorbed by the ambient air and does not contribute to the hydration process anymore. Hence, the total weight of the moist sample decreases over time. Both hydration and evaporation lead to a reduction of the mixing water in liquid phase and this process continues until a thermodynamic equilibrium is reached. At this state, the dry material weight remains constant because the hydration process is finished. Furthermore, no evaporation occurs anymore, because the humidity level within the pore network of the sample is in equilibrium with the ambient conditions as well. However, even at this stage, water in liquid phase is still present in the system. This is the physisorption of water at the inner surface of the pore network and can be determined, following various adsorption theories [26, 27, 28]. This remaining part of the mixing water is the material moisture. The adsorbed liquid water in the pores contains dissolved salt and hydroxide ions, leading to different chemical properties compared to the initial mixing water from the tap. Although the thickness of the adsorbed water layer is in the lower nanometre range [27, 29], it is still in liquid phase. The upper right area of figure I.1 shows the final amount of water in each of the phases: the evaporated water in gaseous phase, the adsorbed water in liquid phase and the absorbed/hydrated water as part of the solid phase.

Finally, the ratio between the amount of chemically bound water divided by the ultimate amount of chemically bound water at thermodynamic equilibrium represents the current state of hydration [30, 31]. At thermodynamic equilibrium, the dry sample weight is supposed to be constant. In case of altering the material itself, e.g. by carbonation, the dry sample weight might alter as well. The older the sample, the stronger are the possible deviations. In our experiment, all samples were freshly made, so the influence of carbonation is negligible. Thus, a monitoring of the hydration process is possible by measuring the dry weight of the material matrix over time. As already mentioned, there

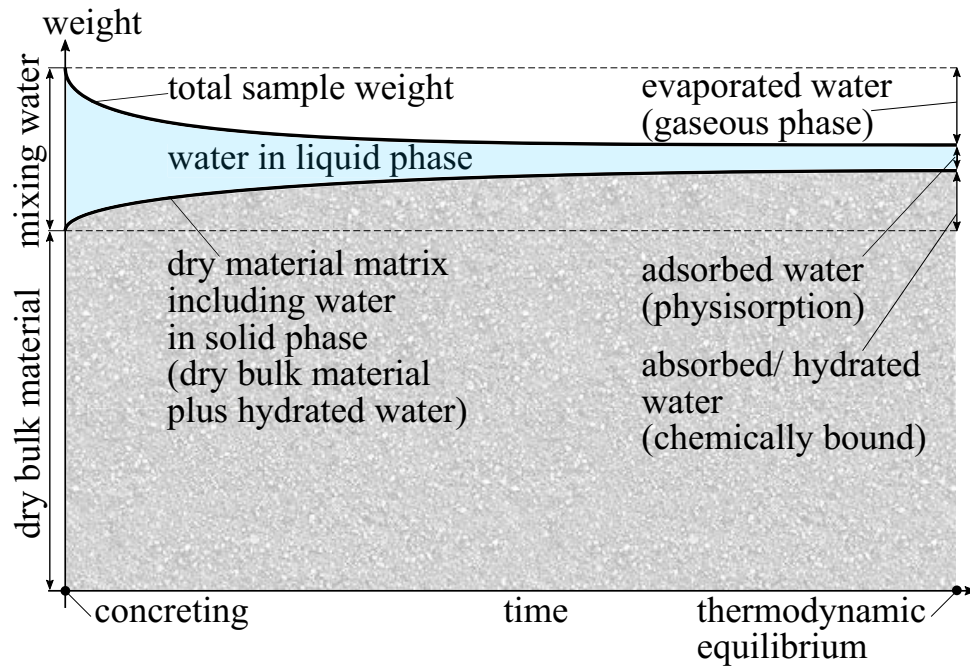


Figure I.1: Schematic sketch of the evolution of the mixing water and its phase transition

are several techniques and settings for material drying. To overcome this uncertainty of choosing the "right" method of drying, a second approach is to measure the amount of water in liquid phase and subtract this from the total weight of the moist sample to yield the dry sample weight. Following the second approach, experimental CCM-measurements are carried out in this study.

I.3 State of the art of measuring the degree of hydration

The hydration process itself includes the formation of several hydration products such as calcium silicate hydrates (C-S-H), ettringite, monosulphate, calcium hydroxide, etc. [22, 23, 24]. In general, two parameters are used to quantify this complex process; the isothermal heat of hydration Q or the amount of chemically bound water w_b [30]. To derive the current state of hydration, these two parameters are set in relation to their final values Q_∞ and $w_{b,\infty}$ when the hydration is completed. Finally, both Q/Q_∞ or $w_b/w_{b,\infty}$ yield theoretically the current state of hydration [30]. Both parameters show an asymptotic approach towards the unit value but never reach this value in practice. This would require an ideal setup including the "perfect" water-to-cement ratio for full hydration and ideal hydration shells around the cement grains [14, 32]. The experimental procedure for measuring Q based on calorimetry is widely established [18, 19] and already standardised [33, 34]. However, adiabatic or isothermal conditions are required, which makes this method only feasible in the laboratory. As a method is required which works reliable in the field as well, calorimetry is not considered further in this study

Another parameter than temperature is required to describe the process in the field. Therefore, several approaches exist to determine the degree of hydration based on w_b , i.e. the amount of bound water. In a first step, the amount of physically bound water has to be determined and/or removed. Probably the most common method is the Darr

drying in an oven [35]. Choosing the right drying temperature is already a widely discussed issue with recommended temperatures between 40 °C and 105 °C for cement-based materials [36, 37, 38, 39, 40]. Ettringite and gypsum might become unstable already at temperatures above ca. 60° C [36, 41, 42], as well as the interlayer water between the C-S-H sheets due to cavitation [43]. It must also be considered that the oven drying may lead to a significant bias in the data, because the hydration process is not stopped immediately after sample extraction. On the contrary, increased ambient temperatures lead to an accelerated hydration as long as sufficient moisture is available within the sample [14, 30]. Oven drying provides in fact only single point measurements and the experimental values might not be representative for the current state of hydration. Therefore, other approaches were developed to determine the material moisture during hydration such as ground penetrating radar [44], time-domain reflectometry [45], electrical impedance and conductivity [46], piezoelectric sensors [47], relative humidity measurements [48, 49], nuclear magnetic resonance relaxometry [50], or infrared spectroscopy combined with scanning electron microscopy [51]. Nevertheless, all these mentioned measurement techniques require a precise calibration for the investigated cement-mixture at controlled ambient conditions. This high laboratory effort prevents these methods from being used in the field. An alternative approach is the use of several Bister-samples instead of investigating the sample of interest directly. All samples are made of the same batch of mixture and exposed to identical environmental conditions. Nevertheless, the challenge of measuring the "true" amount of chemically bound water remains.

Despite the challenges in measuring the DoH, the results are highly dependent on the investigated material. Jennings showed a DoH of around 55 % after three days for a cement-based material with a water-cement ratio of $w/c = 0.4$ based on calorimetry measurements [52]. Similar to this, Di Luzio et al. measured a DoH of 60 % after 7 days for an ordinary Portland cement with $w/c = 0.4$ [31]. Cook et al. investigated mixtures of Type 1 Portland cement with $0.3 \leq w/c \leq 0.7$. After 10 days, the DoH was between 45 % and 55 %, whereas different methods of sample drying were evaluated [53]. A Montalieu cement with $w/c = 0.35$ was investigated by Bentz et al. [32]. There, a DoH of around 82 % was already reached after 4.5 hours. Scrivener et al. found that for a white cement paste with $w/c = 0.4$ that after 10 days only around 5 % of the initial capillary water was present. All these mentioned studies were carried out in the laboratory at controlled ambient conditions and with precisely characterised mixtures. Today, the use of climate-friendly cement and recycled building materials comes more into focus [8, 10, 11, 54]. To determine the DoH of such new and often rather unknown mixtures based on the amount of chemically bound water will be very challenging, even in laboratory. Ideally, the applied measurement technique should be applicable in the field as well.

In this study, we used the calcium carbide method (CCM) to derive the amount of chemically bound water as an indicator of the DoH. The calcium carbide reacts with the evaporable water of sampling material in a pressure vessel. The reaction leads to a measurable pressure increase, which is proportional to the amount of free water [55]. Thereby, this method has several advantages. It is easy to use both in laboratory and in the field. The sampling material is investigated directly without any kind of sample drying. This means there is no time delay and no uncertainty about the drying procedure. Therefore, the measurement value is representative for the current state of hydration and no calibration for the material composition is needed. We investigated two cement-based and two calcium-sulphate-based mixtures for the first 90 days. The CCM measurement are compared with oven dried samples at 40 °C and 105 °C for validation.

I.4 Materials

In this study, two cement-based and two calcium-sulphate-based materials were investigated. The dry bulk material was purchased as bagged goods from a local hardware store. The properties of the different materials are listed in table I.1. As the binder and the aggregates are already premixed, the water demand is given in liter per kilogram dry screed material. The mixing water itself was ordinary tap water. The binder of the screed is identical to concrete, just the maximum aggregate size is 8 mm, which is higher for concrete. For each screed type, three different sample heights h of 50 mm, 60 mm, and 70 mm were investigated. A new sample was required for each of the nine intended measurement days for the destructive CCM testing. In total, 27 samples of each calcium-sulphate screed type, and 54 samples of each cement-based screed type were produced from one respective mixture batch. The number of samples for the cement-based screeds was doubled to investigate the difference between Darr drying at 40 °C and 105 °C. Both ovens had no humidity control, they used just supply air from the ambient. The ambient conditions around the ovens in the experimental hall are estimated to be around 23° C and 40 % relative humidity. ¹

Table I.1: Classification of the used cement-based and calcium-sulphate-based screed types.

binder	type	compressive strength	bending tensile strength	water demand	aggregate size	label
cement (CT)	screed	25 Nmm ⁻²	5 Nmm ⁻²	0.1333 lkg ⁻¹	0 - 5 mm	CT-C25-F5
cement (CT)	rapid screed	40 Nmm ⁻²	7 Nmm ⁻²	0.0875 lkg ⁻¹	0 - 4 mm	CT-C40-F7
calcium-sulphate (CA)	floating screed	25 Nmm ⁻²	5 Nmm ⁻²	0.15 lkg ⁻¹	0 - 4 mm	CA-C25-F5
calcium-sulphate (CA)	floating screed	30 Nmm ⁻²	7 Nmm ⁻²	0.15 lkg ⁻¹	0 - 2 mm	CA-C30-F7

I.5 Experimental approach

CCM requires small portion of sampling material. A certain amount of material of around 10 g to 100 g is extracted and needs to be crushed into small particles. Then, the sampling material is weighted and filled in a pressure vessel with known inner volume. A certain amount of anhydrous calcium carbide is added in a glas-ampulla. Steel balls are placed in the pressure vessel as well for further crushing of the sampling material. Then, the pressure vessel is sealed, and the pressure recording is started. By shaking the vessel by hand, the sampling material is ground and the calcium carbide ampulla cracks. At this point, the chemical reaction starts. [55]

The calcium carbide reacts with the evaporable water of sampling material in the sealed pressure vessel. The reaction takes place at the surface of the calcium carbide particles and must be in contact with the sampling material (through crushing and shaking). Calcium carbide and liquid water react to solid calcium hydroxide and gaseous acetylene ($\text{CaC}_2 + 2\text{H}_2\text{O} \rightarrow \text{Ca}(\text{OH})_2 + \text{C}_2\text{H}_2$). The acetylene occupies more volume than the initial materials, leading to a pressure increase within the pressure vessel. Each molar volume of water leads to the same molar volume of acetylene, independent of the material composition. After the procedure is terminated and the resulting pressure is corrected according to the temperature inside the vessel, the amount of liquid water is known. At this point, the entire chemical reaction is not necessarily finished, i.e. a small amount of

¹product name of the used screeds in the order of table I.1: maxit plan 425, maxit plan 435, maxit plan 470, maxit plan 490

the material moisture has not reacted yet. Calcium carbide might react in the same way with methanol, so the sampling material must be free of methanol to avoid a systematical measurement bias. [55]

According to figure I.1, the weight of the dry material can now be derived. The moist sample material was weighted before filling the sampling material into the pressure vessel. Based on CCM, the weight of liquid water is measured. Subtracting the two weights will give in the dry material weight. This includes the dry bulk material and the hydrated water. Knowing the initial weight of the sister-sample and its w/c-value, the weight of chemically bound water can be determined, independent of the material composition and without the uncertainties of sample drying.

The corresponding equations for the material moisture and weight are briefly summarised. Here, m denotes mass in kg and M stands for the material moisture by weight in kg water per kg material. The material can be considered in two conditions, dry or moist, which leads to different reference masses and moisture values, so that there are two definitions for the material moisture, $M_{moist} = \frac{m_{H_2O}}{m_{moist}}$ or $M_{dry} = \frac{m_{H_2O}}{m_{dry}}$. Equation I.1 gives the relation between the dry mass m_{dry} and the moist mass m_{moist} . The difference between both is the physiosorbed mass of moisture m_{H_2O} .

$$m_{dry} = m_{moist} - m_{H_2O} = m_{moist} - m_{wet} \cdot M_{moist} = m_{moist} \cdot (1 - M_{moist}) \quad (I.1)$$

The Darr method directly yields the dry mass, and hence M_{dry} . Although the CCM approach measures M_{moist} , the underlying calibration functions are mostly given in M_{dry} [55]. Equation I.2 yields the calculation of M_{moist} based on M_{dry} . This formulation is free of any measured mass and therefore generally applicable.

$$M_{moist} = \frac{1 - M_{dry}}{-M_{dry} + \frac{1}{M_{dry}}} \quad (I.2)$$

To describe the hydration process according to figure I.1, the determined masses are normalised by the initial mass $m_{initial}$, which is the summation of the dry bulk material and the mixing water. Following the initial identity of $m_{dry} = m_{moist} - m_{H_2O}$, the two different measurement principles are directly comparable.

$$\frac{m_{moist} \cdot (1 - M_{moist,CCM})}{m_{initial}} \hat{=} \frac{m_{dry,Darr}}{m_{initial}} \quad (I.3)$$

I.6 Testing procedure and sample preparation

To cast the samples, cylindric formworks were designed as shown in Figure I.2. Therefore, sliced polyvinyl chloride pipes were attached and sealed on a filmfaced plywood with silicone. A vertical slit closed by a hose clamp was applied to ensure an easy stripping of the formwork after casting. All screed mixtures were produced according to the manufacturers' instructions and then poured into the formworks. With a vibrating table, an appropriate compression was achieved. Unlike the drawing in Figure I.2, multiple formworks were attached to one single plywood to accelerate the described process of casting and compressing. Because of this, it was not possible to weigh each individual sample immediately after casting. Instead, this was therefore postponed to the day after casting. During this time all fresh samples were covered with a PE foil to limit the evaporation of mixing water.

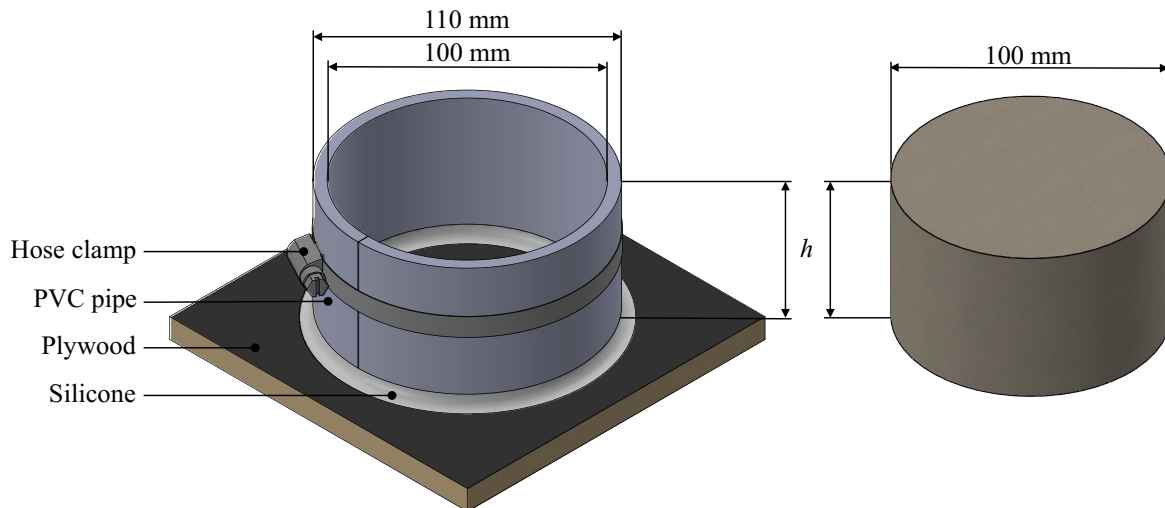


Figure I.2: Formwork (left) to cast the resulting screed sister-samples (right) of 100 mm diameter and varying heights h of 50 mm, 60 mm, and 70 mm.

After a 20 hour curing time, the formworks were removed, and each sample was weighed to obtain $m_{initial}$. Then, the bottom and side surfaces were covered with PE foil and waterproof tape, respectively, to allow a realistic self-desiccation from above. For the remaining testing time, all samples were stored under controlled climatic conditions of 23 °C and 50 % relative humidity. The first measurement day was 7 days after casting followed by tests after 10, 14, 21, 28, 35, 50, 70, and 90 days. For CT-C25-F5 the first measurement had to be discarded due to the use of outdated calcium carbide.

A measurement day included the following procedure:

1. The respective sister-sample is removed from the climate chamber and unwrapped from its waterproof tape and PE foil cover.
2. The sample is weighed to obtain $m_{moist,total}$ for the CCM.
3. CCM testing is performed.
 - (a) A small portion of material was taken off destructively from the sample:
 - i. CT screed: Since there are two samples for each measurement day, 20 g are collected from the upper part of the first, and from the lower part of the second sample. The broken off piece was approximately 30 mm deep on each side, independent of the sample thickness.
 - ii. CA screed: According to the expected moisture content, 20 g (7 days old), 50 g (10 days or older) or 100 g (35 days or older) are collected over the entire height of the sample.
 - (b) CCM procedure is further conducted as described in I.5 to obtain $M_{moist,CCM}$. According to the manufacturer's manual the time intervals for shaking the vessel were: (start) 1 min shaking - 3 min rest - 1 min shaking - 5 min rest - 10 s shaking (end).
4. The remaining sample is weighed to obtain $m_{moist,remain}$ for Darr drying.
5. The remaining sample is then put into an oven:

- (a) CT screed: one sample is dried at 40 °C, one at 105 °C
- (b) CA screed: dried at 40 °C

All measurements were carried out by the same person to reduce the influence of the human factor. This is especially relevant for the CCM testing, where the intensity of shaking could have an influence on the release of reactive liquid water. To avoid this, commercial CCM manufacturer might offer stir sticks connected to an electric drill to generate a recurring crushing of the material. If flinty stones are included in the material, the stir sticks avoids sparking which might ignite the gas inside the pressure vessel. The emitted pressure wave is not a safety issue, but would probably destroy the membrane of the integrated pressure sensor.

During the drying process, the sample weights were controlled in appropriate intervals of one to three days. The samples were removed from the oven and were left for 20 minutes to cool off, before being weighed. According to [35], m_{dry} is reached, when the difference in mass on three consecutive weightings (with at least 24 hours in between) does not change more than 0.1 % of the total mass. The average drying time for CT screed was 21 to 22 days at 40 °C and 7 to 8 days at 105 °C. CA screed dried after 6 to 7 days at 40 °C.

I.7 Results

In a first step, the results of the measured material moisture are compared between the CCM and Darr method. For the latter, the influence of the drying temperature is discussed as well. Afterwards, the amount of chemically bound water is derived.

I.7.1 Comparison of material moisture based on Darr and CCM

Figure I.3 shows the measured material moisture of the calcium-sulphate-based samples over time. For both screed types, an oven temperature of 40 °C is recommended for Darr drying. The first measurements started 7 or 10 days after concreting, showing the highest moisture values for both methods. After around 70 days, both sample moisture values are close to equilibrium. The CCM gives constant material moisture and the Darr drying indicates still a slightly decreasing moisture. Nevertheless, all four lines show the expected asymptotic trend. Furthermore, the correlation is high between the CCM and Darr method. If unintended hydration is going on during oven drying, the material moisture decreases. The opposite is measured for both samples. The Darr drying gives higher moisture values for at least the first 20 days. These measurements indicate that hydration is negligible in the time frame between sample extraction and the end of oven drying. In this case, both approaches seem to be suitable for the measurement of material moisture, and in consequence for the determination of chemically bound water as well.

The same analysis as described above is done for the cement-based sample CT-C25-F5. For cement-based material, there is no unified drying temperature [39]. For practical reasons, 105 °C are chosen which yields the shortest measurement time. Nevertheless, several studies proved that this high drying temperature is already able to dissolve chemically bound water [36, 37, 38]. In this context, the mineral ettringite which is formed during hydration plays a role [22, 23, 24]. The water-rich ettringite mineral becomes unstable at temperatures above ca. 60 °C and/or at low relative humidity below 30 %RH [36, 41, 42]. Hence, oven drying at 105 °C might cause systematical deviations regarding

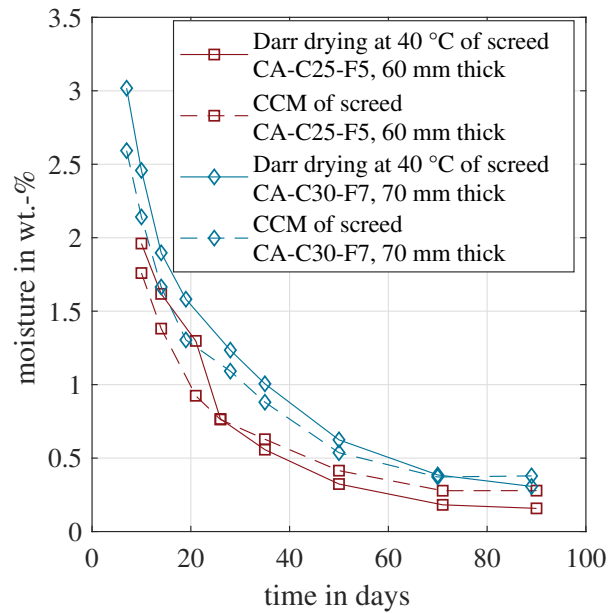


Figure I.3: Evolution of the material moisture measured by CCM and Darr drying for the calcium-sulphate-based samples CA-C25-F5 and CA-C30-F7

the material moisture. Therefore, a second oven drying temperature was chosen of 40 °C with around 15 %RH. Furthermore, sampling material was extracted individually from the upper part of the first, and from the lower part of the second CT sample, as described in I.6.

Figure I.4 depicts the resulting moisture content for all four approaches for CT-C25-F5. The Darr drying was done at 40 °C or 105 °C, respectively. The drying temperature of 105 °C yields significantly higher material moisture values. The deviation between both is between 1.6 wt.-% and 2.1 wt.-%. This clearly indicates that with the 105 °C drying temperature the amount of physiosorbed (evaporable) water cannot be correctly determined. The solid cement structure is partly damaged and chemically bound water is released and evaporated. The sample weight decreases, which is incorrectly recognised as a higher material moisture. In consequence, the 105 °C data will not be considered in further analyses. In addition, the two CCM measurements from the upper and lower part are shown. The upper part, which includes the top surface where the evaporation takes place, shows lower moisture values compared to the lower part. Furthermore, the moisture is significantly below the one recorded for the Darr drying at 40 °C. The main reason is the moisture gradient within the sample. Comparable measurements were carried out with cement-based screed samples with a thickness of 70 mm [17, 56]. Here it is shown that the moisture gradient can vary by more than 2 wt.-% within the sample during hydration and drying. As Darr drying includes the entire sample, the CCM approach should consider the entire cross section as well. In consequence, the values of the upper and lower part are averaged to yield a representative CCM measurement for the entire sample. This mean value is used for further analyses in this study.

In conclusion, the Darr drying at 40 °C quantifies the evaporable moisture, while keeping the solid cement matrix intact. Because the entire sample is dried in the oven, obviously the entire cross section is affected by this method. In consequence, it is compared with the mean CCM of the upper and lower part. This should be a representative value, despite a certain moisture gradient. As shown in figure I.4, the two curves coincide. Within the first

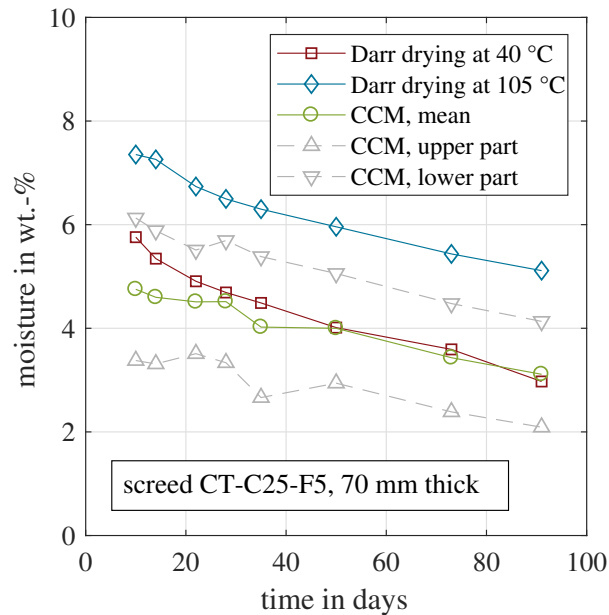


Figure I.4: Evolution of the material moisture measured by CCM and Darr drying for the cement-based samples CT-C25-F5

30 days, some deviations are visible with a maximum deviation of 1 wt.-% on day 10. In the beginning, the samples are very moist and the carbide is probably not able to react with all adsorbed water within the common 10 minutes. With an adapted measurement procedure with an extended time period would probably decrease the deviation between Darr drying and CCM with the first 30 days.

Figure I.5 presents the same analysis for the second cement-based material CT-C40-F7. All measured moisture values are lower compared to CT-C25-F5. This is mainly caused by the lower water demand for CT-C40-F7, see table I.1. A bigger portion of the mixing water is required for the hydration process and less evaporable water remains in the sample. Hence, the measured material moisture is reduced. The material moisture deviations between the two different Darr drying temperatures are even more prominent, if compared to CT-C25-F5, in absolute and relative numbers. For CT-C40-F7, the 105 °C drying results in moisture values almost twice as much as for 40 °C. This indicates that the solid material matrix is even more affected and damaged by the high drying temperature. The CCM measurements of the upper and lower part are closer to each other, mainly caused by the overall reduced material moisture. For this material, the averaged CCM moisture values are above those of the Darr drying at 40 °C. This systematic deviation was also observed for the two other samples with 50 mm and 60 mm thickness. The authors' hypothesis to explain the deviation is the higher amount of cement paste in the material. It is more difficult for the carbide to reach the entire adsorbed water in the pore network. Thus, not all water has reacted after 10 minutes.

For CT-C25-F5, the Darr moisture is above the CCM moisture within the first 40 days. In case of CT-C40-F7, the moisture is similar at the two first measurement days. Then, the Darr moisture decreases more rapidly than the CCM moisture. If unintended hydration during oven drying would occur, both trends must be the opposite. Therefore, the measurements indicate that hydration during Darr drying after sample extraction is negligible and does not affect the amount of chemically bound water.

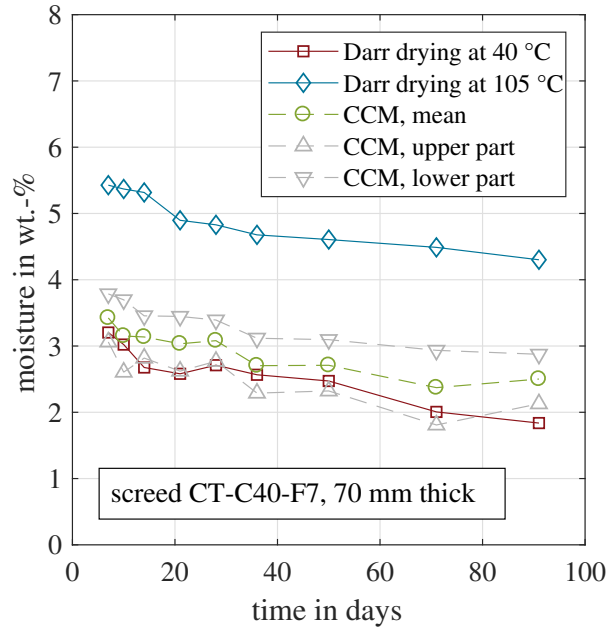


Figure I.5: Evolution of the material moisture measured by CCM and Darr drying for the cement-based samples CT-C40-F7

Based on the material moisture measurements, CCM shows a satisfying correlation to the Darr drying at 40 °C for both investigated materials. In a next step, the amount of chemically bound water will be calculated based on the CCM measurements.

I.7.2 Determination of the chemically bound water based on Darr drying and CCM

According to figure I.1, subtracting the physisorbed (evaporable) water from the sample weight of the moist material gives the dry material weight. This is the weight of the dry bulk material plus the hydrated water. In contrast to other approaches, this method avoids sample drying and/ or a time delay between sampling material extraction and receiving a measurement value.

Figure I.6 shows the results based on this approach for the two calcium-sulphate-based screeds. All weights are normalised by the initial weight during concreting, which is the weight of the dry bulk material plus the weight of the mixing water, according to figure I.1. In figure I.6, the normalised weight of the moist sample is decreasing over time, caused by the evaporation of mixing water. Both samples tend asymptotically towards their final values when the hydration is finished, and the complete sample has reached its equilibrium moisture content [56]. This final condition can probably not be reached after the presented 90 days. According to equation I.3, the depicted dry weight is determined experimentally in two ways. The first approach is based on CCM. The dry mass is gained by measuring the moist sample weight and the material moisture. The second approach is the common Darr drying in the oven at 40 °C. In addition, the normalised dry bulk material is shown. This is the lower limit, if the entire mixing water would evaporate and no water adsorption or adsorption would take place in the bulk material. The theoretical value is a direct function of the w/c value, as shown in equation I.4. Because both materials had the same initial water demand during mixing, the normalised dry bulk material is identically for

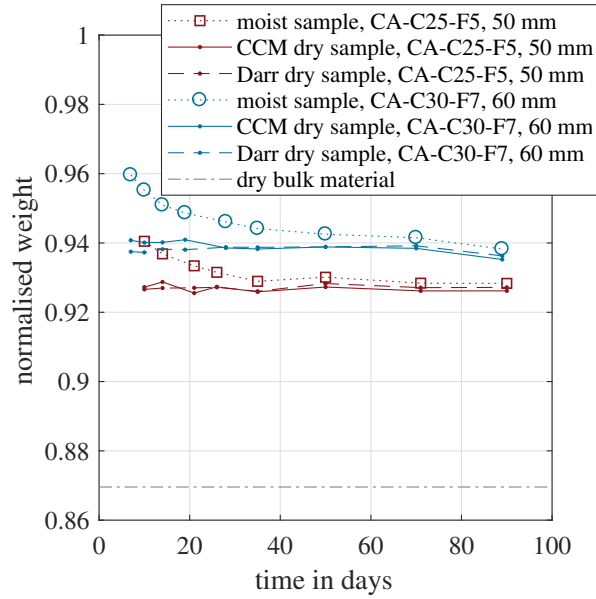


Figure I.6: Evolution of the normalised dry weight over time measured for two samples with a calcium-sulphate-based binder

both screed types.

$$\frac{m_{bulk}}{m_{initial}} = \frac{1}{1 + (w/c)} \quad (\text{I.4})$$

For both samples, the normalised dry weight coincides for the CCM and Darr method. Within the first 20 days, a slight scatter is observable. For the subsequent 70 days, the values are almost identical. Furthermore, for both materials, the values are nearly constant. This indicates that the hydration process is completed already before the first measurement on day seven or ten and proves that the entire solid material matrix has been formed entirely within one week. Although the initial water demand was identical for both samples, the dry material weight is approximately one percent higher for CA-C30-F7. This mixture is designed to withstand a higher compressive strength, as stated in the published data sheet, provided by the manufacturer. This is generally achieved with a higher material compaction due to an increased hydration rate. Related to the available water in the beginning, around 7.7 % additional mixing water was hydrated. Figure I.7 presents the same approach for the two cement-based materials. Because these two mixtures have a different water demand, the lower limit expressed by the dry bulk material weight varies. As expected, the normalised weight of the moist samples decreases with time due to water evaporation. For the CT-C40-F7 sample, the Darr dried samples weight is above the CCM value during all measurement days. In case of CT-C25-F5, the trend is the opposite, except for the last measurement point on day 90.

Between day 7 and 21, both methods show that the dry sample weight increases for the CT-C40-F7. But later, it also decreases again for both methods. These fluctuations are probably caused by the general measurement uncertainty and a clear trend cannot be derived. Eventually, no significant increase in dry weight can be determined. This indicates that for the cement-based materials the hydration is also completed within the first week. This is contradicting other studies, because the formation of C-S-H is supposed to take several months [22, 23, 24]. On the other hand, this formation is a reformation within the solid cement matrix, e.g. ettringite transforms to C-S-H and monosulphate [23]. This

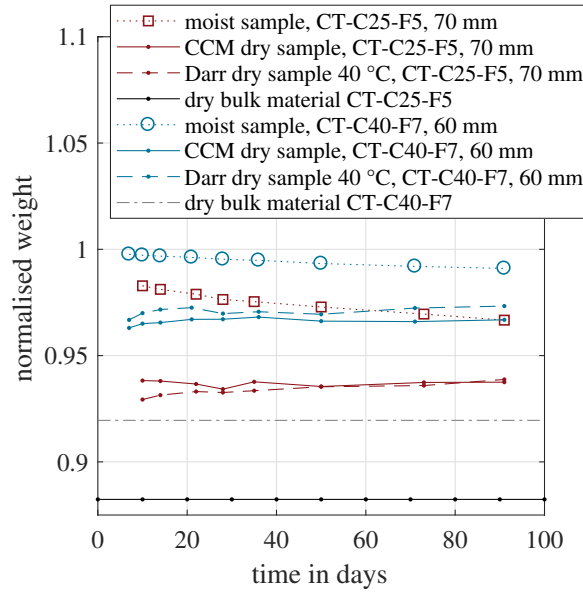


Figure I.7: Evolution of the normalised dry weight over time measured for two samples with a cement-based binder

process might not need evaporable water, although it is an exothermic reaction, which is measurable with calorimetry. In such a case, monitoring the amount of chemically bound water could not disclose the hydration process entirely.

However, this study's central subject is the experimental determination of chemically bound water. In conclusion, the CCM approach coincides well with the Darr dried sample at 40 °C. Therefore, CCM is able to appropriately quantify the amount of chemically bound water and could be used for hydration monitoring. This approach avoids long-term oven drying and delivers contemporary results in the laboratory as well as in the field. Furthermore, by modifying the measurement procedure, this method enables also the on-site quantify of crystalline bonded water of ettringite incorporated in the material sample [57].

I.7.3 Comparison of Darr drying and CCM applied to quantify chemisorbed water

Darr drying and CCM are able to quantify the evolution of the chemisorbed water and the hydration process. In Figure I.8, both methods are compared to each other based on a common linear regression. The regression includes only one coefficient, the slope. A y-axis intercept is excluded for two reasons. First, an offset between both methods is unreasonable, because a totally dry material should be quantified as zero for both methods. Second, the definition area is $\mathbb{D} = \mathbb{R}(0, 1)$, but measured values are all above 0.92. Here, the sampling points have a large leverage towards the origin of coordinates. Thus, small scatter of the data points would have an exaggerated influence on the estimated y-axis intercept.

The slope coefficient s was calculated based on all 102 sampling points of the normalised dry weight. Here, only the Darr drying value at 40 °C were included, which leads to $s = 0.9995$. The corresponding coefficient of determination is $R^2 = 0.958$. The slope value is very close to one and around 96 % of the variance of the data can be explained by this simple linear regression model. This confirms the high agreement between Darr drying at

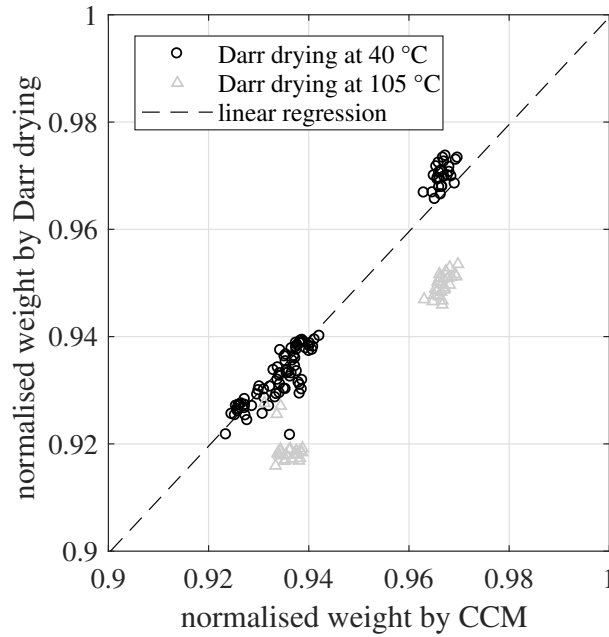


Figure I.8: Linear regression of the normalised weight based on CCM and Darr drying (at 40 °C). The regression comprises only a slope coefficient, excluding a y-axis intercept.

40 °C and CCM for determining the DoH. On the other hand, the Darr values at 105 °C show a systematic negative bias of around two percentage points. One more time, this validates that such a high drying temperature is able to extract chemisorbed water from the investigated material samples. Furthermore, looking on the residuals of the regression, there is no indication that the different sample thicknesses have any influence on the determination of the DoH.

I.8 Conclusion

The essential properties of hydraulically bound materials are determined during the first hours, days and weeks after concreting. A proper hydration process is crucial for structural performance and long-lasting durability. The process can be measured and monitored by calorimetry or by determining the amount of chemically bound water. For the latter approach, the time-consuming Darr drying method is often used which has several systematic measurement uncertainties, such as the selection of the correct drying temperature. In this study, the CCM as an alternative method is presented and evaluated. This method delivers contemporary results, can be used in the field as well and covers all kinds of material compositions and binders. This makes the method highly suitable to monitor the DoH of CO₂-reduced binders, new mixtures, or recycled materials. In case of unexpected ambient conditions such as heat and drought periods, this in situ methods which delivers prompt results enables a dense DoH monitoring if required.

The main findings are:

- CCM directly measures the physiosorbed (evaporable) water and hence, is capable for hydration monitoring
- The measured material moisture and the derived hydration curves of CCM highly coincide with Darr measurements at 40 °C oven temperature

- Darr drying at 105 °C highly affects the solid material structure and dissolves chemically bound water. This systematic deviation influences the measured material moisture by more than 50 % for the cement-based materials investigated here
- The quantification of chemically bound water with the Darr and the CCM method shows for both methods that no significant chemisorption of free water occurs between measurement day 7 and 90 for the calcium-sulphate-based and the cement-based materials.
- The formation of the C-S-H generally takes several months. The formation and reformation of C-S-H, ettringite, monosulphate, calcium hydroxide might represent an exothermal process, which is measurable with calorimetry. But the current measurements indicate, that this process is unaffected by the amount of evaporable or chemically bound water

CCM coincides well with Darr drying at 40 °C. CCM is an alternative to the time-consuming oven drying. Due to its easy handling and independence of the material composition, it can be applied to all scarcely-researched binder types. For both established or new “alternative” materials, the monitoring of the hydration process and its experimental quantification remains crucial for the creation of safe and long-lasting structures.

Bibliography

- [1] Emily Elhacham, Liad Ben-Uri, Jonathan Grozovski, Yinon M Bar-On, and Ron Milo. Global human-made mass exceeds all living biomass. *Nature*, 588(7838):442–444, 2020.
- [2] Fridolin Krausmann, Christian Lauk, Willi Haas, and Dominik Wiedenhofer. From resource extraction to outflows of wastes and emissions: The socioeconomic metabolism of the global economy, 1900–2015. *Global Environmental Change*, 52:131–140, 2018.
- [3] Raili Kajaste and Markku Hurme. Cement industry greenhouse gas emissions–management options and abatement cost. *Journal of Cleaner Production*, 112:4041–4052, 2016.
- [4] International Energy Agency. Technology roadmap low-carbon transition in the cement industry. Technical report, World Business Council for Sustainable Development and International Energy, 2018.
- [5] Uwe Kunert and Heike Link. Verkehrsinfrastruktur: Substanzerhaltung erfordert deutlich höhere Investitionen. *Deutsches Institut für Wirtschaftsforschung-Wochenbericht*, 80(26):32–38, 2013.
- [6] Bundesministerium für Verkehr und digitale Infrastruktur. Verkehr in Zahlen 2020/21, 2020.
- [7] Gero Marzahn, Olaf Mertzsch, and Lisa Kramer. Load-bearing index to grade structural capacities of road bridges. *Beton- und Stahlbeton*, 115(7):542–550, 2020.
- [8] Karen L Scrivener, Vanderley M John, and Ellis M Gartner. Eco-efficient cements: Potential economically viable solutions for a low-CO₂ cement-based materials industry. *Cement and Concrete Research*, 114:2–26, 2018.
- [9] World Wildlife Fund. Klimaschutz in der Beton-und Zementindustrie-Hintergrund und Handlungsoptionen. *World Wildlife Fund Deutschland, Berlin*, 2019.
- [10] J M Kinuthia and J E Oti. Designed non-fired clay mixes for sustainable and low carbon use. *Applied Clay Science*, 59:131–139, 2012.
- [11] Wolfram Schmidt, Michael Commeh, Kolawole Olonade, Gesine Lenore Schiewer, David Dodoo-Arhin, Risikat Dauda, Shirin Fataei, Angela Tetteh Tawiah, Fatma Mohamed, Mareike Thiedeitz, et al. Sustainable circular value chains: From rural waste to feasible urban construction materials solutions. *Developments in the Built Environment*, 6:100047, 2021.
- [12] European Environment Agency. Waste management in the EU. Technical report, European Commission, Brussels, Belgium, 2021.
- [13] Byung Hwan Oh and Soo Won Cha. Nonlinear analysis of temperature and moisture distributions in early-age concrete structures based on degree of hydration. *Materials Journal*, 100(5):361–370, 2003.


- [14] Giovanni Di Luzio and Gianluca Cusatis. Hygro-thermo-chemical modeling of high performance concrete. I: Theory. *Cement and Concrete Composites*, 31(5):301–308, 2009.
- [15] C Strangfeld, P Wiehle, and S M Munsch. About the dominance of mesopores in physisorption in amorphous materials. *Molecules*, 26(7190):1–22, 2021.
- [16] Yunping Xi, Zdeněk P Bažant, Larissa Molina, and Hamlin M Jennings. Moisture diffusion in cementitious materials moisture - capacity and diffusivity. *Advanced Cement Based Materials*, 1(6):258–266, 1994.
- [17] C. Strangfeld. Determination of the diffusion coefficient and the hydraulic conductivity of porous media based on embedded humidity sensors. *Construction and Building Materials*, 263:1–13, 2020.
- [18] Michael Gerstig and Lars Wadsö. A method based on isothermal calorimetry to quantify the influence of moisture on the hydration rate of young cement pastes. *Cement and Concrete Research*, 40(6):867–874, 2010.
- [19] Dehui Wang, Caijun Shi, Nima Farzadnia, Zhenguo Shi, Huangfei Jia, and Zhihua Ou. A review on use of limestone powder in cement-based materials: Mechanism, hydration and microstructures. *Construction and Building Materials*, 181:659–672, 2018.
- [20] Treval Clifford Powers. A discussion of cement hydration in relation to the curing of concrete. In *Proceedings of the 27th Meeting of Highway Research Board, Washington, D.C.*, volume 27, pages 178–188. Highway Research Board, 1948.
- [21] Jun Zhang, Jiahe Wang, and Yuan Gao. Moisture movement in early-age concrete under cement hydration and environmental drying. *Magazine of Concrete Research*, 68(8):391–408, 2016.
- [22] Barbara Lothenbach, Daniel Rentsch, and Erich Wieland. Hydration of a silica fume blended low-alkali shotcrete cement. *Physics and Chemistry of the Earth, Parts A/B/C*, 70:3–16, 2014.
- [23] Koichi Maekawa, Rajesh Chaube, and Toshiharu Kishi. *Modelling of concrete performance*. E & FN Spon, London, 1999.
- [24] Karen L Scrivener, Patrick Juilland, and Paulo JM Monteiro. Advances in understanding hydration of Portland cement. *Cement and Concrete Research*, 78:38–56, 2015.
- [25] Min Li, ChunXiang Qian, and Wei Sun. Mechanical properties of high-strength concrete after fire. *Cement and Concrete Research*, 34(6):1001–1005, 2004.
- [26] Stephen Brunauer, Paul Hugh Emmett, and Edward Teller. Adsorption of gases in multimolecular layers. *Journal of the American Chemical Society*, 60(2):309–319, 1938.
- [27] Arne Hillerborg. A modified absorption theory. *Cement and Concrete Research*, 15(5):809–816, 1985.

- [28] James H Young and GL Nelson. Theory of hysteresis between sorption and desorption isotherms in biological materials. *Transactions of the American Society of Agricultural and Biological Engineers*, 10:260–263, 1967.
- [29] Christoph Strangfeld. Quantification of the Knudsen effect on the effective gas diffusion coefficient in partially saturated pore distributions. *Advanced Engineering Materials*, 2021.
- [30] Ivindra Pane and Will Hansen. Investigation of blended cement hydration by isothermal calorimetry and thermal analysis. *Cement and Concrete Research*, 35(6):1155–1164, 2005.
- [31] Giovanni Di Luzio and Gianluca Cusatis. Hygro-thermo-chemical modeling of high-performance concrete. II: Numerical implementation, calibration, and validation. *Cement and Concrete Composites*, 31(5):309–324, 2009.
- [32] Dale P Bentz, Vincent Waller, and Francois de Larrard. Prediction of adiabatic temperature rise in conventional and high-performance concretes using a 3-D microstructural model. *Cement and Concrete research*, 28(2):285–297, 1998.
- [33] ASTM International. Standard practice for measuring hydration kinetics of hydraulic cementitious mixtures using isothermal calorimetry. *C1679-17*, 2017.
- [34] ISO. ISO 29582-1:2009: Methods of testing cement - Determination of the heat of hydration. *International Standard: Geneva, Switzerland*, 2009.
- [35] DIN. EN ISO 12570:2000: Wärme- und feuchtetechnisches Verhalten von Baustoffen und Bauprodukten - Bestimmung des Feuchtegehaltes durch Trocknen bei erhöhter Temperatur. *Deutsche Norm, German Standard*, 2000.
- [36] I Galan, H Beltagui, M Garcia-Mate, F P Glasser, and M S Imbabi. Impact of drying on pore structures in ettringite-rich cements. *Cement and Concrete Research*, 84:85–94, 2016.
- [37] A Korpa and R Trettin. The influence of different drying methods on cement paste microstructures as reflected by gas adsorption: Comparison between freeze-drying (F-drying), D-drying, P-drying and oven-drying methods. *Cement and Concrete Research*, 36(4):634–649, 2006.
- [38] L Zhang and F P Glasser. Critical examination of drying damage to cement pastes. *Advances in Cement Research*, 12(2):79–88, 2000.
- [39] Z Wu, HS Wong, and NR Buenfeld. Influence of drying-induced microcracking and related size effects on mass transport properties of concrete. *Cement and Concrete Research*, 68:35–48, 2015.
- [40] Zhizhou Wu, H S Wong, and N R Buenfeld. Transport properties of concrete after drying-wetting regimes to elucidate the effects of moisture content, hysteresis and microcracking. *Cement and Concrete Research*, 98:136–154, 2017.
- [41] Q Zhou and F P Glasser. Thermal stability and decomposition mechanisms of ettringite at $<120^{\circ}$ C. *Cement and Concrete Research*, 31(9):1333–1339, 2001.

- [42] Luis G Baquerizo, Thomas Matschei, and Karen L Scrivener. Impact of water activity on the stability of ettringite. *Cement and Concrete Research*, 79:31–44, 2016.
- [43] Monisha Rastogi, Arnaud Müller, Mohsen Ben Haha, and Karen L Scrivener. The role of cavitation in drying cementitious materials. *Cement and Concrete Research*, 154:106710, 2022.
- [44] Wai Lok Lai, Thomas Kind, and Herbert Wiggenhauser. A study of concrete hydration and dielectric relaxation mechanism using ground penetrating radar and short-time Fourier transform. *EURASIP Journal on Advances in Signal Processing*, pages 1–14, 2010.
- [45] Andrea Cataldo, Egidio De Benedetto, and Giuseppe Cannazza. Hydration monitoring and moisture control of cement-based samples through embedded wire-like sensing elements. *IEEE Sensors Journal*, 15(2):1208–1215, 2014.
- [46] S W Tang, X H Cai, Zhen He, Wenjun Zhou, H Y Shao, Z J Li, T Wu, and E Chen. The review of early hydration of cement-based materials by electrical methods. *Construction and Building Materials*, 146:15–29, 2017.
- [47] Arun Narayanan, Amarteja Kocherla, and Kolluru VL Subramaniam. Embedded PZT sensor for monitoring mechanical impedance of hydrating cementitious materials. *Journal of Nondestructive Evaluation*, 36(4):1–13, 2017.
- [48] A S El-Dieb. Self-curing concrete: Water retention, hydration and moisture transport. *Construction and Building Materials*, 21(6):1282–1287, 2007.
- [49] Zhangli Hu, Mateusz Wyrzykowski, and Pietro Lura. Estimation of reaction kinetics of geopolymers at early ages. *Cement and Concrete Research*, 129:105971, 2020.
- [50] M W Bligh, M N d’Eurydice, R R Lloyd, C H Arns, and T D Waite. Investigation of early hydration dynamics and microstructural development in ordinary Portland cement using ^1H NMR relaxometry and isothermal calorimetry. *Cement and Concrete Research*, 83:131–139, 2016.
- [51] Rikard Ylmén, Ulf Jäglid, Britt-Marie Steenari, and Itai Panas. Early hydration and setting of Portland cement monitored by IR, SEM and Vicat techniques. *Cement and Concrete Research*, 39(5):433–439, 2009.
- [52] Hamlin M Jennings. A model for the microstructure of calcium silicate hydrate in cement paste. *Cement and Concrete Research*, 30(1):101–116, 2000.
- [53] Raymond A Cook and Kenneth C Hover. Mercury porosimetry of hardened cement pastes. *Cement and Concrete Research*, 29(6):933–943, 1999.
- [54] Sofiane Amziane and Mohammed Sonebi. Overview on biobased building material made with plant aggregate. *RILEM Technical Letters*, 1:31–38, 2016.
- [55] F. Radtke. Bestimmung des Wassergehaltes mit der Carbid-Methode. Technical report 1.8, Radtke Messtechnik, 2015.

- [56] Christoph Strangfeld and Sabine Kruschwitz. Monitoring of the absolute water content in porous materials based on embedded humidity sensors. *Construction and Building Materials*, 177:511–521, 2018.
- [57] Frank Radtke. On-site determination of crystalline bonded water of ettringite. In *4th International Conference Calcium Aluminates, Avignon, France*, 2014.

II. Poster: Combination of Radar and Neutron Probe to Determine the Mass Moisture of Screeds




BAM
Bundesanstalt für
Materialforschung
und -prüfung

Kombination von Radar und Neutronensonde zur Bestimmung der Massenfeuchte von Estrichen

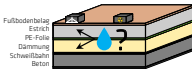
Tim Klewe¹, Christoph Strangfeld¹, Sabine Kruschwitz^{1,2}, Tobias Ritzer³

¹ Bundesanstalt für Materialforschung und -prüfung (BAM)
² Technische Universität Berlin
³ Ingenieurbüro Tobias Ritzer GmbH



2,8 Mrd. €
Leitungswasserschäden
in 2017 [1]

Projekt: Zerstörungsfreie Lokalisierung von Flüssigwasser in Schichtaufbauten



Voruntersuchung an Einzelschicht
Estrich

Probekörper & Datenaufnahme

Probekörper (PK): 800 mm x 800 mm x H
Schwesterproben (SP): 100 mm Ø x H

PK: 12 Stück
SP: 9 je PK

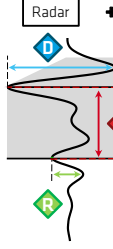
Tag 1 bis >90 nach der Herstellung

- Feuchtemessung mittels Radar (2 GHz) und Neutronensonde
- Referenzverfahren bei PK gravimetrisch und Darr-Trocknung, SP mit Darr-Trocknung und CM-Messungen an 9 Stichtagen

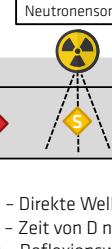
Bezeichnung	Bindemittel	Festigkeit	H in mm
CT1	Zement	normal	50, 60, 70
CA1	Anhydrit	normal	
CT2	Zement	hoch	
CA2	Anhydrit	hoch	

Variablen für Multiple Lineare Regression (MLR)

Radar



+ Neutronensonde

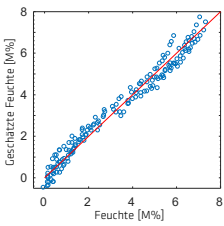


Estrich-PK H

D - Direkte Welle, Amplitude
T - Zeit von D nach R
R - Reflexionswelle, Amplitude
S - Neutronensonde

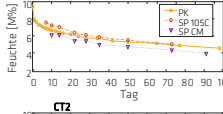
R²_{adj} für verschiedene Variablenkombinationen

0,870	0,488	0,788	0,175
0,959	0,972	0,843	
0,974			

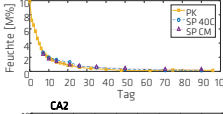


Feuchteverläufe | Bsp.: 60 mm Probekörper

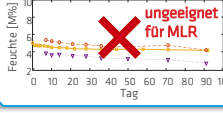
CT1



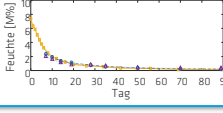
CA1



CT2



CA2



Diskussion

- Radarvariablen ohne Neutronensonde bereits sehr genau
- Kombination aller Variablen zeigt großes Potential zur Bestimmung der Massenfeuchte mittels MLR
- Bei bekannter Höhe wird Variable T am stärksten ($R^2_{adj} = 0,924$)
 - hohe Tiefenabhängigkeit
- Bei bekanntem Bindemittel erreicht S ein $R^2_{adj} = 0,905$
 - hohe Materialabhängigkeit
- Prüfung der Validität über Testdatensatz noch ausstehend

Referenzen
[1] Gesamtverband der Deutschen Versicherungswirtschaft e.V. (<http://www.gdv.de/zahlen-fakten/schaden-und-unfallversicherung/wohngebäudeversicherung/>), abgerufen am 28.03.2019
Icons von www.flaticon.com. Autoren: Metropolisicons, Freepik, Srip, Simpleicon

Sicherheit in Technik und Chemie

www.bam.de

Complete List of Publications

Included in Cumulative Dissertation

Paper A

- **T. Klewe**, C. Strangfeld, S. Kruschwitz, Review of moisture measurements in civil engineering with ground penetrating radar - Applied methods and signal features, *Construction and Building Materials*, Published Article, <https://doi.org/10.1016/j.conbuildmat.2021.122250>, 02.2021

Paper B

- **T. Klewe**, C. Strangfeld, T. Ritzer, S. Kruschwitz, Combining Signal Features of Ground Penetrating Radar to Classify Moisture Damage in Layered Building Floors, *Applied Sciences*, Published Article, <https://doi.org/10.3390/app11198820>, 09.2021

Paper C

- **T. Klewe**, C. Strangfeld, T. Ritzer, S. Kruschwitz, Classification of On-Site Floor Moisture Damage with GPR - Limitations and Chances, Manuscript submitted to the Journal of 'Construction and Building Materials', 08.2022

Other Related Publications

Articles and Conference Papers

- C. Strangfeld, **T. Klewe**, Comparison of the Calcium Carbide Method and Darr Drying to Quantify the Amount of Chemically Bound Water in Early Age Concrete, *Materials*, Published Article, 10.2022, <https://doi.org/10.3390/ma15238422>
- C. Strangfeld, **T. Klewe**, Hygrometric Moisture Measurements Based on Ebedded Sensors to Determine the Mass of Moisture in Porous Building Materials and Layered Structures, *Lecture Notes in Civil Engineering: European Workshop on Structural Health Monitoring*, Conference paper, 01.2021, https://doi.org/10.1007/978-3-030-64594-6_22
- **T. Klewe**, C. Strangfeld, T. Ritzer, S. Kruschwitz, Nondestructive determination of moisture damage in layered building floors, *18th International Conference on*

Ground Penetrating Radar, Conference paper, 07.2020, <https://doi.org/10.1190/gpr2020-045.1>

- **T. Klewe**, C. Strangfeld, T. Ritzer, S. Kruschwitz, Zerstörungsfreie Lokalisierung von Flüssigwasser in Fußböden durch Kombination von Radar und Neutronensonde, *10. Kolloquium Industrieböden*, Conference paper, 3.-4.03.2020

Presentations and Posters

- **T. Klewe**, S. Kruschwitz, J. Wöstmann, Overview of NDT techniques for moisture measurements in building materials, *ENBRI Expert Workshop "Hygrothermal testing - a necessity to guarantee durable buildings"*, Presentation, 21.09.-22.09.2022
- **T. Klewe**, C. Strangfeld, T. Ritzer, S. Kruschwitz, Classification of moisture damage in layered building floors with GPR and neutrone probe, *European Geosciences Union (EGU) General Assembly 2021*, Presentation, 19.04-30.04.2021
- **T. Klewe**, C. Strangfeld, T. Ritzer, S. Kruschwitz, Feuchtemessung an Fußböden mit Radar und Neutronensonde – Ein Vergleich von Labor und Praxis, *81. Jahrestagung der Deutschen Geophysikalischen Gesellschaft (DGG)*, Posterpräsentation, 01.03-05.03.2021
- **T. Klewe**, C. Strangfeld, T. Ritzer, S. Kruschwitz, Multivariate Auswertung von Radarsignalen zur Bestimmung typischer Feuchteschäden in Fußböden, *80. Jahrestagung der Deutschen Geophysikalischen Gesellschaft (DGG)*, Presentation, 18.05.-22.05.2020
- **T. Klewe**, C. Strangfeld, T. Ritzer, S. Kruschwitz, Signalmerkmale des Radarverfahrens zur Klassifizierung von Feuchteschäden in Fußbodenaufbauten, *Fachtagung Bauwerksdiagnose*, Poster, 13.02.2020
- **T. Klewe**, C. Strangfeld, S. Kruschwitz, Untersuchung von Signalmerkmalen des Radarverfahrens zur Feuchtebestimmung an Estrichen, *79. Jahrestagung der Deutschen Geophysikalischen Gesellschaft (DGG)*, Presentation, 05.03.2019
- **T. Klewe**, C. Strangfeld, S. Kruschwitz, T. Ritzer, Kombination von Radar und Neutronensonde zur Bestimmung der Massenfeuchte von Estrichen, *DGZfP-Jahrestagung*, Posterpräsentation, 28.05.2019
- T. Ritzer, **T. Klewe**, C. Strangfeld, S. Kruschwitz, Radarwellen und Neutronenstrahlung – die Lösung für den Feuchteschaden? Forschungsprojekt der BAM und des IB Ritzer zur Feuchtebestimmung von schwimmenden Bodenaufbauten, *Messekongress Schadenmanagement & Assistance*, Presentation, 26.3.2019
- **T. Klewe**, C. Strangfeld, S. Kruschwitz, T. Ritzer, Zerstörungsfreie Lokalisierung von Flüssigwasser in Schichtaufbauten – Projektvorstellung, *Fachtagung Bauwerksdiagnose*, Poster, 15.02.2018